

NUMERICAL SIMULATION OF THE KIRAZLIKÖPRÜ
DAM FAILURE ON THE GÖKIRMAK RIVER

A THESIS SUBMITTED TO
THE GRADUATE SCHOOL OF NATURAL AND APPLIED SCIENCES
OF
MIDDLE EAST TECHNICAL UNIVERSITY

BY

KORAY KARAKAYA

IN PARTIAL FULFILLMENT OF THE REQUIREMENTS
FOR
THE DEGREE OF MASTER OF SCIENCE
IN
CIVIL ENGINEERING

APRIL 2005

Approval of the Graduate School of Natural and Applied Sciences

Prof. Dr. Canan ÖZGEN
Director

I certify that this thesis satisfies all the requirements as a thesis for the degree of Master of Science.

Prof. Dr. Erdal ÇOKÇA
Head of Department

This is to certify that we have read this thesis and that in our opinion it is fully adequate, in scope and quality, as a thesis for the degree of Master of Science.

Assoc. Prof. Dr. Zafer BOZKUŞ
Supervisor

Examining Committee Members

Prof. Dr. Mustafa GÖĞÜŞ	(METU, CE)	_____
Assoc. Prof. Dr. Zafer BOZKUŞ	(METU, CE)	_____
Assoc. Prof. Dr. Nuray TOKYAY	(METU, CE)	_____
Assoc. Prof. Dr. İsmail AYDIN	(METU, CE)	_____
Dr. M. Ali KÖKPINAR	(DSİ)	_____

I hereby declare that all information in this document has been obtained and presented in accordance with academic rules and ethical conduct. I also declare that, as required by these rules and conduct, I have fully cited and referenced all material and results that are not original to this work.

Name, Last name : Koray KARAKAYA

Signature :

ABSTRACT

NUMERICAL SIMULATION OF THE KIRAZLIKÖPRÜ DAM FAILURE ON THE GÖKIRMAK RIVER

Karakaya, Koray

M.S., Department of Civil Engineering

Supervisor : Assoc. Prof. Dr. Zafer Bozkuş

April 2005, 117 pages

Numerical dam break analyses of Kirazlıköprü Dam are performed under various hydraulic scenarios. Kirazlıköprü Dam is located on the Gökırmak River near the city of Bartın. The objective of these analyses is to investigate adverse effects of such dam break failure on the regions downstream of the dam. The numerical model used in the simulations is FLDWAV, which is developed by the National Weather Service (NWS) in the United States. It appears that most adversely effected regions are those that are closest to the dam location. The results of these simulations can be used sufficiently to prepare emergency action plans in case of possible failures.

Keywords: Dam-break, FLDWAV, Numerical simulation

ÖZ

GÖKIRMAK NEHRİ ÜZERİNDEKİ KIRAZLIKÖPRÜ BARAJ YIKILMASININ NÜMERİK BENZEŞİMİ

Karakaya, Koray

Yüksek Lisans, İnşaat Mühendisliği Bölümü

Tez Yöneticisi: Doç. Dr. Zafer Bozkuş

Nisan 2005, 117 Sayfa

Kirazlıköprü Barajı'nın nümerik baraj yıkılması analizleri çeşitli hidrolik senaryolar altında gerçekleştirildi. Kirazlıköprü Barajı, Bartın ili sınırları içinde Gökırmak nehri üzerinde bulunmaktadır. Bu analizlerin amacı baraj yıkılmasının baraj mansabında bulunan bölgelerde oluşturacağı olumsuz etkileri araştırmaktır. Nümerik benzeşimlerde kullanılan model, Amerika'da Ulusal Hava Servisi (NWS) tarafından geliştirilen FLDWAV modelidir. Baraj yerine en yakın bölgelerin en olumsuz etkilenen yerler olduğu ortaya çıkmaktadır. Bu benzeşimlerin sonuçları olası afet durumunda başvurulacak acil eylem planlarının hazırlanmasında yeterli olarak kullanılabilir.

Anahtar Kelimeler: Baraj yıkılması, FLDWAV, Nümerik benzeşim

To My Parents

ACKNOWLEDGMENTS

The author wishes to present his eternal gratitude to his supervisor Assoc. Prof. Dr. Zafer Bozkuş for his assistance, guidance, advices, encouragements and friendly cooperation throughout the research. He is highly appreciated for advising such an interesting and important subject that is really worthy to study extensively with curiosity and great concern.

The author would also like to thank the directors and officials of the State Hydraulic Works (DSİ) for their friendly approach and great effort in gathering all technical data required for the successful completion and execution of this study.

Encouragements and confidence of the author's parents together with his company MİTAŞ's support and understanding throughout the study are gratefully acknowledged.

TABLE OF CONTENTS

PLAGIARISM.....	iii
ABSTRACT.....	iv
ÖZ.....	v
DEDICATION.....	vi
ACKNOWLEDGMENTS.....	vii
TABLE OF CONTENTS.....	viii
LIST OF TABLES.....	xi
LIST OF FIGURES.....	xiii
LIST OF SYMBOLS.....	xvi
CHAPTER	
1. INTRODUCTION.....	1
1.1 General information.....	1
1.2 Objectives of the study.....	3
2. LITERATURE REVIEW.....	4
2.1 Introduction to dam break phenomenon.....	4
2.2 General information on dam failures.....	5
2.3 Historical dam break failures.....	7
2.3.1 Teton Dam.....	8
2.3.2 Buffalo Creek Coal Waste Dam.....	9
2.3.3 Kelly Barnes Dam.....	10

2.3.4 South Fork (Johnstown) Dam.....	12
2.3.5 Austin Dam.....	13
3. DAM BREAK FLOOD FORECASTING.....	15
3.1 History of dam break flood forecasting.....	15
3.2 Tools for dam break flood forecasting.....	16
3.2.1 A generalized routing model: FLDWAV.....	16
3.2.2 Comparison of FLDWAV to DAMBRK and DWOPER models.....	18
3.2.3 Modeling capabilities of FLDWAV.....	18
3.3 Flood Routing.....	20
3.3.1 Flood routing methods.....	21
3.3.2 Expanded Saint-Venant equations.....	22
3.3.3 Solution technique for Saint-Venant equations.....	25
3.3.3.1 Boundary conditions.....	29
3.3.3.2 Internal boundaries.....	33
3.3.3.3 Initial conditions.....	36
3.4 Modeling dam breach.....	38
3.4.1 Breach outflow.....	39
3.4.2 Breach parameters.....	41
3.4.2.1 Overtopping failures.....	42
3.4.2.2 Piping failures.....	45
3.4.2.3 Concrete dams.....	46
3.4.2.4 Earthen dams.....	47

4. A CASE STUDY: KİRAZLIKÖPRÜ DAM.....	50
4.1 Introduction to study area.....	50
4.2 About the Kirazlıköprü Dam.....	52
4.3 Modeling routing reach.....	54
4.4 Modeling of cross sections.....	58
5. KİRAZLIKÖPRÜ DAM BREAK ANALYSES.....	64
5.1 Selection of breach parameters.....	64
5.2 Failure scenarios.....	65
5.3 Simulation results.....	74
6. EVALUATION OF THE RESULTS.....	82
6.1 Evaluation of scenario 1 results.....	83
6.2 Evaluation of scenario 2, 3 and 4 results.....	88
6.3 Evaluation of scenario 5 results.....	95
6.4 Evaluation of scenario 6 results.....	100
6.5 Hazard evaluation of downstream regions	106
7. CONCLUSION.....	110
REFERENCES.....	113
APPENDICES	
A. LAYOUT OF MODELING REACH.....	117

LIST OF TABLES

Table 4.1 Physical and hydrological characteristics of Kirazlıköprü Dam...	52
Table 4.2 Kirazlıköprü Dam reservoir elevation-area-volume data.....	56
Table 5.1 Simulation characteristics of scenarios 1 and 2.....	69
Table 5.2 Simulation characteristics of scenarios 3, 4 and 5.....	70
Table 5.3 Simulation characteristics of scenario 6.....	74
Table 5.4 Summary table of peak flows and their occurrence times for scenario 1.....	76
Table 5.5 Summary table of peak water surface elevations and their occurrence times for scenario 1.....	76
Table 5.6 Summary table of peak flows and their occurrence times for scenario 2.....	77
Table 5.7 Summary table of peak water surface elevations and their occurrence times for scenario 2.....	77
Table 5.8 Summary table of peak flows and their occurrence times for scenario 3.....	78
Table 5.9 Summary table of peak water surface elevations and their occurrence times for scenario 3.....	78
Table 5.10 Summary table of peak flows and their occurrence times for scenario 4.....	79
Table 5.11 Summary table of peak water surface elevations and their occurrence times for scenario 4.....	79

Table 5.12 Summary table of peak flows and peak water surface elevations together with their occurrence times for scenario 5.....	80
Table 5.13 Summary table of peak flows and their occurrence times for scenario 6.....	81
Table 5.14 Summary table of peak water surface elevations and their occurrence times for scenario 6.....	81
Table 6.1 Hazard evaluation of downstream regions.....	109

LIST OF FIGURES

Figure 2.1 Dam break causes.....	6
Figure 3.1 Discrete x-t solution domain.....	26
Figure 3.2 Boundary conditions.....	31
Figure 3.3 Front view of a dam with discharge components.....	35
Figure 3.4 Physical parameters of an ideal overtopping breach	42
Figure 3.5 Formation of piping breach	46
Figure 3.6 Medford Quarry wash pond piping failure.....	46
Figure 3.7 Trapezoidal breach formation of an embankment dam.....	48
Figure 4.1 Plan view of modeling domain.....	51
Figure 4.2 Catastrophic inflow hydrograph of Kirazlıköprü Dam	55
Figure 4.3 Elevation-Area-Volume curve of Kirazlıköprü Dam reservoir.....	55
Figure 4.4 Profile view of routing reach.....	57
Figure 4.5 Definition of an input cross section.....	59
Figure 4.6 Cross section B1.....	61
Figure 4.7 Cross section B2.....	61
Figure 4.8 Cross section B3.....	62
Figure 4.9 Cross section B4.....	62
Figure 4.10 Cross section B6.....	63
Figure 4.11 Cross section B7.....	63
Figure 5.1 Schematic view of breach type 1 formation.....	66

Figure 5.2 Schematic view of breach type 2 formation.....	66
Figure 5.3 Schematic view of breach type 3 formation.....	66
Figure 5.4 Spillway rating curves for different gate openings.....	68
Figure 5.5 Formation of piping breach.....	73
Figure 6.1 Peak discharge profiles for different breach parameters	84
Figure 6.2 Peak flow occurrence time profiles for different breach parameters	86
Figure 6.3 Peak water surface elevation profiles for different breach parameters	87
Figure 6.4 Dam break flood wave attenuation along the routing reach for scenario 1.....	89
Figure 6.5 Peak discharge profiles for different spillway gate openings.....	91
Figure 6.6 Peak water surface elevation profiles for different spillway gate openings.....	92
Figure 6.7 Peak flow occurrence time profiles for different spillway gate openings that lead to dam failure.....	93
Figure 6.8 Peak discharge profiles for different Manning n values.....	97
Figure 6.9 Peak water surface elevation profiles for different Manning n values.....	98
Figure 6.10 Peak flow occurrence time profiles for different Manning n values.....	93
Figure 6.11 Reservoir outflow hydrograph for piping failure ($T_f = 1$ hr).....	101
Figure 6.12 Reservoir outflow hydrograph for piping failure ($T_f = 2$ hr).....	102
Figure 6.13 Reservoir outflow hydrograph for piping failure ($T_f = 3$ hr).....	103

Figure 6.14 Temporal variation of water surface elevation in the
reservoir for 1 hr failure time..... 104

LIST OF SYMBOLS

A	channel/floodplain cross-sectional area of active flow
A_g	fixed gate flow area
A_o	inactive (off-channel storage) cross-sectional area
A_s	surface area of the reservoir at the top of the dam
B	channel/floodplain topwidth at elevation h for active flow portion of cross-section
B_c	topwidth of channel portion of channel/floodplain cross-section
B_f	topwidth of floodplain portion of channel/floodplain cross-section
B_o	off-channel storage topwidth
C_n	Courant number of the Courant-Friedrich-Lewy condition for numerical stability of explicit solutions of Saint-Venant equations
C_w	non-dimensional wind coefficient
D	hydraulic depth
DXM	computational distance step
F_r	Froude number
K	flow conveyance factor
K_c	channel conveyance
L	the momentum effect of lateral flow
L_d	length of the dam crest less L_s and the length of the gates located along the dam crest
L_s	spillway length
N	denotes the sequence number of the last most downstream cross section or total number of cross sections along the river
P	wetted perimeter
Q	discharge or flow
\overline{Q}	average discharge between separate locations

$Q(h)$	discharge as a function of water surface elevation
$Q(t)$	discharge as a function of time
Q_1	discharge at section 1
Q_b	the dam-breach flow
Q_{dam}	dam overtopping flow
Q_{gate}	fixed gate orifice flow
Q_o	initial flow at $t=0$
Q_p	estimated peak breach discharge
Q_s	total non-breach flow at dam or at bridge
Q_t	turbine flow
R	hydraulic radius
S	instantaneous dynamic energy slope
S	storage in level-pool routing
S_a	reservoir surface area
S_c	critical slope
S_f	channel/floodplain boundary friction slope
S_e	expansion-contraction slope
S_i	additional friction slope associated with internal viscous dissipation of non-Newtonian fluids such as mud/debris flows
S_o	the channel/river bottom slope
T_r	the time of rise of hydrograph
V	the velocity of flow
V_r	reservoir volume
W_f	effect of wind resistance on the flow
b	terminal bottom width of dam breach
\bar{b}	average dam breach width
c	local dynamic wave velocity
\hat{c}	kinematic or bulk wave velocity
c_d	discharge coefficient for overtopping flow over the crest of the dam
c_{sp}	uncontrolled spillway discharge coefficient
c_v	velocity of approach correction factor

d	the flow depth associated with the correct Manning n value
f	Darcy friction factor
g	constant for the acceleration due to gravity
h	water surface elevation
h_b	instantaneous elevation of the breach bottom
h_{bm}	final elevation of the breach bottom
h_d	height of dam
h_f	elevation which attained first by the reservoir water surface elevation initiates the formation of the breach
h_{fp}	water surface elevation of the floodplain
h_k	elevation of topwidth at k^{th} entry to topwidth-elevation table
h_N	starting water surface elevation at downstream boundary location
h_p	centerline elevation of the pipe breach of a dam
h_{sp}	uncontrolled spillway crest elevation
h_t	downstream tailwater elevation
k_d	submergence correction for tailwater effects on dam overtopping flow
k_s	broad-crested weir submergence correction factor
n	the Manning n, a coefficient for frictional resistance
q	lateral inflow or outflow per linear length of channel
q_o	average unit width discharge (average discharge/average channel topwidth)
s_{co}	sinuosity factor for conversation of mass equation
s_m	sinuosity factor for conversation of momentum equation
t	time
t_b	time since beginning of breach formation
x	the longitudinal distance along the river
α	weighting factor ($0 < \alpha \leq 1$) in dynamic tributary equation
β	the momentum coefficient for velocity distribution
θ	weighting factor in implicit finite-difference scheme for Saint-Venant equation
μ	constant in Manning's equation (1.49 for English system of units and 1.0 for SI units)

τ dam-breach time of formation or time of failure
 ψ represents any variable

CHAPTER 1

INTRODUCTION

1.1 GENERAL INFORMATION

Dams are man made barriers constructed across water courses for the benefit of mankind. They are constructed in order to improve living conditions of the society they are serving. By the existence of dams any society can increase their living standard which yields to civilization in turn. The quantity of dams constructed may be considered as an indication of civilization degree of a country.

Some of the vital uses of dams are municipal and industrial water supply, flood control after heavy precipitation, hydroelectric power production, irrigation, recreation and improvement of water quality. On the other hand, dams constitute great danger to the life and property of people living in the regions downstream of the dam since they have potential to fail like many other man made structures. Due to several reasons a dam may fail and lead to catastrophe. Since they keep great amounts of water in their reservoirs they are always potential hazards. A dam fails when a breach opening forms in its body and large amount of water stored in its reservoir escapes through that opening. Release of such a large amount of impounded water into the downstream valley may trigger a catastrophic flood.

When compared to floods triggered by heavy precipitation, dam failure originated floods usually lead to much higher peak flows in magnitude. These values greatly exceed all previous floods caused by heavy

precipitations. More importantly, the occurrence time of peak water flows is much shorter than the ones encountered in any hydrologic event. This means warning time of people living downstream is significantly shorter.

It is not possible to prevent all dam failures; however, it is possible to avoid great number of victims during dam failure catastrophe. This can only be achieved by proper evacuation of people living downstream of the dam before the flood wave arrives and sweeps away everything. In order to relieve adverse effects of such catastrophes, emergency action plans can be established based on data available through numerical and physical models. By the help of these models, inundation information and travel time of flood waves can be forecasted in any dam failure incident and these results can form the guidelines in emergency management. This type of planning may include preparation of inundation maps, tables of warning times for each district and establishment of early warning systems which is the one and only way to avoid a large number of victims.

The potential for catastrophic flooding due to a dam failure was brought to the attention of government officials, emergency action personnel, engineers and researchers in the United States during the 1970's by several major catastrophic floods due to dam failures such as, the Buffalo Creek coal-waste dam in 1972, the Teton Dam in 1976, the Laurel Run Dam in 1977, and the Kelly Barnes Dam in 1977, all of which resulted in significant loss of life and property. Since that period, extensive researches and studies on dam failure phenomenon have been going on intensively in the United States.

In Turkey, recently, there has been an ever increasing interest for predicting the potential hazards of dam failure incident and for performing numerical analyses of dam break failures in order to make data available to the officials for emergency management (Bozkuş, 1994; Bozkuş and Kasap, 1998; Bozkuş and Güner, 2001).

1.2 OBJECTIVES OF THE STUDY

The main purpose of this study is to perform numerical dam break analyses of the Kirazlıköprü Dam in the province of Bartın in North Western part of Turkey. Unfortunately, this region of Turkey is notorious for its major floods in spring. In the past few years, there have been severe flooding events in the Western Black Sea Region of Turkey that had led to significant property losses. Due to the hydrologic basin characteristics of this region, flooding occurs very frequently and there is always a potential for dam break failure. A recent project called TEFER (Turkey Emergency Flood & Earthquake Recovery), which is financed by a foreign consortium, is going on in order to minimize adverse effects of flooding and to establish countermeasures in the western parts of Turkey. Kirazlıköprü dam and its basin are also involved in this project and the aim of this study is to take part in this project by sharing findings and results of analyses.

This study will aim to provide flood hydrographs at selected locations downstream of the Kirazlıköprü Dam as a result of numerical dam break analyses. The simulations shall be conducted under several hydraulic conditions and peak flow rates together with peak water surface elevations shall be obtained for the worst case scenario in order for the officials of the city to make proper emergency action plans of Bartın. Needless to say, the dam break analysis of Kirazlıköprü Dam is inevitable for the city of Bartın whose population is about 185,000. Performing such analyses gives us vital information necessary during the emergency in order to alert people on time and to evacuate them to safe places before the predicted flood wave arrives. There is no doubt that an unpredicted dam failure can lead to great number of human life losses. The pre-event prediction of dam break failures would give us great benefits and people can be alerted before the disaster hits. This valuable information shall be obtained by the use of numerical model FLDWAV, which is developed by the NWS (National Weather Service) in the United States.

CHAPTER 2

LITERATURE REVIEW

2.1 INTRODUCTION TO DAM BREAK PHENOMENON

Although dams provide society with many essential benefits, catastrophic flooding occurs when a dam fails and the impounded water escapes through the breach opening to cause loss of large number of lives and property in the downstream valley. Usually, the magnitude of the dam-break flow greatly exceeds all previous floods that have occurred in the past and the response time to warn people is much shorter than for precipitation runoff floods.

A distinguishing feature of dam-break floods is the great magnitude of the peak discharge when compared to any precipitation runoff generated floods that could occur in the same valley. The dam-break flood is usually many times greater than the runoff flood of record in magnitude. Another distinguishing characteristic of dam-break floods is the extremely short period of time from the beginning of rise to the occurrence of the peak. This also means that duration of the flood is very short. In almost all cases, the time to peak is the same as the interval of time required for the breach to develop completely when it starts to form. This time of failure may be in the order of minutes for most dams, although some very large dams may have a time of failure of an hour or greater. This feature of dam-break floods, along with the great magnitude of the peak flow, makes the dam-breach flood to have acceleration components of a far greater significance than those associated with a precipitation runoff generated flood.

Within the United States, as well as in many nations throughout the world, there are many dams that are 30 or more years old. Many of the older dams are of serious concern because of increased hazard potential for the downstream development and increased risk of failure due to structural deterioration and inadequate spillway capacity. A report by the U.S. Army (1981) gives an inventory of approximately 70,000 dams in the United States with heights greater than 25 ft (7.62 m) or storage volumes greater than 50 acre-ft ($61.66 \times 10^3 \text{ m}^3$). The report also classifies 20,000 of these dams as being “so located that failure of the dam could result in loss of human life and appreciable property damage...”

The potential for catastrophic flooding due to a dam failure was brought to the attention of politicians, emergency action personnel, engineers, and some portions of the population within the United States during the 1970's by several catastrophic floods due to dam failures, such as the Buffalo Creek coal-waste dam in 1972, the Teton Dam in 1976, the Laurel Run Dam in 1977, and the Kelly Barnes Dam in 1977 (Fread, 1997).

2.2 GENERAL INFORMATION ON DAM FAILURES

According to reports by the International Commission on Large Dams (ICOLD, 1973) and the United States Committee on Large Dams in cooperation with the American Society of Civil Engineers (ASCE/USCOLD, 1975), about 38 percent of all dam failures are caused by overtopping of the dam due to inadequate spillway capacity and by spillways being collapsed during large inflows to the reservoir from heavy precipitation runoff. About 33 percent of dam failures are caused by seepage or piping through the dam or along internal conduits, while about 23 percent of the failures are associated with foundation problems, and the remaining failures are due to slope embankment slides, damage or liquefaction of earthen dams from earthquakes, and overtopping of the dam by landslide-generated waves

within the reservoir. Figure 2.1 shows the percentage distribution of dam failure causes below.

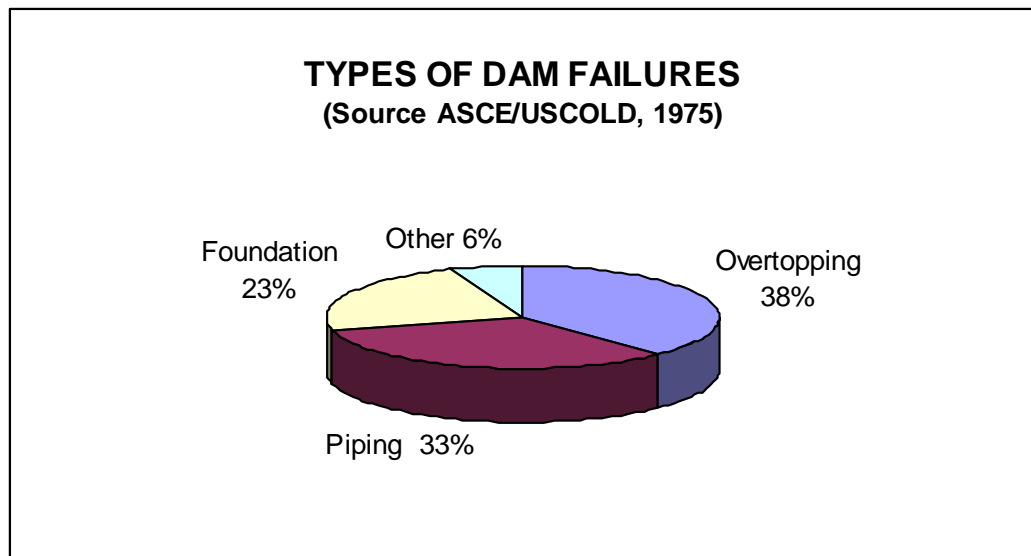


Figure 2.1 Dam break causes

Large portion of the existing dams have been constructed many years ago and now they do not meet recent design specifications. Most of the unsafe dams have inadequate spillway capacity and risk of being overtopped is very high for these dams. Approximately 35% of dams built by non-federal interests in the USA are in an unsafe condition. About three quarter of these dams are unsafe because of poor spillway capacity (Hagen, 1982). The percentages of dams that fail, among the total of constructed dams, have decreased during this century due to basic improvements in the design and construction (Serafim, 1981).

A large dam is always considered to be a potential source of hazard, especially to densely populated areas at downstream. This arises from the fact that, there is always a failure probability due to miscalculations, inadequate evaluation of any critical design condition or an error in

operational procedures, among many other reasons. According to statistics, dams of significant size fail in the United States at an average rate of more than one per year (Ellingwood et al., 1993).

Simulation of embankment dam breach events and the resulting floods are very important for characterizing and reducing threats due to potential dam failures. Development of effective emergency action plans requires accurate prediction of inundation levels and the flood arrival time at a given location. If population centers are located well downstream of a dam, details of the breaching process have little effect on the results. However, if population centers are close to dam location, then reasonable prediction of breach parameters (e.g. breach width, depth, time of formation) is very critical and important. If breach parameters can not be predicted with reasonable accuracy, increased conservatism with associated costs are required (Wahl, 1997).

2.3 HISTORICAL DAM BREAK FAILURES

Floods resulting from the failure of constructed dams have produced some of the most devastating disasters of the last two centuries. When dams fail, property damage is inevitable, but loss of life can vary dramatically with the extent of the inundation area, the size of the population at risk, and the amount of warning time available. Sixty percent of the more than 11,100 deaths associated with all dam failures worldwide have occurred in just three failures: Vaiont, Italy, 1963 (2,600 dead; overtopping of concrete arch dam by landslide generated wave); Johnston Dam, Pennsylvania, 1889 (2,200 dead; overtopping of embankment dam); and Machau II, India, 1974 (2,000 dead; overtopping of embankment dam during construction). In each of these cases, large populations were given little or no warning at all. It is reported that the average number of deaths per dam failure is 19 times greater when there is inadequate or no warning (Costa, 1985).

A presentation was prepared by Wayne Graham in the United States Bureau of Reclamation (Graham, 2001). The title of the presentation was “Human and Economic Consequences of Dam Failure “, which has focused on 13 dam failures in the United States. The presentation included a discussion of dam characteristics, cause of dam failure, dam failure warning, evacuation, and human and economic losses.

Details of some dam failure incidents presented in Graham's study can be found in the following sections.

2.3.1 TETON DAM

Location: near Wilford, Idaho

Dam Characteristics:

Dam Type: earthfill

Dam Height: 93 m

Reservoir Volume: 308.3x10⁶ m³ released

Spillway: water never reached spillway

History of Dam:

Purpose: irrigation

Dam completed: under final construction/first filling

Dam failed: Saturday June 5, 1976 at 11:57 a.m.; first filling

Failure cause: Piping of dam core in foundation key trench

Details on Detection of Failure/Deciding to warn:

00:30 a.m. and 7 a.m.: dam unattended

7 a.m. to 8 a.m.: Survey crew discovers turbid leakage

9:30 a.m.: PCE considers alerting residents but decides emergency situation is not imminent and is concerned about causing panic.

10 a.m.: larger leak, flowing turbid water

10:30 a.m. to 10:45 a.m.: PCE notifies sheriff's offices and advises them to alert citizens.

Details on dissemination of warnings and technologies used:

Police, radio, television, telephone, neighbor word of mouth. (Included live commercial radio broadcasts from reporters in aircraft and at Teton Dam)

Description of flooding resulting from dam failure:

Over 3,700 houses destroyed or damaged. 400 to 500 km² flooded.

The losses included:

11 deaths (6 from drowning, 3 heart failure, 1 accidental gun shot and 1 suicide) with about 25,000 people at risk. 800 injuries. Total damage of \$400 million.

2.3.2 BUFFALO CREEK COAL WASTE DAM

Location: Near Saunders, West Virginia

Dam Characteristics:

Dam type: Coal waste

Dam height: 14 m

Reservoir volume: 50x10⁴ m³

Spillway: Small pipe

History of Dam:

Purpose: Improve water quality, dispose of coal waste

Dam completed: Continually changing

Dam failed: February 26, 1972 about 8 a.m. (0 years old)

Failure cause: Slumping of dam face during 2-year rain.

Details on detection of failure/Deciding to warn:

Owner reps were on site monitoring conditions prior to dam failure. At least two dam owner officials urged the Logan County Sheriff's force to refrain from a massive alert and migration.

Details on dissemination of warnings and technologies used:

Company officials issued no warnings. The senior dam safety official on the site dismissed two deputy sheriffs at about 6:30 a.m. who had been called to the scene to aid evacuation.

Details on response to the warning:

Resident's reaction to inadequate warnings that were issued was dampened due to at least 4 previous false alarms.

Description of flooding resulting from dam failure:

Wave traveled downstream through the 24 km long valley at 8 kmph. Over 1,000 homes either destroyed or damaged.

The losses included:

125 deaths; 4,000 people homeless. All of the fatalities occurred in the first 24 km downstream from the dam. Total damage of \$50 million.

2.3.3 KELLY BARNES DAM

Location: On Toccoa Creek, near Toccoa Falls, Georgia.

Dam Characteristics:

Dam type: Earthfill

Dam height: About 12 m

Dam crest length: 122 m

Reservoir volume: $77.7 \times 10^4 \text{ m}^3$ at time of failure

History of Dam:

Purpose: Originally for hydropower. Hydropower abandoned in 1957 and then used for recreation.

Dam completed: 1899. Enlarged/modified in 1937 and after 1945.

Dam failed: Sunday, November 6, 1977 at 1:20 a.m.

Failure cause: Saturation due to heavy rain caused downstream slope failure.

Details on detection of failure/deciding to warn:

Two volunteer firemen examined the dam around 10:30 p.m. on November 5, 1977 and reported that dam was solid and that there was no need for concern or alarm.

Details on dissemination of warnings and technologies used:

With concern over rising water, not dam failure, 1 or 2 families were warned by volunteer firemen just minutes before dam failure.

Details on response to warning:

Most people were not warned. It would have been horrible condition for evacuation due to dark, rain and cold.

Description of flooding resulting from dam failure:

Flood reached depths of 2.5 to 3 m in populated floodplain.

The losses included:

39 fatalities, all within 3 km of the dam. 9 houses, 18 house trailers, 2 college buildings demolished. 4 houses and 5 college buildings damaged. Total damage of \$2.8 million.

2.3.4 SOUTH FORK (JOHNSTOWN) DAM

Location: On South Fork Little Conemaugh River, Pennsylvania.

Dam Characteristics:

Dam type: Earthfill

Dam height: 22 m

Reservoir volume: $14.18 \times 10^6 \text{ m}^3$

History of Dam:

Purpose: Originally for supplying water to canal system; at time of failure it was owned by South Fork Hunting and Fishing Club of Pittsburgh.

Dam completed: 1853

Dam failed: May 31, 1889 about 3:10 p.m. (about 36 years old)

Failure cause: Overtopping during an approximate 25-year storm (Drainage area of about 124 km^2)

Details on detection of failure/Deciding to warn:

People were at dam trying to prevent dam failure. Between 11:30 and noon the resident engineer, on horseback, reached the town of South Fork (3 km from dam) with a warning. Word was telegraphed to Johnstown that was in danger.

Details on dissemination of warnings and technologies used:

Warnings were not widely disseminated.

Details on response to warning:

Little attention paid to warnings due to false alarms in prior years.

Description of flooding resulting from dam failure:

Floodwater reached Johnstown, 22 km, about 1 hour after failure. Large number of buildings destroyed. At time of failure, Johnstown was inundated by up to 3 m of floodwater.

The losses included:

About 2,209 fatalities; 20,000 people at risk. All, or nearly all, of the fatalities occurred in the first 22.5 km downstream from South Fork Dam.

2.3.5 AUSTIN DAM

Location: On Freeman Run, about 2.4 km upstream from Austin, Pennsylvania. The dam is located in western PA., about 210 km northeast of Pittsburgh.

Dam Characteristics:

Dam type: Concrete gravity

Dam height: Between 13 and 15 m

Dam crest length: 166 m

Reservoir volume: Between 68×10^4 and 105×10^4 m³

Spillway: 15 m long and 76.2 cm deep

History of Dam:

Dam completed: November 1909

Partial failure: January 1910; part of dam moved 46 cm at base and 86 cm at the top.

Dam failed: 2 p.m. or 2:20 p.m., September 30, 1911 (2 years old)

Failure cause: Weakness of the foundation, or of the bond between the foundation and concrete.

Details on detection of failure/Deciding to warn:

Harry Davis, boarding in a house on the mountain slope near the dam phoned Austin operators at whose warning the paper mill whistle sounded about 2 p.m. The phone operators warned others but many ignored the warnings.

Details on dissemination of warnings and technologies used:

The mill whistle had blown twice earlier in the day as false signals had been received from telephone company employees who had been repairing telephone lines. The two false alarms were the cause of many people losing their lives as many people assumed the whistle (sounded to warn of dam failure) was another false alarm. Warnings were issued to people in Costello, about 8 km downstream from the dam. A person riding a bicycle traveled from the south side of Austin to Costello to spread the warning.

Description of flooding resulting from dam failure:

The water traveled from the dam to the town of Austin, a distance of 2.5 km, in either 11 minutes or in up to 20 to 30 minutes. This results in a travel time of between 5 and 13 km per hour.

The losses included:

At least 78 fatalities, all in the first 3 km downstream from the dam, i.e. in the Austin area (about 3 or 4 percent of Austin's 2300 population).

CHAPTER 3

DAM BREAK FLOOD FORECASTING

3.1 HISTORY OF DAM BREAK FLOOD FORECASTING

The 1964 failure of Baldwin Hills Dam, near Los Angeles, California, and the near failure of Lower Van Norman (San Fernando) Dam in 1971 prompted the State of California to enact statutes requiring dam owners to prepare dam failure inundation maps. Thus, need for developing procedures for estimating dam-break flood hydrographs came out. Before enactment of the California statutes, there were only a few publications regarding methodologies for estimating dam-break outflow hydrographs.

The Bureau of Reclamation of the United States made comprehensive reviews on its dam safety program after numerous dam failures that occurred in the mid 1970's, including Buffalo Creek coal waste dam (West Virginia, 1972), Teton Dam (Idaho, 1976), Laurel Run Dam and Sandy Run Dam (Pennsylvania, 1977), and Kelly Barnes Dam (Georgia, 1977). In many of these reviews, planning of emergency readiness with inundation maps was emphasized. The Federal Guidelines for Dam Safety, dated June 25, 1979, stated that inundation maps should be prepared. These events highlighted the need for developing procedures for estimating dam-break outflow hydrographs (Wahl, 1998).

3.2 TOOLS FOR DAM BREAK FLOOD FORECASTING

Today there are numerous tools available for analyzing dam failures and their resulting outflow hydrographs. Some of the well known and most widely used are the National Weather Service (NWS) Dam-Break Flood Forecasting Model, *DAMBRK*; the U.S. Army Corps of Engineers Hydrologic Center Flood Hydrograph package, *HEC-1* (Hydrologic Engineering Center, 1981); and the NWS Simplified Dam-Break Flood Forecasting Model, *SMPDBK* (Weatmore and Fread, 1983). *DAMBRK* is the most widely used one among these models. Wurbs (1987) discussed and compared the state-of-the-art models available at that time and recommended the use of *DAMBRK* or *SMPDBK*, depending on the level of accuracy required and resources and input data available. Westphal and Thompson (1987) also compared *DAMBRK* and *SMPDBK* and recommended the use of *SMPDBK* as a screening tool and *DAMBRK* for more detailed analyses. All these models treat the routing of the dam-break flood in much greater detail than the actual breaching process. The National Weather Service *BREACH* model (Fread, 1988) and other similar models simulate the breach formation process in greater detail.

3.2.1 A GENERALIZED ROUTING MODEL: FLDWAV

A generalized flood routing model, *FLDWAV*, has been developed by the National Weather Service (NWS) in the United States. *FLDWAV*, Version 1.0, released in November 1998 replaced the *NWS DAMBRK* (released in 1988) and *DWOPER* (released in 1984) models since it allows the utilization of their combined capabilities, as well as provide new hydraulic simulation features. While *DAMBRK* has the ability to analyze the flow of a single stream, *DWOPER* has the additional capability to model flows through a system of interconnected waterways. In addition to the capabilities of *DAMBRK* and *DWOPER*, *FLDWAV* also has the capability to analyze flows in mixed-flow regimes.

FLDWAV is a generalized flood routing (unsteady flow simulation) model. The governing equations of the model are the complete one-dimensional Saint-Venant equations of unsteady flow which are coupled with internal boundary equations representing the rapidly varied (broad-crested weir) flow through structures such as dams and bridge/embankments which can develop a user-specified time-dependent breach. Also, appropriate external boundary equations at the upstream and downstream ends of the routing reach are utilized. The system of equations is solved by an iterative, nonlinear, weighted four-point implicit finite-difference method. The flow may be either subcritical or supercritical or a combination of each varying in space and time from one to the other; fluid properties may obey either the principles of Newtonian (water) flow or non-Newtonian (mud/debris) flow. The hydrograph to be routed may be user-specified as an input time series, or it can be developed by the model via user-specified breach parameters (size, shape, time of development). The possible presence of downstream dams which control the flow and may be breached by the flood, bridge/embankment flow constrictions, tributary inflows, river sinuosity, levees located along the tributaries and/or downstream river, and tidal effects are each properly considered during the downstream propagation of the flood. *FLDWAV* also may be used to route mud and debris flows or rainfall/snowmelt floods using user-specified upstream hydrographs. High water profiles along the valley, flood arrival times, and discharge and stage (water-surface elevation) hydrographs at user selected locations are standard model output. Model input/output may be in either English or metric (SI) units.

FLDWAV can be used by hydrologists and engineers for a wide range of unsteady flow applications including real-time flood forecasting in a dendritic system of rivers, dam-break analyses for sunny day piping or overtopping associated with a Probable Maximum Flood, design of waterway improvements, floodplain inundation mapping, irrigation system design, debris flow inundation mapping, and storm sewer analysis and design.

3.2.2 COMPARISON OF FLDWAV TO DAMBRK and DWOPER MODELS

The NWS *FLDWAV* model is a combination of the NWS *DAMBRK* and *DWOPER* models. Although these models are quite powerful, limitations exist that weaken their flexibility. Limitations of *DWOPER* include its inability to interpolate cross sections when needed, its inability to handle supercritical flow, its inability to model dam breaks and a variety of reservoir outflow controls, and its limited levee capability. *DAMBRK* can only model single rivers. Fixed arrays for the number of time steps and number of cross sections severely limit the size of river systems that could be modeled without breaking up the problem into several datasets. *FLDWAV* includes the best capabilities of both models and a few enhancements that make it the model of choice.

3.2.3 MODELING CAPABILITIES OF FLDWAV

The *FLDWAV* computer program is designed to analyze large flood events usually caused by breach of a dam and to predict the movement of a large flood wave in the real-time forecasting done by the NWS River Forecasting System (NWSRFS). *FLDWAV* has the following capabilities:

- **Flow system:** *FLDWAV* can model single channel or dendritic systems, straight or meandering channels, or divided channels.
- **Flow regime:** *FLDWAV* can model free surface flows in subcritical, supercritical, and mixed-flow regimes or pressurized conduit flows.
- **Fluid type:** *FLDWAV* can model Newtonian (clear water) fluids and non-Newtonian fluids (mud/debris).
- **Off-channel storage:** *FLDWAV* can define ineffective flow areas in cross sections to be used to model ineffective flow areas.
- **Flow controls:** *FLDWAV* can model time-dependent dam breaches, time-dependent gate controls, flow over spillways, from through waterfalls

and short rapids, pressure and weir flow of bridges and breaches of bridge embankments, low flows through bridge embankments, and multiple levee over-topping and breaches.

- *FLDWAV* has the capacity to interpolate cross sections
- *FLDWAV* can read rating curve data as input. This feature is generally available in unsteady flow models. This feature gives *FLDWAV* the capability to use the stage-discharge relationships of control structures developed by other hydraulic models/analyses or obtained through observation.
- *FLDWAV* can use an optimization procedure to determine the Manning's roughness coefficients necessary to calibrate to observed high-water marks. This calibration is achieved through an efficient automatic adjustment of the roughness coefficients such that the differences between computed and observed water surface elevations are minimized.
- *FLDWAV* can route unsteady flows occurring simultaneously in a system of interconnected rivers. Any of the rivers may have one or more structures such as dams, bridges, levees which control the flow and which may breach if failure conditions are reached.
- *FLDWAV* can calculate initial conditions that consist of initial water surface elevations and discharges at each of the input cross section location. *FLDWAV* can start up in either a steady state or an unsteady state condition.
- *FLDWAV* has the capability of using multiple routing techniques in a river system. Currently, there are four routing techniques available: dynamic implicit, dynamic explicit, level pool (storage), and diffusion. Each reach between adjacent cross sections can be assigned a separate routing technique.

The model consists of mainly three functional parts:

1. *Description of the dam failure model*, i.e., the temporal and geometrical description of the breach

2. *Computation of the outflow hydrograph* through the breach opening as affected by the breach description, reservoir inflow, reservoir storage characteristics, spillway outflows, and downstream tailwater elevations.

3. *Routing of the reservoir outflow hydrograph* through the downstream valley in order to determine changes in the hydrograph due to valley storage, frictional resistance, downstream bridges or dams, and to determine the resulting water surface elevations and flood wave arrival times.

Due to new enhancements and wide range of hydraulic capabilities, the *FLDWAV* model was selected in this study to perform dam break analyses of Kirazlıköprü Dam.

3.3 FLOOD ROUTING

The essential component of the *FLDWAV* model is the computational hydraulic routing algorithm which determines the extent and time of occurrence of flooding in a river or system of interconnected rivers when they are subjected to unsteady flow. The unsteady flood hydrograph is attenuated, lagged, distorted as it is routed through the valley due to the effects of floodplain storage, frictional resistance to flow, flood wave acceleration components, flow losses/gains and downstream channel constrictions or flow control structures. The modifications done to the flood wave are the attenuation of the flood peak magnitude, dispersion of the temporal varying flood wave volume, and changes in the propagation speed of the flood wave.

There are two basic types of flood waves. The first one is the runoff generated waves resulting either from precipitation or snow-melt and the second one is the dam-break generated flood waves. The magnitude of the peak flow of a dam-break generated flood wave is usually much greater than the runoff flood of record that has occurred in the same river. Another distinguishing characteristics of dam-break floods is the very short duration t ,

and particularly the extremely short period of time from the beginning of rise until the time of occurrence of the peak flow. This time to peak is synonymous with the period of breach formation time in almost all cases. It can range from a few minutes to about an hour or greater. Due to the fact that dam-break flood waves have acceleration components of a far greater significance than those associated with runoff generated flood waves, the time to peak is considerably rapid.

3.3.1 FLOOD ROUTING METHODS

There are two basic flood routing methods: the hydrologic and the hydraulic methods. When compared to hydraulic methods, the hydrologic methods usually provide a more approximate analysis of the progression of a flood wave through a river. The hydrologic methods are used for convenience and economy. They are most appropriate, as far as accuracy is concerned, when the flood wave acceleration effects are negligible compared to the effects of gravity and channel friction. Also, they are best used when backwater effects are negligible and when the flood wave is very similar in shape and magnitude to previous flood waves for which observed stage and discharge values are available for the calibration of hydrologic routing parameters.

In the *FLDWAV* model, a particular hydraulic method, known as the *dynamic wave* method based on the complete one-dimensional Saint-Venant unsteady flow equations, is used for routing unsteady flood waves. This selection has been done due to the method's ability to provide more accuracy in simulating the unsteady flood wave than that provided by the hydrologic methods. The dynamic wave method is also superior to the other less complex hydraulic methods such as the kinematic wave and diffusion wave method as far as accuracy is concerned. Of the many available hydrologic and hydraulic routing methods, only the dynamic wave method accounts for the acceleration effects associated with the dam-break flood

wave and the influence of downstream unsteady backwater effects produced by channel constrictions, dams, bridge-road embankments, and tributary flows. Also, the dynamic wave method is advantageous since the computational time can be made rather insignificant if advantages of certain implicit numerical solution techniques are utilized (Fread, 1973, 1977, 1978, 1985, 1998).

The dynamic wave method is based on the complete one-dimensional equations of unsteady flow which are known as Saint-Venant equations. These equations can be used to route flood hydrographs through rivers comprising of both channel and floodplain. This method is based on an expanded version of the original equations developed by Barré de Saint-Venant (1871). The Saint-Venant equations can be appropriately used to simulate abrupt waves such as the dam-break wave. This is a “through computation” method which does not provide special treatment for shock waves. This method does not isolate a single shock wave, should it occur, nor apply the shock equations to it while simultaneously using the Saint-Venant equations for all other portions of the flow. The *FLDWAV* model is primarily based on the complete Saint-Venant equations of unsteady flow.

3.3.2 EXPANDED SAINT-VENANT EQUATIONS

The Saint-Venant equations, expressed in conservative form (Fread, 1974), with additional terms for the effect of expansion/contraction (Fread, 1978), channel sinuosity (DeLong, 1986, 1989) and non-Newtonian flow (Fread, 1988) consist of conservation of mass equation, i.e.

$$\frac{\partial Q}{\partial x} + \frac{\partial s_{co}(A + A_o)}{\partial t} - q = 0 \quad (3.1)$$

and a conservation of momentum equation, i.e.

$$\frac{\partial(s_m Q)}{\partial t} + \frac{\partial(\beta Q^2 / A)}{\partial x} + gA\left(\frac{\partial h}{\partial x} + S_f + S_e + S_i\right) + L + W_f B = 0 \quad (3.2)$$

where,

Q: discharge or flow

h: water surface elevation

A: active cross-sectional area of flow

A₀: inactive (off-channel storage) cross-sectional area

s_{co}, s_m: sinuosity factors after DeLong (1986, 1989) which vary with h

x: longitudinal distance along the river

t: time

q: lateral inflow or outflow per linear distance along the channel

β: momentum coefficient for velocity distribution

g: acceleration due to gravity

S_f: channel/floodplain boundary friction slope

S_e: expansion-contraction slope

S_i: additional friction slope associated with internal viscous dissipation of non-Newtonian fluids such as mud/debris flows

B: active river topwidth at water surface elevation h

W_f: effect of wind resistance on the surface of the flow

L: momentum effect of lateral flow.

The boundary friction slope (S_f) in Eq. (3.2) is evaluated from Manning's equation for uniform, steady flow, i.e.

$$S_f = \frac{n^2 |Q|Q}{\mu^2 A^2 R^{4/3}} = \frac{|Q|Q}{K^2} \quad (3.3)$$

in which n is the Manning roughness coefficient, μ is a units conversion factor, 1.49 for English units and 1.0 for SI units, R is the hydraulic radius,

and K is the flow conveyance factor. When the conveyance factor (K) is used to represent S_f , the river cross-sectional properties are designated as left floodplain, channel, and right floodplain rather than a single composite section. The conveyance factor is defined as below;

$$K_l = \frac{\mu}{n_l} A_l R_l^{2/3} \quad (3.4)$$

$$K_r = \frac{\mu}{n_r} A_r R_r^{2/3} \quad (3.5)$$

$$K_c = \frac{\mu}{n_c} \frac{A_c R_c^{2/3}}{s_m^{1/2}} \quad (3.6)$$

$$K = K_l + K_c + K_r \quad (3.7)$$

in which the subscripts l , c , and r designate left floodplain, channel, and right floodplain, respectively. The sinuosity factors (s_{co} and s_m), the momentum coefficient for velocity distribution (β), the expansion-contraction slope (S_e), additional friction slope associated with non-Newtonian flows (S_i), wind effect (W_f) and the momentum effect of lateral flow (L) are expressed by means of some analytical or empirical relations. For detailed information on these expressions one can look up in the user documentation of *FLDWAV* model.

The active cross-sectional area (A) and inactive (off-channel storage) area (A_0) are obtained from hydrographic surveys or topography maps. They are user-specified in *FLDWAV* as a table of topwidth (B) versus elevation (h) at selected cross sections along the routing valley. The number of topwidth vs. elevation values has to be the same for all selected cross sections. Within the model, the topwidth table is integrated using the trapezoidal rule to obtain a table of cross-sectional area versus elevation. Linear interpolation is used for intermediate elevations and areas associated with elevations exceeding the maximum values in the specified table are linearly extrapolated.

The Manning coefficient (n) is user-specified for each reach between adjacent cross sections and varies with elevation (h) or discharge according to user specified tabular values similar to the topwidths table. Linear interpolation is used for n values associated with intermediate elevations. Values of n for elevations exceeding the tabular values are not extrapolated, but they are assigned the n values associated with the maximum elevation of the user-specified table.

3.3.3 SOLUTION TECHNIQUE FOR SAINT-VENANT EQUATIONS

The expanded Saint-Venant equations, Eqs (3.1-3.2), constitute a system of nonlinear, partial differential equations with two independent variables, x and t , and two dependent variables, h and Q . The remaining terms are either functions of x , t , h , and Q , or they are constants. Eqs. (3.1-3.2) may be solved numerically by performing two basic steps. First, the partial differential equations are represented by a corresponding set of approximate finite-difference algebraic equations. Then, the system of algebraic equations is solved in conformance with prescribed initial and boundary conditions.

In order to solve Eqs. (3.1-3.2), either *explicit* or *implicit* finite-difference techniques can be used. *Explicit* methods are simple in application but they are restricted by mathematical stability considerations to very small computational time steps. These computational time steps can be on the order of a few seconds for most dam-break waves and a few minutes for run-off generated waves. Such small time steps cause the *explicit* methods to be very inefficient in the use of computer time. *Implicit* finite-difference techniques, however, have no restrictions on the size of the time step due to mathematical stability. But this time, convergence considerations may require computational time step sizes to be limited (Fread, 1998).

One of the various implicit schemes that have been developed is the “weighted four-point” scheme. This scheme was first used by Preissmann (1961) and somewhat later by Fread (1974, 1978). It appears to be most advantageous since it can readily be used with unequal distance and time steps and its stability-convergence properties can be conveniently controlled. In the *weighted, four-point implicit finite-difference scheme*, the continuous x-t (space-time) region in which solutions of h and Q are sought, is represented by a rectangular net of discrete points shown in Figure 3.1. The net points are determined by the intersection of lines drawn parallel to the x and t axes. Those parallel to the t axis represent locations of cross sections. They have a spacing of Δx_i , which need not be constant. Those parallel to the x axis represent time lines. They have a spacing of Δt_i , which also need not be constant. Each point in the rectangular network can be identified by a subscript (i) which designates the x position and a superscript (j) which designates the particular time line.

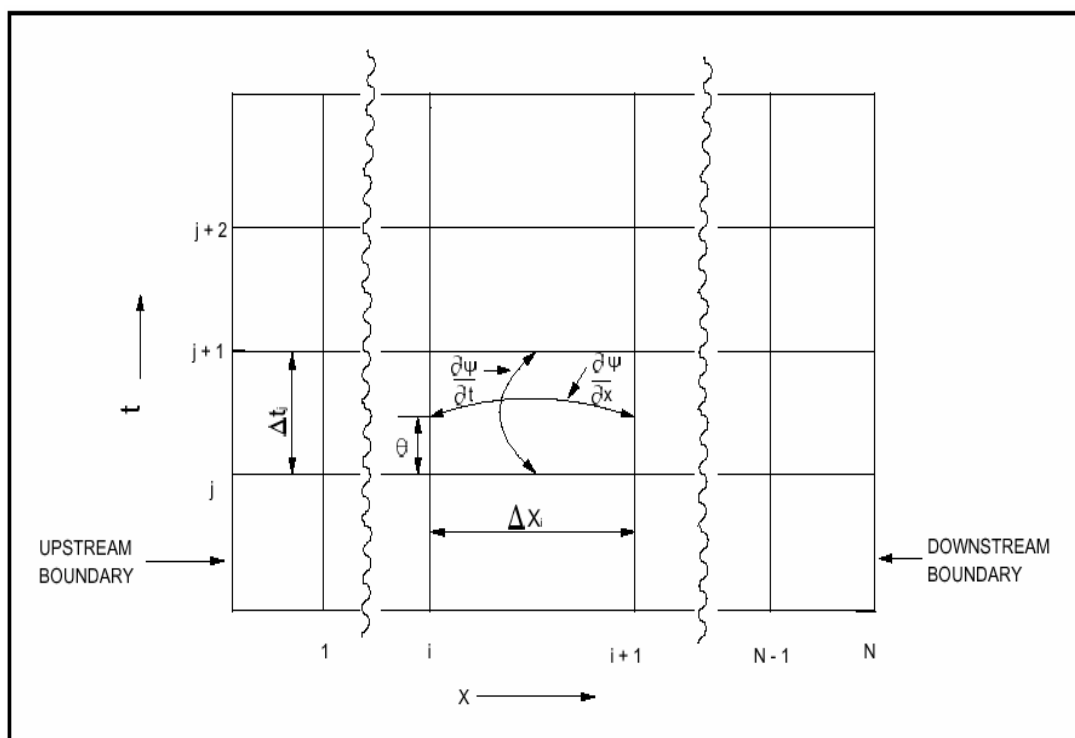


Figure 3.1 Discrete x-t solution domain

The time derivatives are approximated by a forward-difference quotient centered between the i^{th} and $i+1$ points along the x axis, i.e,

$$\frac{\partial \psi}{\partial t} = \frac{\psi_i^{j+1} + \psi_{i+1}^{j+1} - \psi_i^j - \psi_{i+1}^j}{2\Delta t_j} \quad (3.8)$$

Where ψ represents any variable (Q, h, A, A_o , s_{co} , s_m , etc.).

The spatial derivatives are approximated by a forward-difference quotient positioned between two adjacent time lines according to weighting factors θ and $(1 - \theta)$, i.e,

$$\frac{\partial \psi}{\partial x} = \theta \left[\frac{\psi_{i+1}^{j+1} - \psi_i^{j+1}}{\Delta x_i} \right] + (1 - \theta) \left[\frac{\psi_{i+1}^j - \psi_i^j}{\Delta x_i} \right] \quad (3.9)$$

Variables other than derivatives are approximated at the time level where the spatial derivatives are evaluated by using the same weighting factors, i.e,

$$\psi = \theta \left[\frac{\psi_i^{j+1} + \psi_{i+1}^{j+1}}{2} \right] + (1 - \theta) \left[\frac{\psi_i^j + \psi_{i+1}^j}{2} \right] \quad (3.10)$$

A θ weighting factor of 1.0 yields the fully implicit or backward difference scheme used by Baltzer and Lai (1968). A weighting factor of 0.5 yields the box scheme used by Amein and Fang (1970). The influence of the θ weighting factor on the accuracy of the computations was examined by Fread (1974), who concluded that the accuracy tends to decrease as θ departs from 0.5 and approaches to 1.0.

When the finite-difference operators defined by Eqs. (3.8-3.10) are used to replace the derivatives and other variables in Eqs. (3.1-3.2), the following weighted, four-point implicit, finite difference equations are obtained:

$$\theta \left[\frac{Q_{i+1}^{j+1} - Q_i^{j+1}}{\Delta x_i} \right] - \theta q_i^{j+1} + (1 - \theta) \left[\frac{Q_{i+1}^j - Q_i^j}{\Delta x_i} \right] - (1 - \theta) q_i^j + \left[\frac{s_{co_i}^{j+1} (A + A_o)_i^{j+1} + s_{co_i}^{j+1} (A + A_o)_{i+1}^{j+1} - s_{co_i}^j (A + A_o)_i^j - s_{co_i}^j (A + A_o)_{i+1}^j}{2\Delta t_j} \right] = 0 \quad (3.11)$$

$$\left[\frac{(s_{m_i} Q_i)^{j+1} + (s_{m_i} Q_{i+1})^{j+1} - (s_{m_i} Q_i)^j - (s_{m_i} Q_{i+1})^j}{2\Delta t_j} \right] + \theta \left[\frac{(\beta Q^2 / A)_{i+1}^{j+1} - (\beta Q^2 / A)_i^{j+1}}{\Delta x_i} + g\bar{A}^{j+1} \left(\frac{h_{i+1}^{j+1} - h_i^{j+1}}{\Delta x_i} + \bar{S}_f^{j+1} + S_e^{j+1} + \bar{S}_i^{j+1} \right) + L_i^{j+1} + (W_f \bar{B})_i^{j+1} \right] + (1 - \theta) \left[\frac{(\beta Q^2 / A)_{i+1}^j - (\beta Q^2 / A)_i^j}{\Delta x_i} + g\bar{A}^j \left(\frac{h_{i+1}^j - h_i^j}{\Delta x_i} + \bar{S}_f^j + S_e^j + \bar{S}_i^j \right) + L_i^j + (W_f \bar{B})_i^j \right] = 0 \quad (3.12)$$

Where:

$$\bar{A} = \frac{A_i + A_{i+1}}{2} \quad (3.13)$$

$$\bar{S}_f = \left[\frac{n_i^2 \bar{Q} |\bar{Q}|}{\mu^2 \bar{A}^2 \bar{R}^{4/3}} \right] = \frac{\bar{Q} |\bar{Q}|}{\bar{K}^2} \quad (3.14)$$

$$\bar{Q} = \frac{Q_i + Q_{i+1}}{2} \quad (3.15)$$

$$\bar{R} = \frac{\bar{A}}{\bar{B}} \quad \text{Or} \quad \bar{R} = \frac{\bar{A}}{\bar{P}} \quad (3.16)$$

$$\bar{B} = \frac{B_i + B_{i+1}}{2} \quad (3.17)$$

$$\bar{K} = \frac{K_i + K_{i+1}}{2} \quad (3.18)$$

$$\bar{P} = \frac{P_i + P_{i+1}}{2} \quad (3.19)$$

where, P_i is the wetted perimeter.

The terms associated with the j^{th} time line are known from either the initial conditions or previous computations. The initial conditions refer to values of h_i^j and Q_i^j at each node along the x axis for the first time line, that is $j=1$.

Eqs. (3.11-3.12) can not be solved in an explicit or direct manner for the unknowns since there are four unknowns $Q_i^{j+1}, h_i^{j+1}, Q_{i+1}^{j+1}, h_{i+1}^{j+1}$ and only two equations. However, if Eqs. (3.11-3.12) are applied to each of the (N-1) rectangular grids shown in Figure 3.1 between the upstream and downstream boundaries, a total of (2N-2) equations with 2N unknowns can be formulated. Herein, N denotes the total number of nodes or cross sections. Then, prescribed boundary conditions for subcritical flows, one at the upstream boundary and one at the downstream boundary, provide the necessary two additional equations for the system to be determinate. This means there are same number of equations and number of unknowns. The resulting system of 2N nonlinear equations with 2N unknowns is solved by a functional iterative procedure, the *Newton-Raphson method* (Amein and Fang, 1970).

3.3.3.1 BOUNDARY CONDITIONS

Unsteady flows usually occur because of the flow conditions at the most upstream location of the routing reach. This is known as the upstream boundary condition. Also, at the most downstream location of the routing reach, another boundary condition also influences the flow behavior within the river reach being simulated. This is known as the downstream boundary condition.

The upstream boundary condition is required to obtain a solution of the Saint-Venant equations. In the *FLDWAV* model, this is user-specified by either means of discharge or water surface elevation hydrograph, i.e,

$$Q_1 = Q(t) \quad (3.20)$$

or,

$$h_1 = h(t) \quad (3.21)$$

in which Q_1 is the flow at section 1, which is the most upstream cross section in Figure 3.2, $Q(t)$ represents a time series of user-specified flow at each time (t) , h_1 is the water-surface elevation or stage at section 1, and $h(t)$ represents a time series of user-specified water surface elevation at each time (t) . The hydrograph values can be specified in both constant and variable time intervals. Intermediate values are interpolated from the table of discharge or water surface elevation versus time. The upstream hydrograph should be user-specified for the total duration of time that the Saint-Venant equations are to be solved.

The downstream boundary shown in Figure 3.2 is located at the downstream extremity of the routing reach of a single river or the main-stem river of dendritic (tree-type) rivers. Depending on the physical characteristics of the downstream section, the *FLDWAV* model allows the user to specify the appropriate one of the following six downstream boundary equations:

1. *Single-value rating:*

$$Q_N^{j+1} = Q(h) \quad (3.22)$$

in which $Q(h)$ represents a user-specified tabular relation of Q and h .

2. *Generated dynamic loop-rating* using the Manning equation with a dynamic energy slope term (S) computed by one of two below options:

$$Q_N^{j+1} = \frac{\mu}{n_N} A_N^{j+1} R_N^{j+1 \frac{2}{3}} S_{N-1}^{\frac{1}{2}} = K_N^{j+1} S_{N-1}^{\frac{1}{2}} \quad (3.23)$$

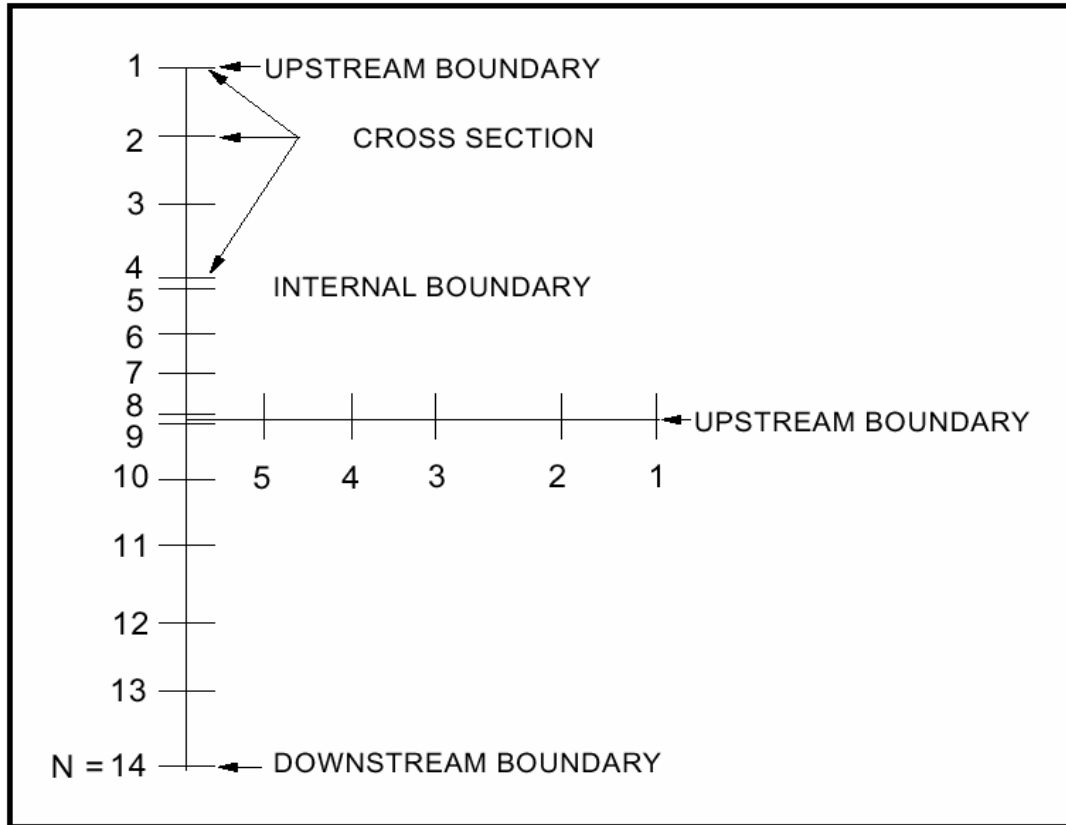


Figure 3.2 Boundary conditions

where:

$$S_{N-1} = \frac{h_{N-1} - h_N}{\Delta x_{N-1}} + \frac{(Q'_N - Q_N)}{0.5g(A_N + A_{N-1})\Delta t} + \frac{(Q_{N-1}^2 / A_{N-1} - Q_N^2 / A_N)}{0.5g(A_N + A_{N-1})\Delta x_{N-1}} \quad (3.24)$$

or,

$$S_{N-1} = \frac{n_N^2 \overline{Q} \overline{Q}}{\mu^2 \overline{A} \overline{R}^{4/3}} \quad (3.25)$$

in which Q'_N is the discharge at time t^{j+1} and all other terms in the equation are at the j^{th} time ($t-\Delta t$), $\mu=1.49$ for English units and 1.0 for SI units, and $\overline{A}, \overline{Q}, \overline{R}$ are reach average values for the N-1 reach according to Eqs. (3.13-3.16).

3. *Generated single-value rating* in which Eq. (3.23) is used, but S is user-specified as the channel bottom slope in the vicinity of the Nth cross section.

4. *Critical flow rating* that occurs at a waterfall or beginning of a short, steep rapids:

$$Q_N^{j+1} = \left[g \frac{(A_N^{j+1})^3}{B_N^{j+1}} \right]^{0.5} \quad (3.26)$$

5. *Water surface elevation time series*:

$$h_N^{j+1} = h(t) \quad (3.27)$$

in which $h(t)$ represents a user-specified time series of water surface elevation at each time (t) at the N^{th} cross section.

6. *Discharge time series*:

$$Q_N^{j+1} = Q(t) \quad (3.28)$$

in which $Q(t)$ represents a user-specified time series of discharge at each time (t) at the N^{th} cross section.

If channel control exist, i.e., the flow at section N is controlled by the channel properties, than either Eq. (3.22) or (3.23) can be selected. Eq. (3.22) is useful if an empirical $Q(h)$ relation is available which is essentially single-valued, in other words, for each water surface elevation there is only one discharge. When a known $Q(h)$ relation does not exist, option (3) can be used; or when the relation is not single-valued, then the dynamic loop-rating, Eq (3.23) may be used. The loop-rating allows two water-surface elevations to exist for each discharge value. On the rising limb of the hydrograph, the water surface elevation is usually less than that which occurs for the same discharge on the recession limb (Fread, 1998).

The dynamic loop-rating. Eq. (3.23) may be subject to numerical instability when the channel bottom slope S_0 is less than about one ft/mi. In this situation, the S term as computed by Eq. (3.24) may be user-specified to be computed by Eq. (3.25) which yields more stable results than those using Eq. (3.24). If the solution remains unstable, the downstream boundary can

be relocated a sufficient distance further downstream of the original downstream boundary location and Eq. (3.23) with $S=S_0$ can be user-specified. A channel control boundary, Eq. (3.22) or (3.23) should not be located where changes in flow further downstream can effect the flow at the chosen boundary location, e.g., just upstream of where a significant tributary flow enters, or within the backwater effect of a bridge, dam, or tidal fluctuation. A single-value rating, Eq (3.22), may also be used when the downstream boundary is a dam where the total flow through the dam is controlled by the water surface elevation occurring immediately upstream of the dam and not by the water elevation downstream of the dam due to tailwater submergence conditions affecting spillway or gated outflows (Fread, 1997).

3.3.3.2 INTERNAL BOUNDARIES

There can be structures such as dams, bridges or short rapids along a waterway where the Saint-Venant equations are not applicable. At these internal locations, the flow is rapidly varied (spatially) rather than gradually varied. And a flow has to be gradually varied in order to apply Saint-Venant equations. Empirical water surface elevation versus discharge relations such as that for weir flow can be utilized for simulating rapidly varied flow. In *FLDWAV*, unsteady flows are routed along the waterway including locations of rapidly varied flow by utilizing internal boundaries. At internal boundaries, cross sections are user-specified for the upstream and downstream extremities of the short reach where rapidly varied flow takes place. Since, as with any other Δx reach, two equations (the Saint-Venant equations) are required, the internal boundary Δx reach also requires two equations. The first of the required equations represents the conservation of mass with negligible time dependent storage and lateral flow, and the second is an empirical, spatially-rapidly-varied flow equation representing weir, orifice, critical flow, etc. The internal boundary equations are:

$$Q_i = Q_{i+1} \quad (3.29)$$

$$Q_i = Q_s + Q_b \quad (3.30)$$

in which Q_s and Q_b are the spillway and breach flow, respectively. The flows Q_i and Q_{i+1} and the elevations h_i and h_{i+1} are in balance with the other flows and elevations occurring simultaneously throughout the entire flow system which may consist of additional dams or bridges. *FLDWAV* can simulate the progression of a dam-break flood or any type of unsteady flow through an unlimited number of dams or bridges sequentially located in any combination.

A **dam** can have several components that pass discharge, including spillways, gates, and turbines (Fread, 1988). A typical dam that can be modeled within *FLDWAV* is shown in Figure 3.3. Flow may pass through the structure via any of these components as well as over the top of the dam. In the event of failure, flow may also pass through the breach which is formed during the failure process. A dam may be considered an internal boundary defined by a short Δx_i reach between sections i and $i+1$ in which the flow is governed by Eqs. (3.28-3.29). In Eq. (3.28), the spillway flow Q_s is computed from the following expression:

$$Q_s = Q_{spillway} + Q_{gate} + Q_{dam} + Q_t \quad (3.31)$$

where, $Q_{spillway}$, Q_{gate} , Q_{dam} , and Q_t represent flow through the respective components (Fread, 1998).

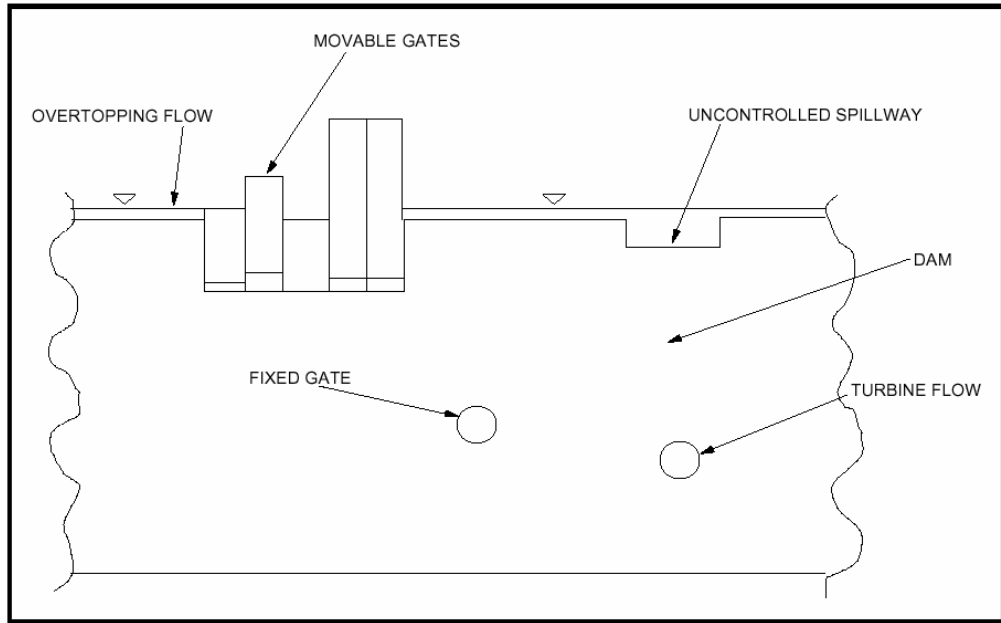


Figure 3.3 Front view of a dam with discharge components

Uncontrolled spillway flow which passes through the dam can be modeled as weir flow (e.g. emergency spillway or main spillway). The flow can be represented by either an empirical head-discharge rating curve similar to Eq. (3.22) which is user-specified, or automatically generated using the following:

$$Q_{spillway} = k_{sp} c_{sp} L_{sp} (h - h_{sp})^{1.5} \quad (3.32)$$

in which c_{sp} is the user-specified uncontrolled spillway discharge coefficient, $(h - h_{sp})$ is the computed head, h_{sp} is the user-specified uncontrolled spillway crest elevation, L_{sp} is the user-specified spillway length, and k_{sp} is an automatically computed submergence correction factor for tailwater effects, i.e.,

$$k_{sp} = 1 - 27.8 \left(\frac{h_{tw} - h_{sp}}{h - h_{sp}} - 0.67 \right)^3 \quad (3.33)$$

where, h_{tw} and h are the tailwater and reservoir pool elevations, respectively.

Several **gates** may exist in a dam. When the gates are fixed, the flow through a fixed-gated spillway is computed using the following:

$$Q_{gate} = \sqrt{2g} c_g A_g (h - h_g)^{0.5} \quad (3.34)$$

where, A_g is the user specified gate flow area (fixed in time), c_g is the user specified fixed-gated spillway discharge coefficient, $(h-h_g)$ is the computed head, and h_g is the user specified centerline elevation of the gated spillway or it is the automatically computed tailwater elevation if the latter is greater. If several gate openings share a common gate sill, they can be combined into one gate and user specified as an averaged fixed-gate opening. The fixed-gated spillway flow can also be represented as a table of head versus discharge values (Fread, 1998).

Turbine flow (Q_t) usually represents a constant flow which is head independent; however, it may also be variable with time. Since *FLDWAV* requires the initial condition to have a nonzero minimum flow, the Q_t parameter may also be used to pass a minimum flow through the dam when the initial pool elevation is below any spillway crests or gate sill elevations such that spillway and/or gate flows are zero (Fread, 1998).

3.3.3.3 INITIAL CONDITIONS

In order to solve the Saint-Venant unsteady flow equations, the state of the flow (h_i and Q_i) must be known at all cross sections ($i=1, 2, 3, \dots, N$) at the beginning of the simulation. This is known as the *initial conditions* of the flow. The initial conditions may be either a steady or unsteady flow condition. In the steady state condition, the *FLDWAV* model assumes the flow to be

steady, nonuniform flow with the flow at each cross section initially computed as:

$$Q_i = Q_{i-1} + q_{i-1} \Delta x_{i-1} \quad (3.35)$$

where, Q_i is the known steady discharge at $t=0$ at the upstream boundary, and q_i is any user specified lateral inflow at $t=0$ from tributaries existing between the user specified cross sections placed at intervals of Δx along the valley. Tributaries may be dynamic rivers which will be modeled using the unsteady flow equations, or local lateral inflows which must be user specified as one or more time series. If the local lateral inflows are relatively small compared to the expected maximum flood, they may be omitted in the simulation. Discharges at $t=0$ are usually assumed to be nonzero. In other words, an initially dry downstream channel is not usually simulated in *FLDWAV*. Because, when modeling regular water low flows, it is important to maintain a sufficient base flow to prevent numerical instability when solving the Saint-Venant finite difference Eqs. (3.11-3.12).

The water surface elevations (h_i) associated with the steady flow must be determined at $t=0$. The user may specify known h_i values at various locations along the routing reach. Usually, the reservoir pool elevation behind a dam is specified. The remaining elevations will be generated by *FLDWAV*. If the flow is subcritical, this is accomplished by using the iterative Newton-Raphson method to solve the flowing backwater equation for h_i (Fread and Harbaugh, 1971).

$$\left(\frac{Q^2}{A} \right)_{i+1} - \left(\frac{Q^2}{A} \right)_i + g \bar{A}_i (h_{i+1} - h_i + \Delta x_i \bar{S}_f) = 0 \quad (3.36)$$

in which \bar{A} , \bar{S}_f , and \bar{S}_i are defined by Eqs. (3.13), and (3.14), respectively. Eq. (3.35) is a simplified form of the momentum Eq. (3.2) where the first term

is taken as zero for steady flow; and L and W_f are assumed to be zero. The computations proceed in the upstream direction ($i=N, N-1, \dots, 3, 2, 1$). The starting water surface elevation (h_N) may be user specified, or obtained from the user specified downstream boundary condition for either a discharge of Q_N , Eq. (3.23) or Eq. (3.26), or the elevation h_N at $t=0$, Eq. (3.27).

3.4 MODELING DAM BREACH

The breach is the opening formed in the dam as it fails. The actual failure mechanics are understood only partially for earthen dams and less for concrete dams. Prior to about 1970, efforts to predict downstream flooding due to dam failures usually assumed that the dam failed completely and instantaneously, e.g., Ritter (1892), Schocklitsch (1917), Ré (1946), Dressler (1954), Stoker (1957), Su and Barnes (1969), and Sakkas and Strelkoff (1973). Others, such as the Army Corps of engineers (1960) recognized the need to assume a partial rather than complete breach; however, it was still assumed the breach occurred instantaneously. The assumptions of instantaneous and complete breaches were used for reasons of convenience when applying certain mathematical techniques for analyzing dam-breach flood waves. The assumptions are somewhat appropriate for concrete arch dams, but are not appropriate for earthen dams and concrete gravity dams. For these dams, as well concrete arch dams, the breach should be considered to develop over a finite interval of time (τ) and to encompass only a portion of the dam except for concrete arch dams (Fread, 1977).

Partial dam breaches with $\tau > 0$ result in considerably smaller dam-breach floods than instantaneous ($\tau = 0$) and complete breaches. It is readily apparent that a smaller breach will allow less peak outflow than a larger breach; however, it is not quite as apparent that a larger failure time results in less peak outflow. As the dam breach forms, the outflow through the

breach reduces the reservoir storage contained by the dam, resulting in a reduction of the reservoir water level. The rate of flow through the breach is proportional to the height (head) of the water above the breach bottom. Therefore, as the breach forms, the water level reduces; and when the breach is fully formed, the resulting head of water is less than that if the breach formed instantaneously or even at a faster rate. The smaller head of water available to produce flow through the breach when it completely forms (both in the vertical and horizontal directions) results in a smaller peak outflow and a smaller dam-breach flood. The extent of flood peak reduction due to a larger failure time is directly proportional to the magnitude of the final breach width and inversely proportional to the magnitude of the reservoir storage volume (Fread, 1997).

3.4.1 BREACH OUTFLOW

The breach outflow (Q_b) is computed as broad-crested weir flow (Fread, 1988), i.e.,

$$Q_b = c_v k_s \left[3.1 b_i (h - h_b)^{1.5} + 2.45 z (h - h_b)^{2.5} \right] \quad (3.37)$$

in which c_v is a small computed correction for velocity of approach, b_i is the computed instantaneous breach bottom width, h is the computed elevation of the water surface just upstream of the structure, h_b is the computed elevation of the breach bottom which is assumed to be a function of the breach formation time (τ), z is the user specified side slope of the breach, and k_s is the computed submergence correction due to downstream tailwater elevation (h_t), i.e.,

$$k_s = 1.0 - 27.8 \left[\frac{h_t - h_b}{h - h_b} - 0.67 \right]^3 \quad \text{if } (h_t - h_b)/(h - h_b) > 0.67 \quad (3.38)$$

otherwise, $k_s = 1.0$.

The velocity of approach correction factor (c_v) is computed from the following (Brater, 1959):

$$c_v = 1.0 + 0.023 \frac{Q_b^2}{[B_d^2 (h - h_{bm})^2 (h - h_b)]} \quad (3.39)$$

in which B_d is the reservoir width at the dam and h_{bm} is the user-specified final elevation of the breach bottom. If the breach is formed by piping, z is assumed zero (rectangular shape) and Eq. (3.37) is replaced by an orifice equation, i.e.,

$$Q_b = 4.8A_p (h - \bar{h})^{1/2} \quad (3.40)$$

where:

$$A_p = 2b_i (h_p - h_b) \quad (3.41)$$

in which h_p is the user-specified centerline elevation of the pipe, and $\bar{h} = h_p$ or $\bar{h} = h_{tw}$ if $h_{tw} > h_p$ in which h_{tw} is the tailwater surface elevation just downstream of the dam. The breach flow automatically ceases to be orifice flow and becomes broad-crested weir flow when the reservoir elevation (h) lowers sufficiently or pipe enlarges sufficiently that (Fread, 1998):

$$h < 3h_p - 2h_b \quad (3.42)$$

3.4.2 BREACH PARAMETERS

The failure of an embankment dam can be analyzed in two steps. First, the breach formed in the dam body has to be modeled and then the outflow from this breach has to be routed through the downstream valley in order to determine the resulting flooding conditions at downstream regions. When population centers are located very close to the dam axis, it is crucial to predict breach parameters accurately to allow for development of effective emergency action plans, design of early warning systems, and characterization of threats to lives and property. If the population at risk is located well downstream from the dam, selection of breach parameters has little effect on the results (Wahl, 1998).

The actual failure mechanics are not well understood for either earthen dams or concrete dams. Therefore, breach simulation and breach parameter prediction contain the greatest uncertainty of all aspects of dam-break flood forecasting (Wurbs, 1987). Most of the breach parameter prediction methods rely on data from historical dam failures or numerical models that do not simulate the exact erosion mechanisms. Case study data provide only limited information, based on a relatively small database of dam failures, primarily of small dams. Case study data are especially weak for making predictions of the time needed to initiate a breach, the rate of breach formation, and the total time required for failure (Wahl, 1998). These parameters are the most vital ones that influence the dam-break analyses results significantly; therefore, it is very important to predict them accurately.

The routing tasks through the breach and through the downstream valley are handled in most of the widely used numerical models with various one-dimensional routing methods. However, many of them do not simulate the breach directly. The user has to predict the breach characteristics and provide this information as input to the computer model.

Breach characteristics include the parameters required to describe the breach physically. Physical parameters are the breach depth, breach width and side slope of the breach. These parameters are quite enough to determine the size and shape of the breach. Temporal parameters define the time required for breach initiation and formation. The physical parameters are shown graphically in Figure 3.4.

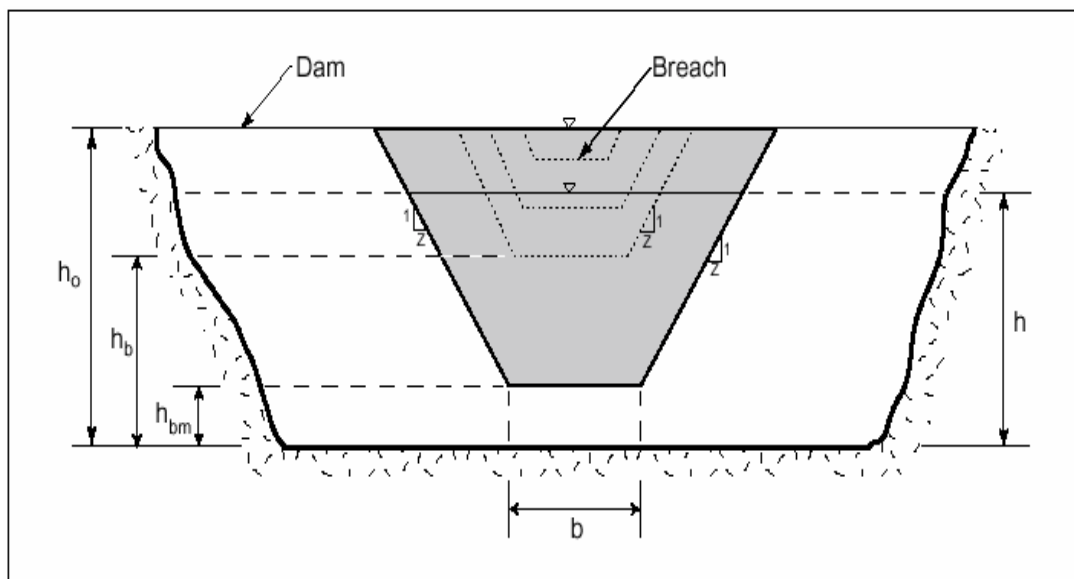


Figure 3.4 Physical parameters of an ideal overtopping breach

3.4.2.1 OVERTOPPING FAILURES

An overtopping failure breach can be simulated as a rectangular, triangular, or trapezoidal shape that grows progressively downward from the dam crest with time. Then, the flow through the breach is calculated using a broad-crested weir equation at any instant.

The final breach shape is specified by a parameter z identifying the side slope of the breach, i.e, 1 vertical : z horizontal, parameter h_{bm} which is the

final breach bottom elevation and parameter b which is the final bottom width of the breach. The values of z may range from 0 to 2. Its value depends on the angle of repose and compaction degree of the dam embankment materials through which the breach develops. By specifying various combinations of b and z , rectangular, triangular, or trapezoidal breach shapes can be formed. For example, $z=0$ and $b>0$ produces a rectangular shaped breach, $z>0$ and $b=0$ produces a triangular shaped breach and finally $z>0$ and $b>0$ leads to a trapezoidal breach.

As shown in Figure 3.4, the breach bottom width starts at a point on the dam crest and enlarges at a linear or quadratic rate over the failure time τ until the final width b is reached and the breach bottom elevation has eroded to the elevation h_{bm} , which is usually, but not necessarily, the invert elevation of the dam cross-section. The instantaneous breach bottom elevation may be expressed by the below relation;

$$h_b = h_0 - (h_0 - h_{bm}) \left(\frac{t_b}{\tau} \right)^\rho \quad \text{if } 0 < t_b < \tau \quad (3.43)$$

in which:

h_{bm} = final elevation of the breach bottom

t_b = elapsed time since the beginning of breach formation

ρ = breach formation rate exponent

h_0 = height of the dam

Parameter ρ specifies the formation rate of a breach and it may range from 1 to 4, with $\rho=1$ corresponding to a linear breach formation rate and $\rho>1$ corresponding to a nonlinear quadratic formation rate.

Furthermore, the instantaneous breach bottom width b_i may be expressed by the following relation;

$$b_i = b \left(\frac{t_b}{\tau} \right)^\rho \quad \text{if } 0 < t_b < \tau \quad (3.44)$$

The final breach bottom width and the rate of breach formation can dramatically affect the peak flow and peak water surface elevations downstream from the dam. Some case studies report either the average breach width or the breach width at the dam crest instead of breach bottom width. Accurate prediction of breach side slope is generally of secondary importance to predicting the breach width and bottom elevation (Wahl, 1998).

The temporal parameters of breach formation are the *breach initiation time* and *breach formation time*. The latter is most often referred to as *failure time*. The time of failure as used in *FLDWAV* is the time elapsed between the first breaching of the upstream face of the dam until the breach is fully formed. For overtopping failures, the beginning of breach formation is just after the downstream face of the dam has eroded away and the resulting crevasse has progressed back across the width of the dam crest to reach the upstream dam face (Fread, 1998). The breach initiation time begins with the first flow over the dam that initiates warning and evacuation of downstream population. It ends at the start of the breach formation phase. In the breach initiation phase, the dam does not fail, and there is small amount of flow overtopping the dam crest. The failure of the dam may be prevented by stopping the overtopping flow during the breach initiation phase. On the other hand, during the breach formation phase, outflow from the dam increases rapidly and the failure of the dam is inevitable. It is very important to recognize and account for these two phases since the breach initiation time directly affects the time available required for warning and evacuation of downstream populations. Unfortunately, it is a very difficult task to distinguish between two phases during a failure and presently there is a little guidance available from the case studies for the prediction of breach initiation times (Wahl, 1998).

3.4.2.2 PIPING FAILURES

A piping failure occurs when breach formation takes place at some point below the top of the dam due to seepage or erosion of an internal conduit through the dam body by the escaping water (See Figure 3.6). In the literature, the piping is also referred to as “Sunny day piping” which implies that there is no need for any heavy precipitation runoff to result in piping failure of a dam. The dam may also fail even there is no inflow to the reservoir in a sunny day. Failure times for piping failures are considerably longer than those for overtopping failures. The reason for this is the fact that upstream face of the dam embankment is slowly eroded in the very early phase of the piping development. As the erosion proceeds, a larger and larger opening is formed and eventually caving-in of the top portion of the dam occurs (Fread, 1998).

A piping failure is simulated as a rectangular orifice breach that grows with time and is centered at any specified elevation within the dam (See Figure 3.5). Instantaneous flow through the breach is calculated with either orifice (Eqs. 3.40-3.41) or weir equations (Eqs. 3.37-3.39) depending on the relation between water surface elevation in the reservoir and the top of the orifice. Within the *FLDWAV*, it is possible to simulate a piping failure by specifying an initial piping centerline elevation h_p and setting side slope parameter z to 0 since *FLDWAV* simulates piping as a rectangular orifice breach. While generally a linear breach formation rate is assumed for overtopping failures, values of $\rho \geq 2$ are appropriate for simulating piping failures.

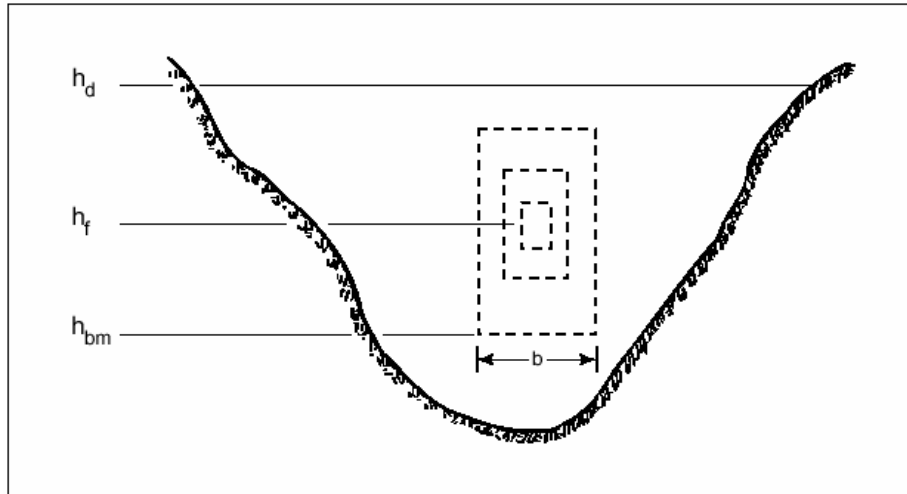


Figure 3.5 Formation of piping breach



Figure 3.6 Medford Quarry wash pond piping failure

3.4.2.3 CONCRETE DAMS

Concrete gravity dams tend to have a partial breach as one or more monolith sections formed during the construction of the dam are forced apart

by the escaping water. The time for breach formation is in the range of a few minutes. It is a hard task to estimate the actual breach width since it is difficult to predict the number of monoliths that may fail or displace during overtopping.

Concrete arch dams tend to fail completely and failure times are in the range of only a few minutes. Side slope parameter z with a value of zero can be used in order to simulate a rectangular breach for concrete gravity and arch dams.

3.4.2.4 EARTHEN DAMS

Majority of the dams that have been constructed are earthen dams. Failure of earthen dams is neither completely, nor simultaneously. The breach requires a finite interval of time τ for its formation through erosion of the dam materials by the escaping water. The failure time may be in the range of a few minutes to a few hours (usually less than 1) depending on the height of the dam, type of the materials used in construction, the extent of compaction of the materials, and the magnitude and duration of the escaping flow (Fread, 1998). Embankment dam breaches are typically assumed to be approximately trapezoidal in shape (See Figure 3.7). This kind of breach geometry can be described physically in terms of breach height, average breach width, and breach side slope which are also referred to as ultimate breach parameters. These parameters are typically estimated using case study based predictive equations that relate breach parameters to characteristics of dam and reservoir, such as dam height and storage volume. Such relations have high uncertainty due to scatter in the available case study data and are based on a database of dam failure case studies that includes only a few examples of large dams or large reservoirs (Wahl, 1997).

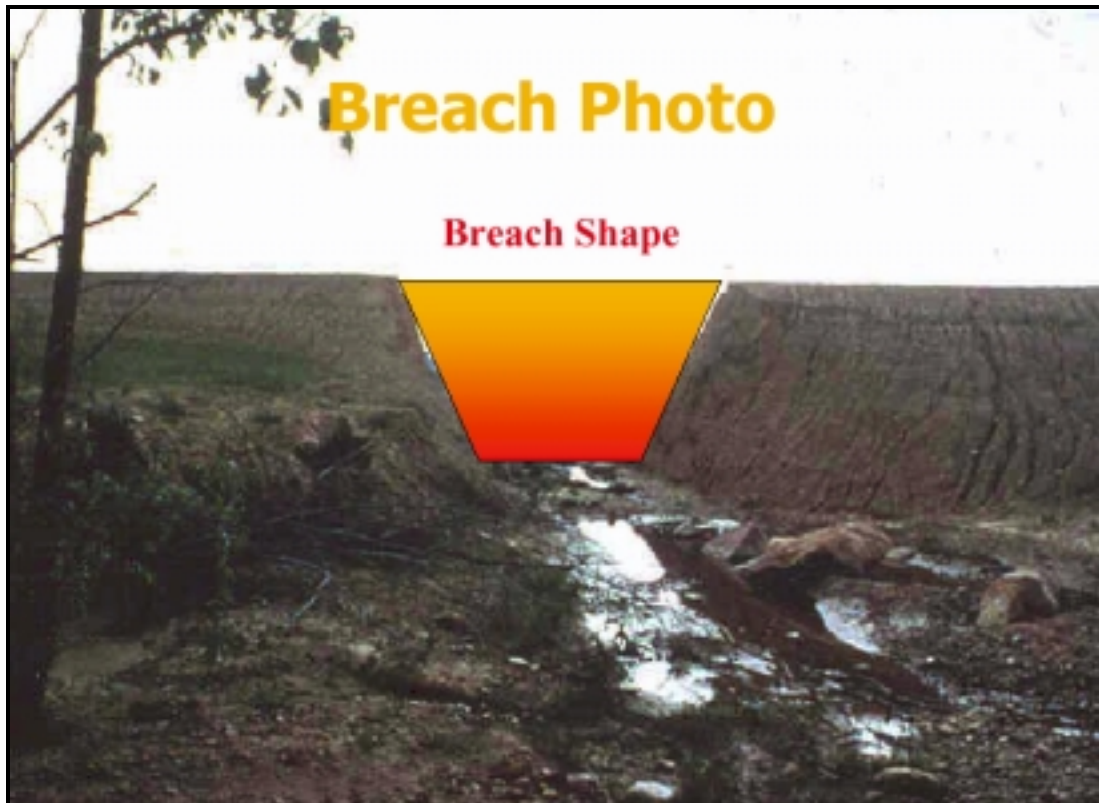


Figure 3.7 Trapezoidal breach formation of an embankment dam

To carry out a dam break flood routing simulation, breach parameters must be predicted and provided to the numerical flood routing model as input. There are many methods for predicting the breach parameters. Comparative analysis of similar case studies, and the use of predictor equations based on numerous case studies are the most convenient approaches. Another approach is the use of hydraulic and sediment transport principles for the physical simulation of dam breaching. The available predictor equations differ widely depending on the investigator and the type of dam failure. The simplest ones predict the average breach width as a function of dam height. The fully formed breach in embankment dams tend to have an average breach width \bar{b} in the range $h_d < \bar{b} < 3h_d$ where h_d is the height of the dam. All of these methods are based on regression analysis of data collected from

actual dam failures. Large dam failure incidents are not involved in the database which is used to develop these predictor equations. 75 percent of dams have heights less than 15 meters in the database (Wahl, 1998). Froelich (1995) developed prediction equations for average breach width and failure time depending on characteristics of dam:

$$\bar{b} = 0.1803K_0V_w^{0.32}h_b^{0.19} \quad (3.45)$$

$$t_f = 0.00254(V_w)^{0.53}h_b^{-0.9} \quad (3.46)$$

in which:

K_0 = 1.4 for overtopping, 1.0 for piping

V_w = volume of water stored in the reservoir

h_b = height of breach (usually assumed to be equal to the dam height)

CHAPTER 4

A CASE STUDY: KIRAZLIKÖPRÜ DAM

4.1 INTRODUCTION TO STUDY AREA

Situated in the western part of Black Sea Region, Bartın is a city that suffers from floods frequently. Due to its climate, this part of Turkey is the rainiest region and the mean annual precipitation is very high compared to other regions. The city is settled between two main tributaries of Bartın River, which are Kozcağız and Bartın Creeks. Bartın River has also two secondary tributaries called Gökırmak and Arit Creeks.

Bartın Creek starts from Ovacuma at an approximate elevation of 1000m. It has the initial name Ova Creek while flowing in the westward direction till the confluence with Ulus Creek. Thereafter, it is called Gökırmak and flows in north-west direction to get connected with another tributary of Bartın Creek, called Arit Creek. In the meantime, Kozcağız Creek, which is the main tributary of Bartın River, flows in North-East direction through the Bartın city center and it connects with the Bartın Creek (Gökırmak and Arit tributaries) on the North-West of the city. From that point to Black Sea, the connection of the three tributaries is named as Bartın River and it travels around 12 km to the Black Sea entrance. Bartın River has a watershed of 2100 km² at the Black Sea entrance and the mean annual precipitation in the watershed is 1033.5 mm. The plan view of modeling domain can be seen in Figure 4.1.

The city has encountered major floods within the last 30 years. Three most severe floods occurred in 1975, 1982 and 1991. Especially, the last one was a catastrophic flood and it has caused loss of lives and damage to property.

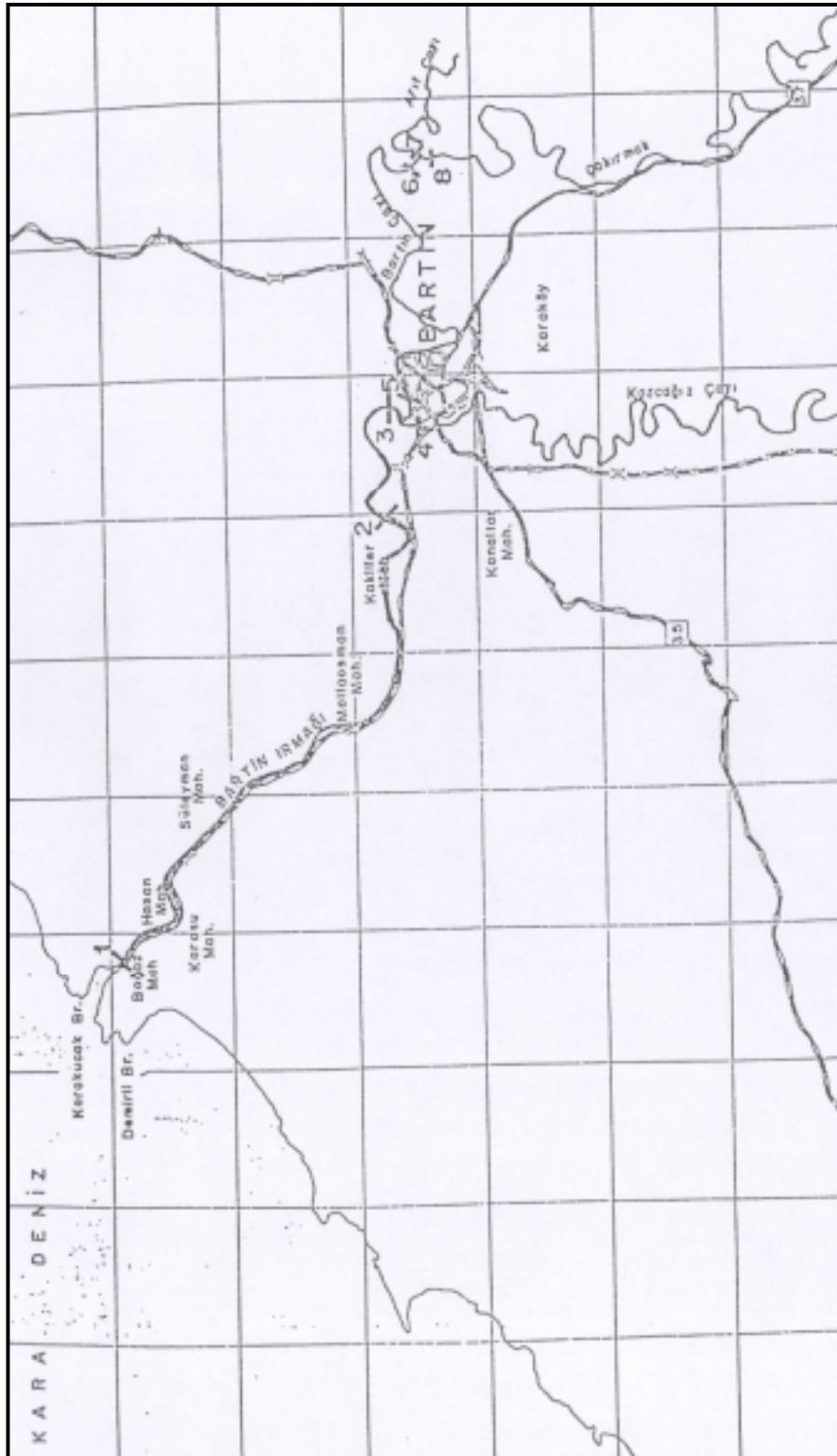


Figure 4.1 Plan view of modeling domain

4.2 ABOUT THE KIRAZLIKÖPRÜ DAM

Kirazlıköprü Dam is located in the South-East of the Bartın city and it is about 20 km far from the city center. It is being constructed on the Gökırmak Creek at an invert elevation of 52 m from the mean sea level. Gökırmak Creek is one of the two main tributaries of Bartın Creek and flows to north-west in the south-east of Bartın city. It is the major stream flowing just upstream of Bartın.

The construction of Kirazlıköprü Dam started in 1998 and the construction is still going on at the moment. The major purpose of Kirazlıköprü Dam shall be flood control of Bartın city center. The dam will also supply water for the irrigation of downstream agricultural areas in the Gökırmak valley. Hydroelectric power production is the last purpose of the dam. It is also hoped that the construction of Kirazlıköprü Dam will prevent excessive sediment deposition in the reach of Bartın River between Bartın city center and Bartın Port.

Due to the frequent flooding in the Bartın River and its tributaries, considerable amount of loss to human lives and property may occur. In order to prevent this kind of disasters, Kirazlıköprü Dam is thought to be the key structure (Claimed in the “Master Plan Report” of Kirazlıköprü Dam).

Some of the physical and hydrological characteristics of the Kirazlıköprü Dam and its reservoir can be found in Table 4.1.

Table 4.1 Physical and hydrological characteristics of Kirazlıköprü Dam

HYDROLOGY:	
Constructed on	Gökırmak (Kocanaz) Creek
Catchment area	890 km ²
Annual mean inflow	513.73 hm ³
Average yield	5.61 hm ³

Table 4.1 Continued

DAM BODY:	
Purpose	Flood control+Irrigation+Hydropower
Dam type	Rockfill with clay corewall
Thalweg elevation	52 m
Crest elevation	105.25 m
Height above foundation level	69 m
Height above thalweg level	53.25 m
Crest length	240 m
Crest width	10 m
Upstream embankment slope	2.5 vertical : 1.0 horizontal
Downstream embankment slope	2.0 vertical : 1.0 horizontal
Total embankment volume	2,200,000 m ³
DAM RESERVOIR:	
Minimum water surface level	75 m
Normal water surface level	102.9 m
Maximum water surface level	102.9 m
Reservoir volume at min. water level	8 hm ³
Reservoir volume at normal water level	66.1 hm ³
Reservoir volume at max. water level	66.1 hm ³
Active storage	58.1 hm ³
Reservoir surface area at min. water level	0.85 km ²
Reservoir surface area at normal water level	10.9 km ²
Reservoir surface area at max. water level	10.9 km ²
SPILLWAY:	
Type	Radial gated
Design flood peak	3935 m ³ /s
Number of gates	4
Gate dimensions	10x14 m
Crest length	47.5 m
Crest elevation	89.25 m
DIVERSION TUNNEL	
Number of diversion tunnels	2
Tunnel lengths	L1=545 m, L2=604 m
Tunnel diameter	6 m
Tunnel discharge (Q ₂₅)	545 m ³ /s
BOTTOM OUTLET	
Discharge at min. water level	29.75 m ³ /s
Discharge at normal water level	37.5 m ³ /s
TURBINES	
Energy tunnel discharge	31.5 m ³ /s
Annual hydropower production	41.2 GWh

4.3 MODELING ROUTING REACH

In the Kirazlıköprü dam break analyses, a routing reach of around 20.4 km length is modeled. The routing reach starts at the Kirazlıköprü Dam axis, which is situated in the Kirazlık region, and runs till the very proximity of the confluence between Gökırmak and Arit tributaries. The river runs through the Gökırmak Plain and the valley is wide most of the time. There are many agricultural areas in the valley.

When modeling a river reach using a flood routing tool, primarily the external boundary conditions must be established. External boundary conditions consist of upstream and downstream boundary conditions. In the present study, catastrophic inflow hydrograph of Kirazlıköprü Dam, which is shown in Figure 4.2, is used as the upstream boundary condition. For the downstream extremity of the routing reach, a looped rating curve generated based on Manning's equation, where the friction slope is computed based on the momentum equation, is applied (Eqs. 3.23-3.24). The most downstream cross section in the reach is far enough from the confluence of Arit and Gökırmak Creeks, such that flow conditions are not affected by tributary inflow.

Unsteady flow routing in the reservoir can be approximated by a simple technique called level-pool routing. This simple method is sometimes called reservoir storage routing, which is acceptable for routing in reservoirs which are not excessively long and in which the inflow hydrograph is not rapidly changing with time (Fread, 1992). This method is especially preferred when cross section data of the reservoir is not available for use in dynamic routing. The simple level-pool routing technique is based on the principle of conservation of mass, i.e.,

$$Q_i(t) - Q_{i+1}(t) = \frac{dS}{dt} \quad (4.1)$$

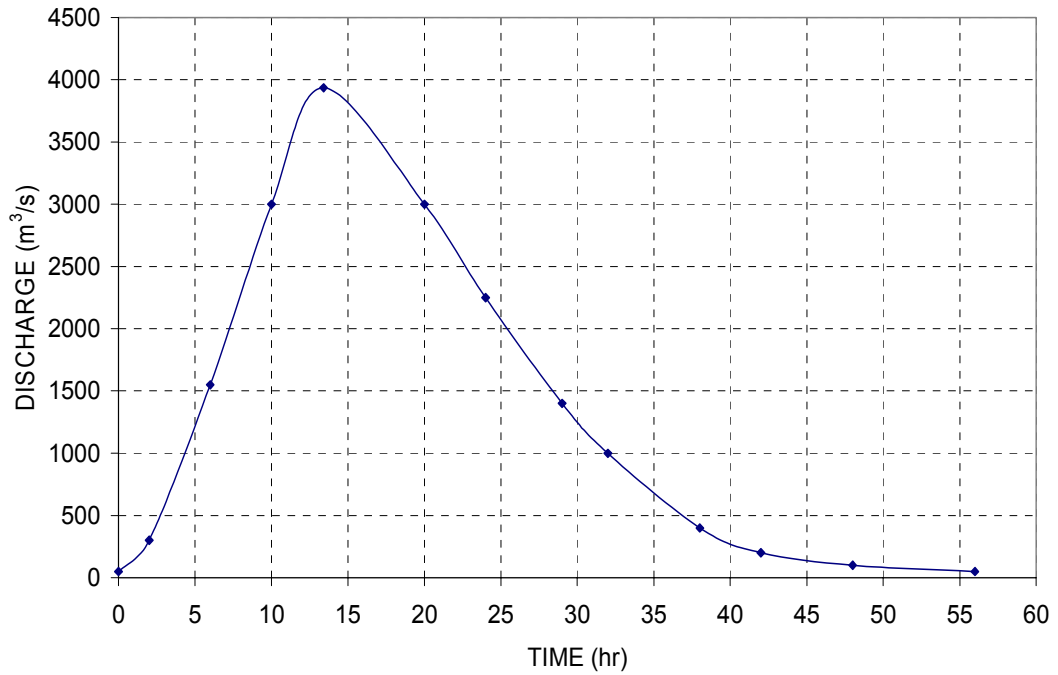


Figure 4.2 Catastrophic inflow hydrograph of Kirazlıköprü Dam

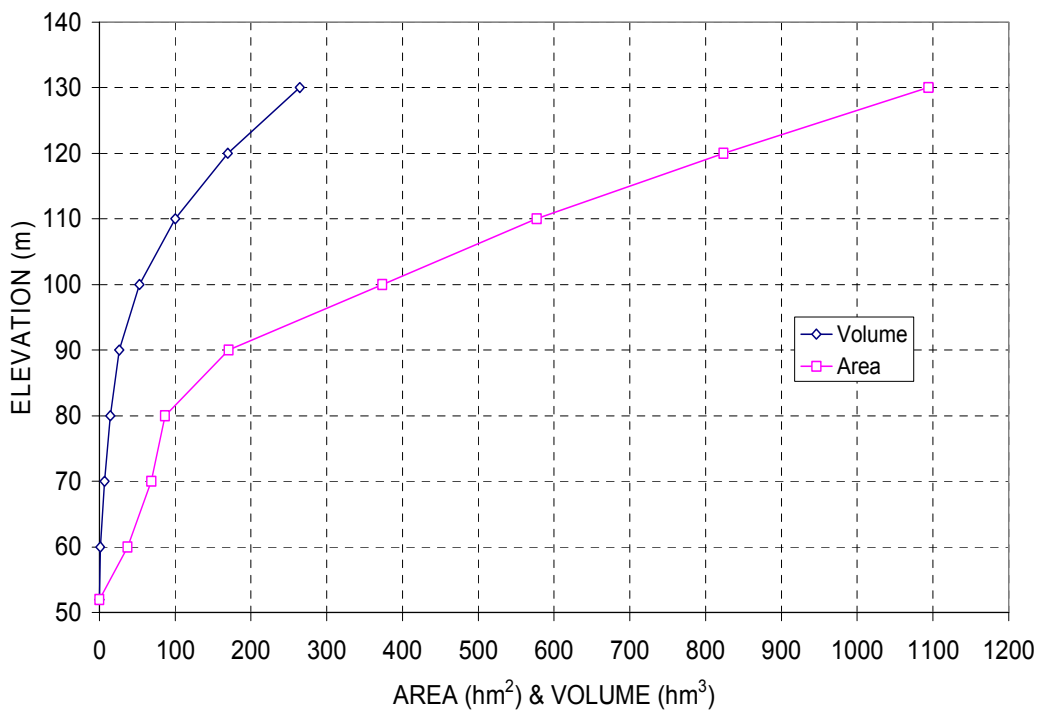


Figure 4.3 Elevation-Area-Volume curve of Kirazlıköprü Dam reservoir

in which, inflow (Q_i) and outflow (Q_{i+1}) are functions of t , and the storage S is a function of the water surface elevation h , which changes with time t . In this method, the reservoir is assumed always to have a horizontal water surface throughout its length. For the storage routing of inflow hydrograph, elevation-area-volume data of the reservoir, as shown in table 4.2, is used.

Table 4.2 Kirazlıköprü Dam reservoir Elevation-Area-Volume data

KIRAZLIKÖPRÜ DAM ELEVATION AREA VOLUME DATA		
Elevation (m)	Area (hm ²)	Volume (hm ³)
52	0	0
60	37.05	1.28375
70	68.65	6.72475
80	86.7	14.387
90	170.6	26.2395
100	373.4	52.9895
110	577.3	100.067
120	823.7	169.352
130	1094.3	264.472

After the routing reach is established by the external boundary locations, cross sections are obtained to represent the reach. Cross section data is measured at any point along the channel/floodplain on the plane perpendicular to the direction of flow. Cross section locations are measured from upstream to downstream starting at the dam axis and continuing downstream. In this study, cross section data were obtained from Directorate of Maps in the State Hydraulic Works (DSİ). Cross section data are obtained from geologic surveys. Fortunately, under the scope of TEFER (Turkey Emergency Flood & Earthquake Recovery) project, there has been a recent study in obtaining the cross sectional data of Gökırmak, Kozcağız, Arıt, and Bartın Creeks. This study makes use of eight available cross sectional data obtained from geological survey in TEFER project. However, two of them are deleted, since they cause numerical problems due to abrupt changes in the size and shape of successive cross sections. In order to improve cross

sectional data and to extend the range of available data, topographic maps with scales of 1/100000 and 1/25000 are used. Therefore, the cross sections used in the present study are a combination of both geological survey data and information extracted from topographic maps. The intention in extending especially the elevation range of cross sections is to account for expected high water surface elevations that would result from dam break flooding.

The cross sections are numbered sequentially from upstream to downstream as shown in Figure 4.4. In this figure, station kilometer (St. Km.) of each cross section can also be found. The plan view of input cross sections on the Gökırmak Creek can be found in appendix A. Having represented the routing reach by cross sections, the initial conditions at each cross section are next established at each location. Finally, the Saint-Venant equations and boundary equations are solved simultaneously to obtain peak flood conditions at selected cross sections.

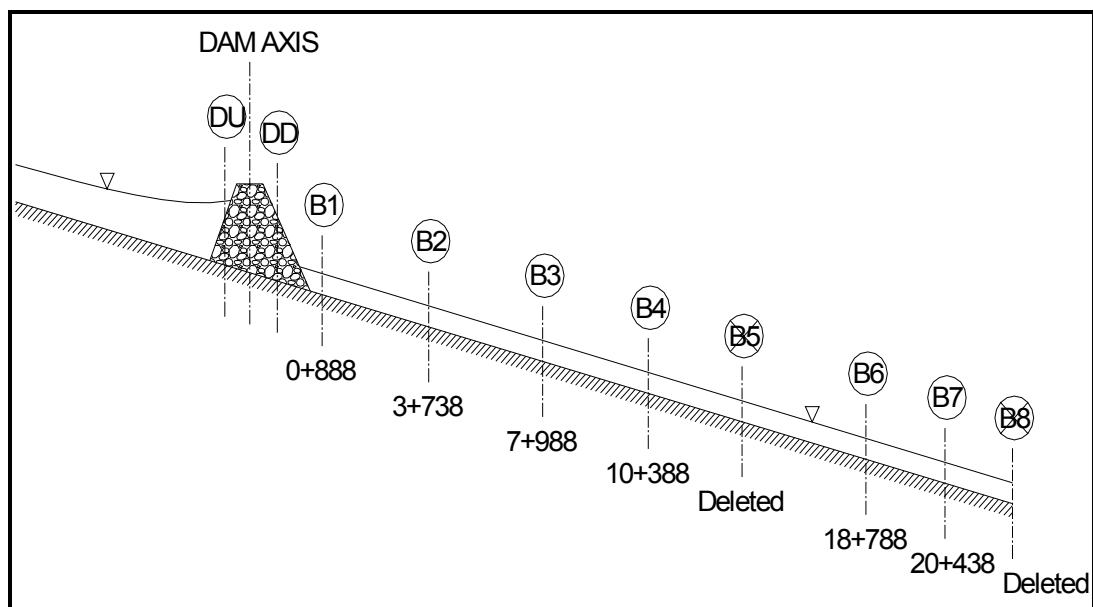


Figure 4.4 Profile view of routing reach

The labels of the cross sections are taken from the original geological survey map of Gökırmak Creek. The cross sections with labels B5 and B8 are not used in the dam break simulation of Kirazlıköprü Dam due to their very small size, which causes convergence problems during solution of Saint-Venant equations. In Figure 4.4, section DU represents the cross section of valley just upstream of the dam, and similarly, section DD represents the cross section just downstream of the dam. Initial letter D holds for the dam and the second letter holds for just downstream or just upstream of the dam. The section DU is the first input section in the *FLDWAV* input files (data sets); therefore, its St.Km. is set to be 0+000. *FLDWAV* needs these two sections at the dam in order to model a small reach which contains an internal boundary condition, which is Kirazlıköprü Dam in this case.

4.4 MODELING OF CROSS SECTIONS

Much of the uniqueness of a specific flow routing application using *FLDWAV* is captured in the cross sections located at selected points along the routing reach (Fread, 1998). Input cross sections may be of any geometrical shape. In *FLDWAV* cross sections are described by tabular values of channel/floodplain topwidth and water surface elevation. In this study, eight sets of top width-elevation values are used. This number is quite good to provide sufficiently accurate description of input cross sections. Area-elevation tables are automatically generated within the *FLDWAV* model from the input topwidth-elevation data. During the solution of Saint-Venant equations, any areas or widths associated with a particular water depth are linearly interpolated from the tabular values specified by the user.

During specification of topwidths, cross section is divided into subsections. That portion of the cross section in which flow is conveyed or in which the velocity in the downstream direction is considerable, is called the channel section or the active section. There can be portions of a cross section where the velocity in the flow direction is negligible relative to the velocity in the

active section (See Figure 4.5). The inactive portion is called off-channel storage, and it does not convey any flow in the downstream direction. The area of this inactive portion is represented by the term A_0 in the Saint-Venant conservation of mass equation (Eq. 3.1). Off-channel storage areas (A_0) can be used effectively to account for embayments, ravines, or tributaries which connect to the flow channel but do not pass flow and serve only to store the flow (Fread, 1998). In this study, since there is not any major tributary connecting to the routing reach, and due to lack of precise information regarding inactive flow portions, off-channel storage option is not used and topwidth values of off-channel storage are entered as zero in the topwidth-elevation tables.

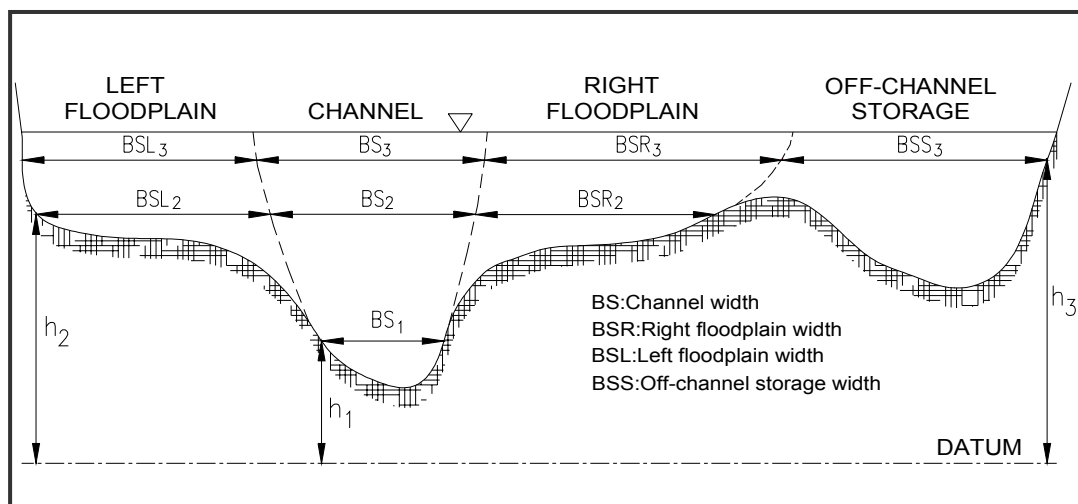


Figure 4.5 Definition of an input cross section

The friction slope S_f in the Saint-Venant equations may be evaluated by using two different methods. In the first method, the average of channel and floodplain values of Manning n , A (active flow area), and R (Hydraulic radius) are utilized. On the other hand, the second method uses separate Manning n , A , and R values for the channel and floodplains. The former is called as *composite option*, and the latter is called *conveyance option*. In the conveyance (K) option, the conveyances are calculated separately for the channel, right and left floodplains, and then the total conveyance of a

particular cross section is obtained by the summation of these separate conveyances. In the dam break flood routing analyses of the Kirazlıköprü Dam, conveyance option is used to take advantage of elimination of numerical convergence problems. Numerical problems occur when the cross section geometry consists of an incised channel and a very wide and flat floodplain. In this case, the derivative db/dh , which is necessary to evaluate for the solution of Saint-Venant equations, is somewhat discontinuous in the vicinity of the channel bank at the beginning of the floodplain portion of the valley. The slope dK/dh is more smoothly varying in this region, and hence, eliminates numerical difficulties (Fread, 1998). The topwidths and Manning n values are entered to the model separately for the channel, right and left floodplains.

The sinuosity factor, which is defined as the ratio of the flow path along the meandering channel to the flow path distance along the floodplain, is set to be unity in this study. This assumption is based on the fact that, when the water flows in very high depths as in the case of a dam break flood, both the main channel flow and floodplain flow follow the same path.

The six input cross sections utilized in the dam break simulation of Kirazlıköprü Dam can be seen in Figures 4.6 through 4.12.

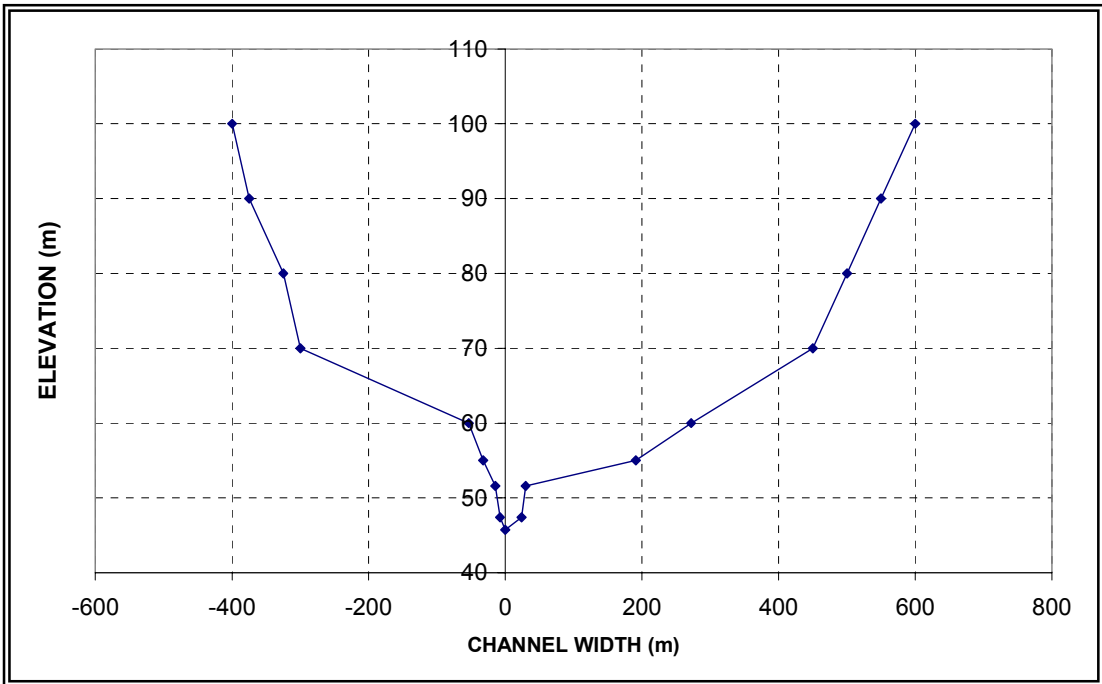


Figure 4.6 Cross section B1

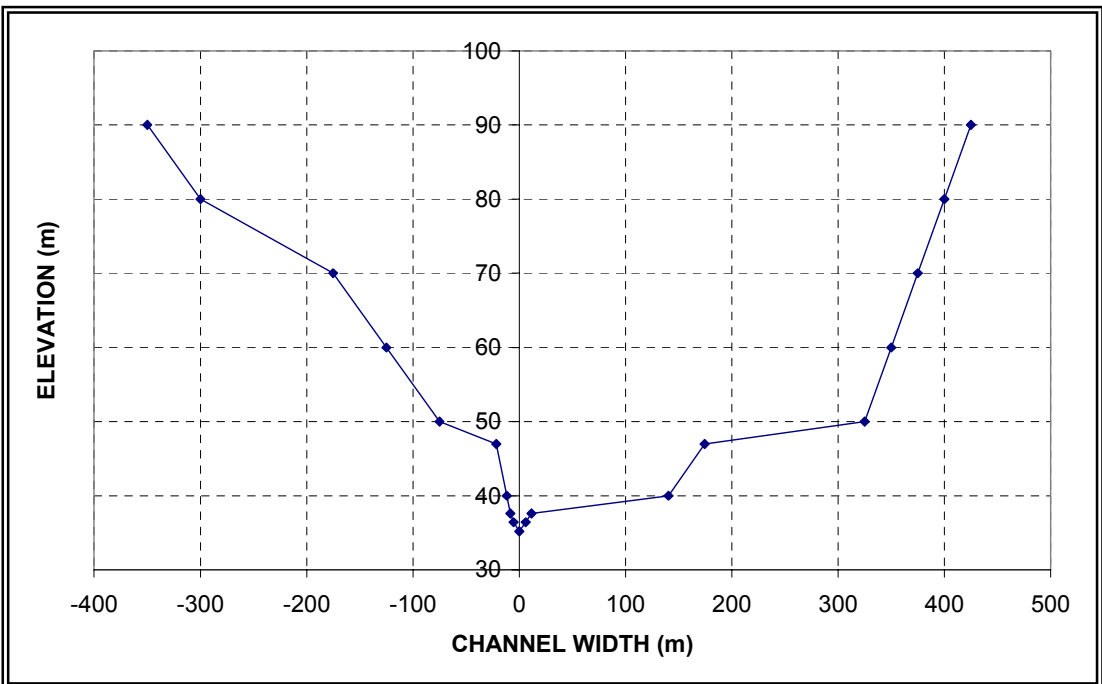


Figure 4.7 Cross section B2

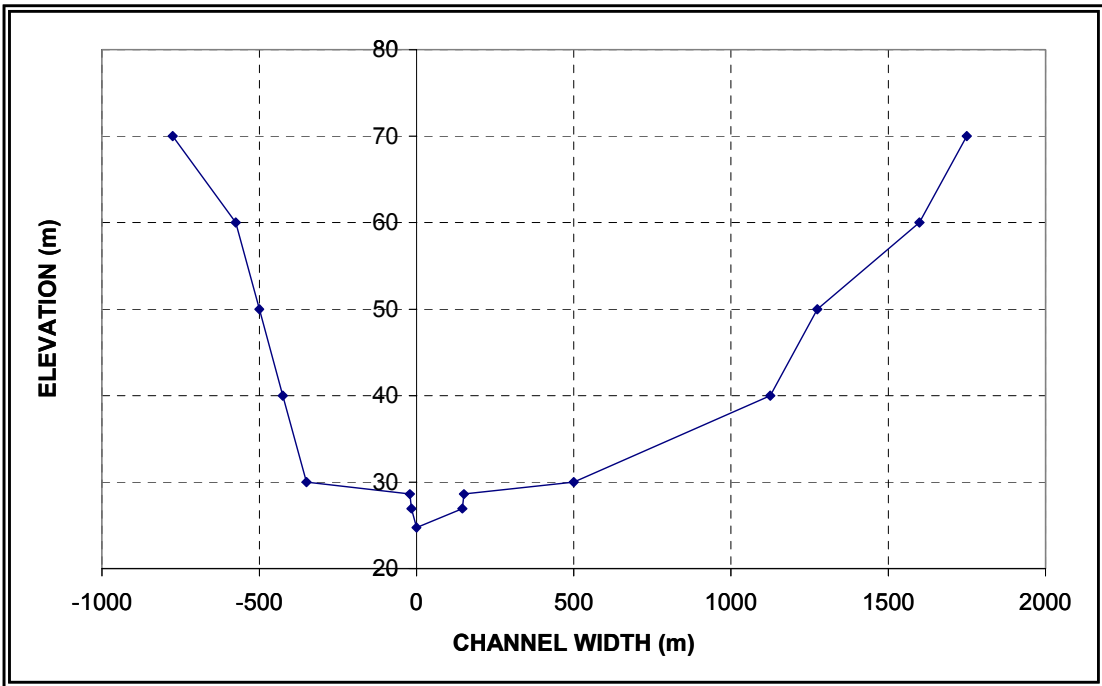


Figure 4.8 Cross section B3

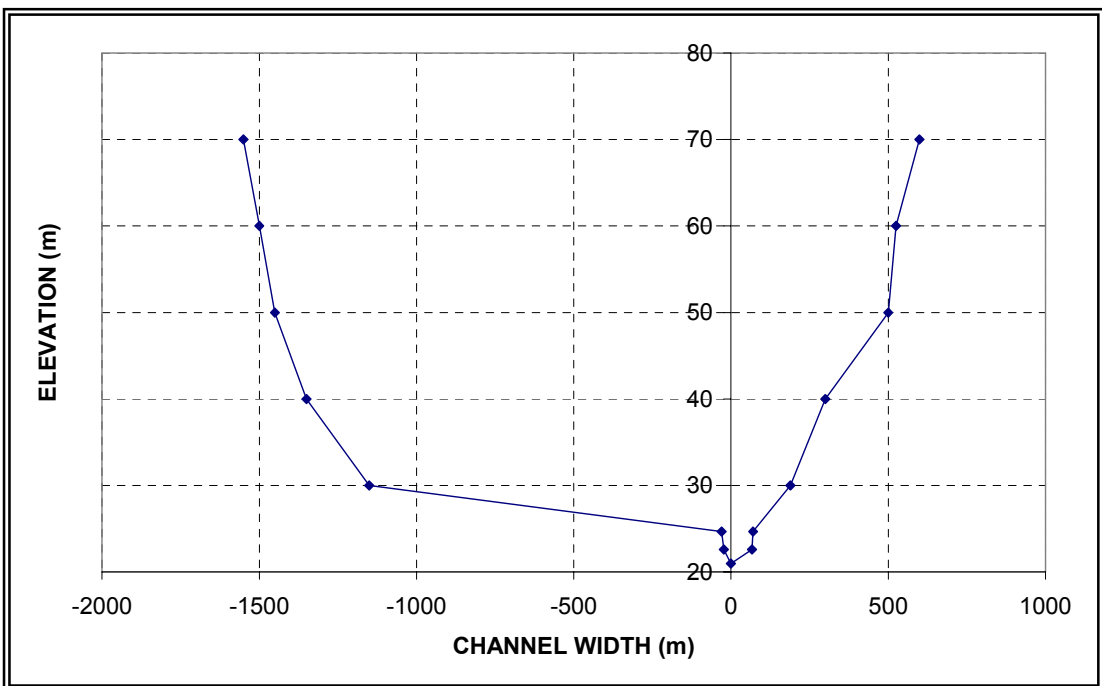


Figure 4.9 Cross section B4

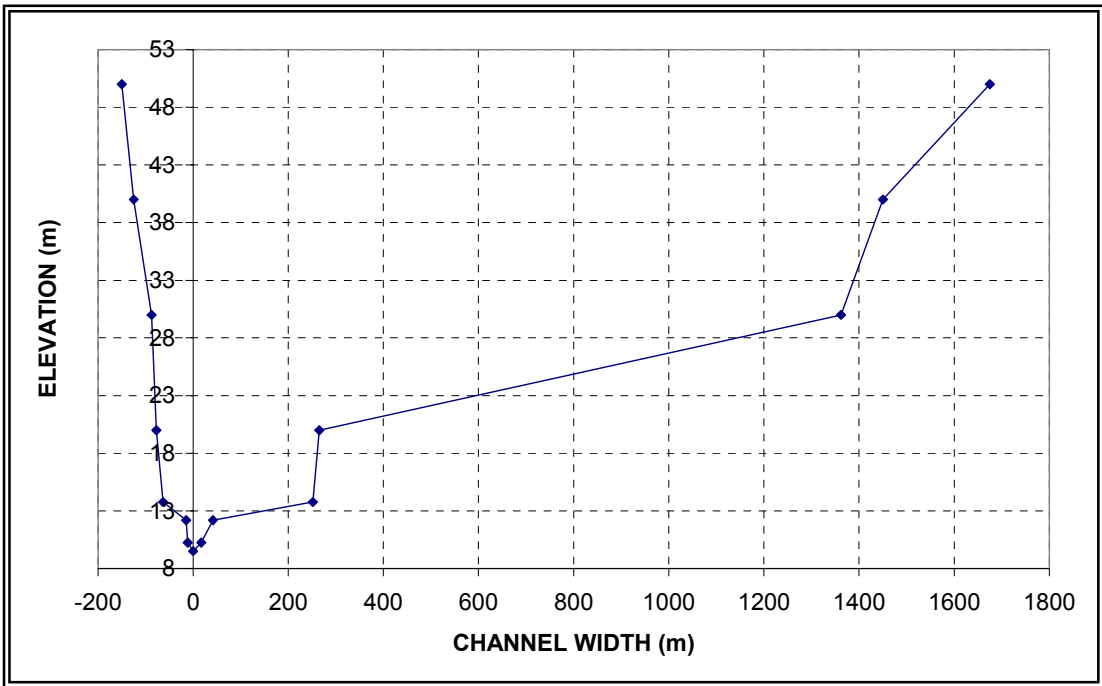


Figure 4.10 Cross section B6

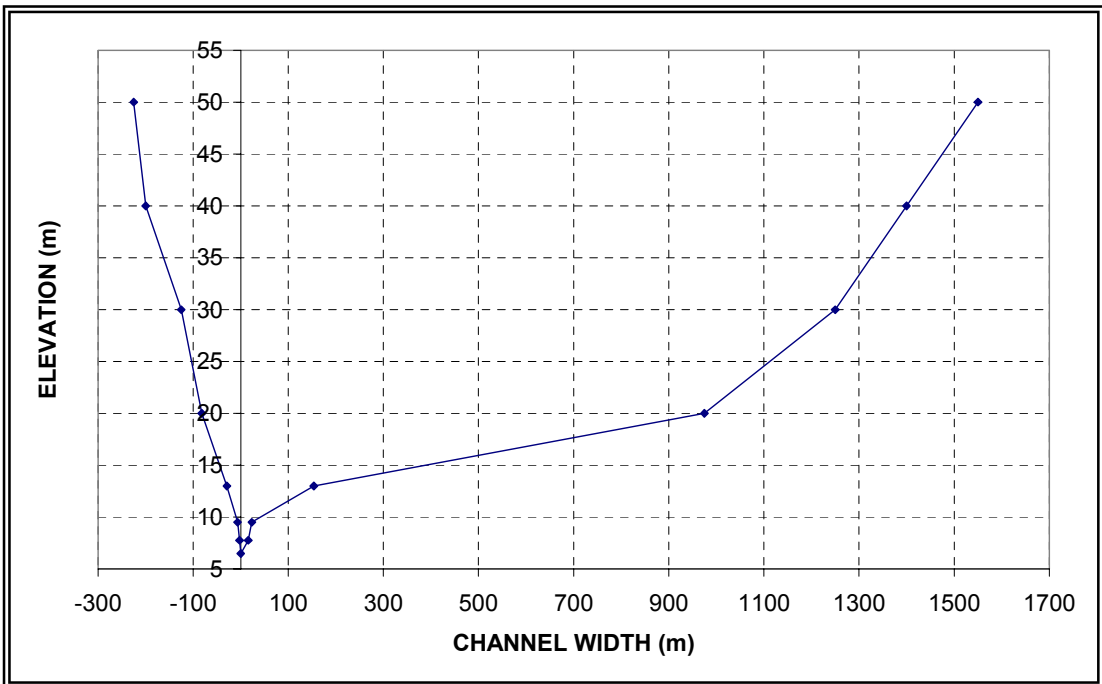


Figure 4.11 Cross section B7

CHAPTER 5

KİRAZLIKÖPRÜ DAM BREAK ANALYSES

Dam break flood forecasting has some uncertainties. Breach simulation and breach parameter prediction contain the greatest uncertainty of all aspects of dam break flood forecasting (Wurbs, 1987). Therefore, selection of breach parameters introduces a varying degree of uncertainty in the downstream flooding predictions. In this study, different failure scenarios are considered together with several breach parameters, in order to compensate for the uncertainty involved in any aspect of flood forecasting. This chapter describes the most likely failure scenarios and breach parameters that would lead to most unfavorable flooding conditions downstream. The results of all analyses shall be evaluated and presented in a comparative manner.

5.1 SELECTION OF BREACH PARAMETERS

To carry out a dam break flood routing simulation, breach parameters have to be estimated and provided as inputs to the flood routing model. Variation of breach parameters can affect peak discharge and inundation levels, which in turn affects warning time to evacuate populations living downstream of the dam. Since, most of the uncertainty is involved in the breach parameters; they have to be predicted with reasonable accuracy. Today, there are numerous breach parameter prediction tools that rely either on case study data from past dam failures or numerical models that do not simulate the erosion mechanisms and flow regimes that are relevant to a dam breach (Wahl, 1998).

In the dam break analyses of Kirazlıköprü Dam, instead of using a single value for each breach parameter, sensitivity analyses of breach parameters are performed by using several breach parameters. This intention is due to the fact that, dam break flood forecasting results may not be reliable and accurate since prediction of breach parameters involves great uncertainty. Moreover, the aim of this study is not to find out precise breach parameters that would result from probable failure of Kirazlıköprü Dam. Instead, it is intended to determine the failure scenario and breach parameters that would lead to most unfavorable flooding conditions in downstream valley. This can be accomplished by trying several breach parameters and to deduce the worst scenario by using a comparative approach between separate failure scenarios and breach parameters.

Based on the above discussion, a minimum, moderate and maximum value for each breach parameter is determined. In order to set up this range, breach parameter prediction equations derived by Froelich (1995) are used. Some of the dam and reservoir characteristics are entered into the formula proposed by Froelich, and the moderate values are approximated to the results given by these formulas. Minimum and maximum values are then estimated based on the moderate value. Consequently, three trial values for breach bottom width, breach bottom elevation and failure time are used for the dam break analyses of Kirazlıköprü Dam under different failure scenarios. The variation of breach parameters are further illustrated in Figures 5.1, 5.2 and 5.3

5.2 FAILURE SCENARIOS

Due to the high level of uncertainty encountered in dam break flood forecasting, several dam failure scenarios are examined in this study. This is needed to obtain more reliable results for the preparation of effective emergency warning systems and evacuation plans.

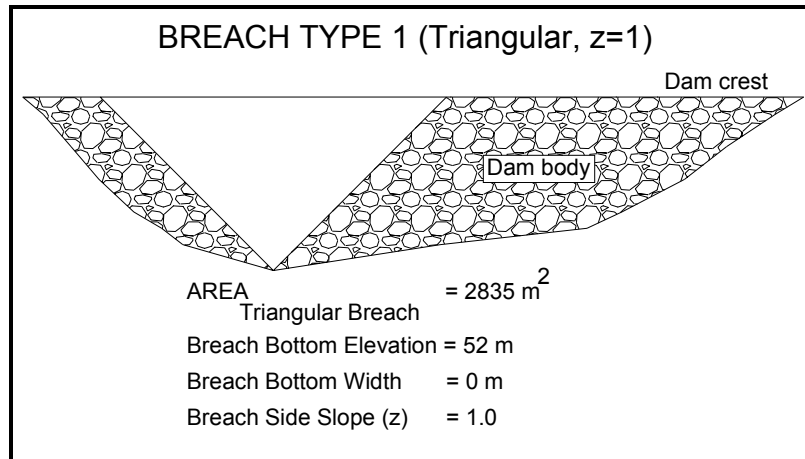


Figure 5.1 Schematic view of breach type 1 formation

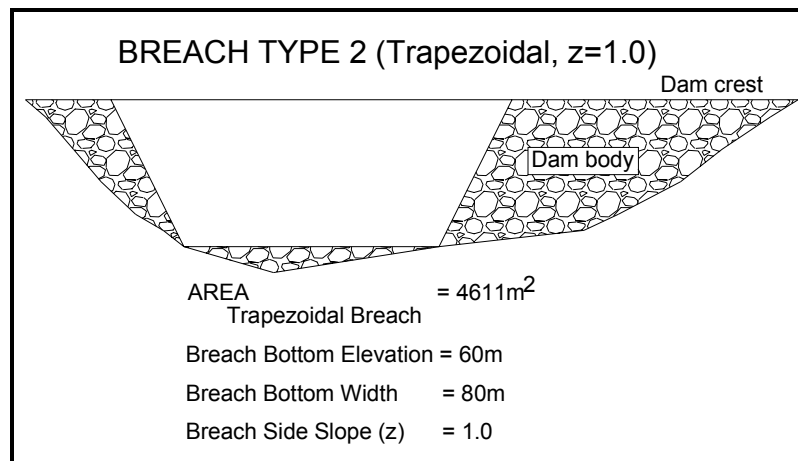


Figure 5.2 Schematic view of breach type 2 formation

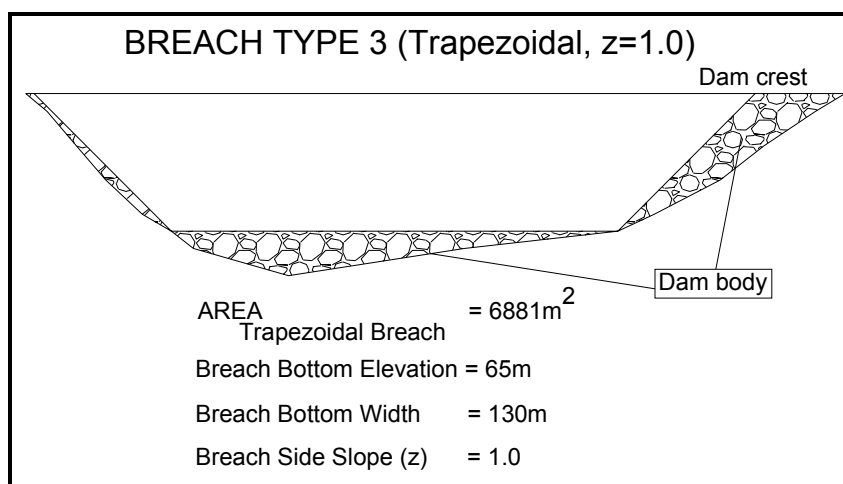


Figure 5.3 Schematic view of breach type 3 formation

Dam failure scenarios employed in this study can be classified in six main categories. The scenarios are derived by changing major parameters that affect dam break phenomenon and downstream flooding conditions to a great extent. Each scenario is identified by a run number. These run numbers also correspond to the name of input data files read in the flood routing model. As mentioned in the previous chapters in detail, the most frequently encountered reasons for dam break failures are overtopping and piping. In this study, it is intended to analyze both overtopping and piping failure of Kirazlıköprü Dam. The first five scenarios all simulate the overtopping failure and the last scenario analyzes piping failure of Kirazlıköprü Dam.

As shown in Table 5.1, run numbers starting from 1.1 to 1.9 constitute scenario 1. The basic assumption in this scenario is that, the spillway gates can not be opened when the catastrophic inflow hydrograph enters into the reservoir of Kirazlıköprü Dam. This can be due to malfunction of any part of the radial spillway gate, or due to the unawareness of the personnel responsible for the operation of the gates. Furthermore, initial water surface level in the reservoir is supposed to be at the maximum level in order to examine the scenario under maximum hydrologic conditions, which in turn results in most unfavorable flooding conditions in the downstream valley. In scenario 1, each run number has different breach parameters. The variable breach parameters are breach side slope, failure time, breach bottom width and breach bottom elevation. In other words, three different breach openings, as shown in Figures 5.1-5.3, are analyzed with three different failure times, which means nine runs in total for scenario 1. The idea behind the utilization of several breach parameters is to investigate the affect of breach parameter variation on the analyses results. Additionally, breach parameter sensitivity analysis is performed in this study since selection of breach parameters before a particular breach forms, i.e., in the absence of observations, introduces a varying degree of uncertainty in the downstream flooding results (Fread, 1998).

In scenarios 2 and 3, it is considered that spillway gates could be opened to an extent. The height of the radial spillway gates of the Kirazlıköprü Dam is 10 m. Fortunately; rating curve data of the spillway with respect to different gate openings are available. Spillway flow with different gate openings can also be modeled in FLDWAV by specifying respective rating curve data in the model. Spillway rating curve for each gate opening is shown in Figure 5.4. In scenario 2, analyses are carried out with the same breach parameters as utilized in scenario 1 with a gate opening of 2 m. In scenario 3, the same application is examined this time with a gate opening of 6 m. In order to have a better insight of effect of gate opening amount on the downstream flooding, scenario 4 is generated. After obtaining the most critical run in scenario 1 that leads to most devastating results in the downstream valley, the run under discussion is subject to examination under all gate openings. The results of this scenario shall give a clear understanding of gate opening effect.

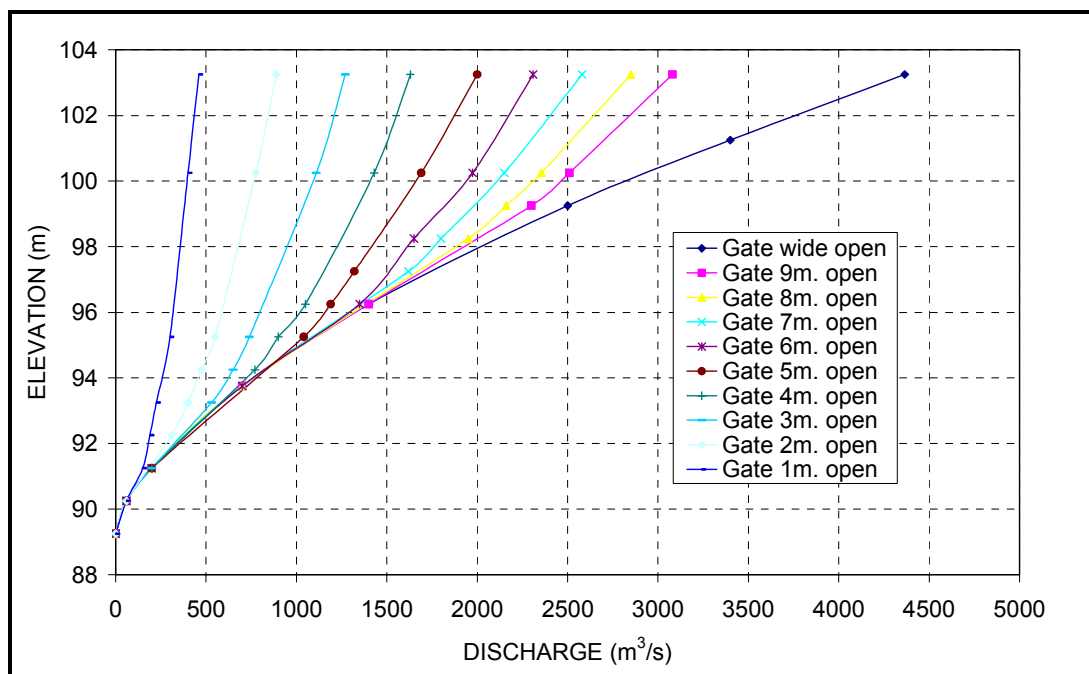


Figure 5.4 Spillway rating curves for different gate openings

Table 5.1 Simulation characteristics of Scenarios 1 and 2

BREACH PARAMETERS VARIATION MATRIX								
Run Number	Spillway Gates	Failure Time (hr)	Breach Shape	Breach Bottom Elevation (MSL)	Breach Side Slope (z)	Breach Bottom Width (m)	Breach Area (m ²)	
SCENARIO 1	1.1	Closed	0.5	Triangular	52	1	0	2835
	1.2	Closed	0.5	Trapezoidal	60	0.5	80	4611
	1.3	Closed	0.5	Trapezoidal	65	1	130	6881
	1.4	Closed	1	Triangular	52	1	0	2835
	1.5	Closed	1	Trapezoidal	60	0.5	80	4611
	1.6	Closed	1	Trapezoidal	65	1	130	6881
	1.7	Closed	2	Triangular	52	1	0	2835
	1.8	Closed	2	Trapezoidal	60	0.5	80	4611
	1.9	Closed	2	Trapezoidal	65	1	130	6881
SCENARIO 2	2.1	Partial Open (d=2m)	0.5	Triangular	52	1	0	2835
	2.2	Partial Open (d=2m)	0.5	Trapezoidal	60	0.5	80	4611
	2.3	Partial Open (d=2m)	0.5	Trapezoidal	65	1	130	6881
	2.4	Partial Open (d=2m)	1	Triangular	52	1	0	2835
	2.5	Partial Open (d=2m)	1	Trapezoidal	60	0.5	80	4611
	2.6	Partial Open (d=2m)	1	Trapezoidal	65	1	130	6881
	2.7	Partial Open (d=2m)	2	Triangular	52	1	0	2835
	2.8	Partial Open (d=2m)	2	Trapezoidal	60	0.5	80	4611
	2.9	Partial Open (d=2m)	2	Trapezoidal	65	1	130	6881

Table 5.2 Simulation characteristics of Scenarios 3, 4 and 5

BREACH PARAMETERS VARIATION MATRIX								
Run Number	Spillway Gates	Failure Time (hr)	Breach Shape	Breach Bottom Elevation (MSL)	Breach Side Slope (z)	Breach Bottom Width (m)	Breach Area (m ²)	
SCENARIO 3	3.1	Partial Open (d=6m)	0.5	Triangular	52	1	0	2835
	3.2	Partial Open (d=6m)	0.5	Trapezoidal	60	0.5	80	4611
	3.3	Partial Open (d=6m)	0.5	Trapezoidal	65	1	130	6881
	3.4	Partial Open (d=6m)	1	Triangular	52	1	0	2835
	3.5	Partial Open (d=6m)	1	Trapezoidal	60	0.5	80	4611
	3.6	Partial Open (d=6m)	1	Trapezoidal	65	1	130	6881
	3.7	Partial Open (d=6m)	2	Triangular	52	1	0	2835
	3.8	Partial Open (d=6m)	2	Trapezoidal	60	0.5	80	4611
	3.9	Partial Open (d=6m)	2	Trapezoidal	65	1	130	6881
SCENARIOS 4 and 5	4.1	Closed	0.5	Trapezoidal	65	1	130	6881
	4.2	Partial Open (d=1m)	0.5	Trapezoidal	65	1	130	6881
	4.3	Partial Open (d=3m)	0.5	Trapezoidal	65	1	130	6881
	4.4	Partial Open (d=4m)	0.5	Trapezoidal	65	1	130	6881
	4.5	Partial Open (d=5m)	0.5	Trapezoidal	65	1	130	6881
	4.6	Partial Open (d=7m)	0.5	Trapezoidal	65	1	130	6881
	4.7	Partial Open (d=8m)	0.5	Trapezoidal	65	1	130	6881
	4.8	Partial Open (d=9m)	0.5	Trapezoidal	65	1	130	6881
	4.9	Wide Open	0.5	Trapezoidal	65	1	130	6881
	5.1	Manning 0.06&0.1	0.5	Trapezoidal	65	1	130	6881
	1.3	Manning 0.04&0.06	0.5	Trapezoidal	65	1	130	6881
	5.2	Manning 0.02&0.04	0.5	Trapezoidal	65	1	130	6881

The main goal of scenario 5 is to explore the effect of Manning roughness coefficient on the dam break simulation results. Manning n is used to simulate the resistance to flow due to channel roughness. This roughness may be caused by bed forms, bank vegetation, river bend effects, and circulation eddy losses. The Manning n varies with the magnitude of the flow. As the flow increases and more portions of the bank and floodplain become inundated, the vegetation such as grass, brush, shrubs, and trees located at these elevations causes an increase in the resistance to flow. Besides, the Manning n may be larger for small floodplain depths than for larger depths due to flattening of the brush, thick weeds, or tall grass as the flow depths and velocities increase. Seasonal influences may also effect the selection of the Manning n (Fread, 1989).

Unfortunately, predictive Manning n methodologies have been confined to floods originated from precipitation runoffs. But, great magnitude of flows caused by dam breaching produces flow in portions of floodplains which were never inundated. Therefore, it is not beneficial to use previous evaluations of n from measured elevation/discharges or to use any calibration technique. The dam break flood is much more capable of creating and transporting large amount of debris than runoff-generated floods. The higher velocities of the dam breach flood will cause additional energy losses due to temporary obstructions formed by accumulation of transported debris at permanent features across the river such as bridge piers. Therefore, the Manning n values often need to be increased in order to account for the additional energy losses associated with the dam break flows (Fread, 1998).

Considering the above discussion regarding Manning n selection, the uncertainty associated with the selection of Manning n can be quite significant for dam break flood simulation. Therefore, instead of utilizing a fixed Manning n value for the channel and floodplain, it is decided to use three different sets of Manning n values, separately for the channel and

floodplains. In scenarios 1 through 4, Manning n value of 0.04 is used for the channel portion and 0.06 is used for the left and right floodplains. These values were obtained from one of the studies of Bozkuş (1992). In his study, he has worked on determination of water surface profiles of the Bartın River. This study was initiated soon after the floods in 1991. Since the same region is studied in this present study, the values are acceptable for use in dam break simulation. But, these values are considered to be average values and in order to make a sensitivity analysis, two sets of minimum and average Manning n values are also utilized. For the lower range, Manning values of 0.02 for the channel and 0.04 for the floodplains are employed. And for the upper range, Manning values of 0.06 for the channel and 0.1 for the floodplains are utilized. The latter set of Manning roughness coefficients were also used by Yazıcılar (1997). In order to obtain these values, she has used a method of estimating n examined by Chow, which is known as The Soil Conservation Service (SCS) Method. She has also made use of the local engineers' experience and the local authority observations. So, these values also seem to be useful and acceptable.

In scenario 5, the run, which gives the most unfavorable flooding conditions downstream in scenarios 1 through 4, is reanalyzed by utilizing different Manning n coefficients. Breach parameters are kept the same and only Manning n values are varied. The results will reveal the extent of Manning n effect on the peak flood results.

Finally, in scenario 6, piping failure of Kirazlıköprü Dam is simulated. As explained before in detail, piping is the formation of an internal conduit at some point below the dam crest due to seepage or erosion. The breach forms in rectangular shape centered at a certain elevation. In the literature, it is stated that piping starts at a height in between $1/2 h_d$ and $3/2 h_d$ from the thalveg elevation, where h_d is the height of the dam (Paquier, 1998). In this study, a rectangular piping breach with terminal breach width of 80 m,

terminal breach bottom elevation of 60 m, and piping centerline elevation of 82 m is simulated. The schematic view of piping breach formation can be seen in Figure 5.5.

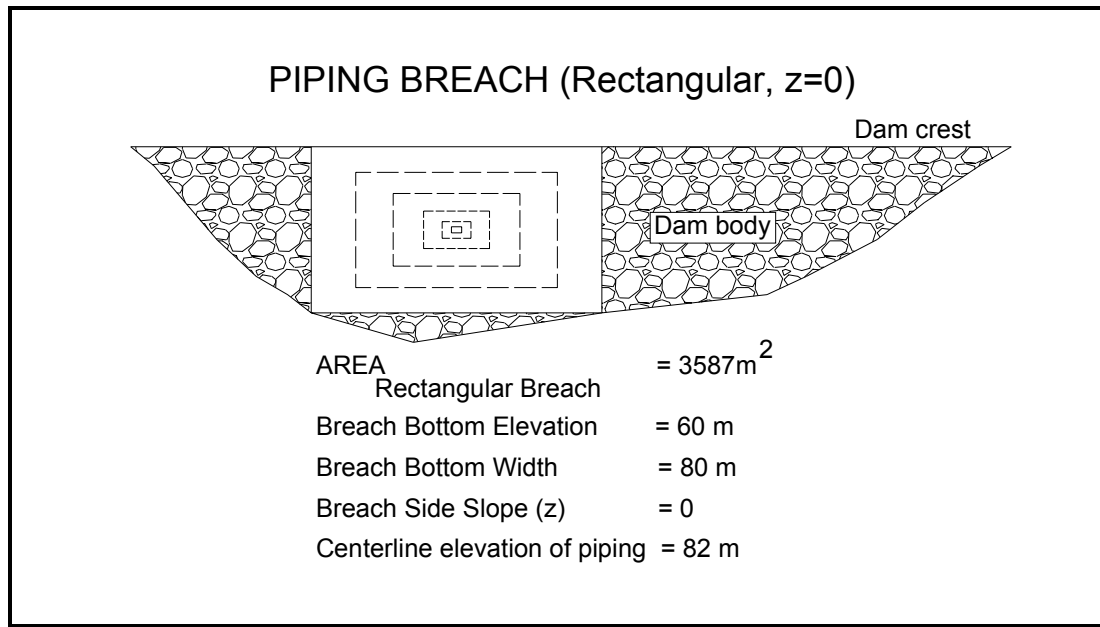


Figure 5.5 Formation of piping breach

In the piping failure simulation of Kirazlıköprü Dam, the initial water surface elevation is set to be equal to normal water level of the reservoir, i.e., 102.9 m. The failure is assumed to occur in a sunny day; therefore, the values of inflow hydrograph are all entered zero in the numerical model. This is due to the fact that there is no need for a storm to occur for piping failure. It can even be modeled in a sunny day. In addition, spillway gates of the dam are all closed. Breach parameters excluding failure time (τ) and breach formation rate (ρ) are constant in all runs. Since, the main purpose in this scenario is to investigate the effect of breach formation rate (ρ) on the downstream flooding conditions and peak flood travel times. The impact of failure time (τ) together with breach formation rate (ρ) is also examined. Basic characteristics of scenario 6 can be found in table 5.3.

Table 5.3 Simulation characteristics of Scenario 6

BREACH PARAMETERS VARIATION MATRIX									
Run Number	Spillway Gates	Failure Time, τ (hr)	Breach Formation Rate, ρ	Breach Shape	Breach Bottom Elevation (MSL)	Breach Side Slope (z)	Breach Bottom Width (m)	Breach Area (m ²)	
SCENARIO 6	6.1	Closed	1	1	Rectangular	62	0	80	3587
	6.2	Closed	1	2	Rectangular	62	0	80	3587
	6.3	Closed	1	3	Rectangular	62	0	80	3587
	6.4	Closed	2	1	Rectangular	62	0	80	3587
	6.5	Closed	2	2	Rectangular	62	0	80	3587
	6.6	Closed	2	3	Rectangular	62	0	80	3587
	6.7	Closed	3	1	Rectangular	62	0	80	3587
	6.8	Closed	3	2	Rectangular	62	0	80	3587
	6.9	Closed	3	3	Rectangular	62	0	80	3587

In common to all scenarios explained above, a constant discharge of 69 m³/s is entered in the model as the initial discharge in the routing reach. This value is the summation of bottom outlet discharge at normal water surface level (37.5 m³/s) and energy tunnel discharge (31.5 m³/s), as specified in Table 4.1. This flow is constantly released from the reservoir to the downstream valley. *FLDWAV* is a “wet” model. That means, it has to have some base flow in it and it can not start up dry, i.e., no flow in the reach. Therefore, this constant discharge is utilized in order to maintain initial conditions in the valley.

5.3 SIMULATION RESULTS

Having defined possible failure scenarios, *FLDWAV* model is employed for the failure analyses of the Kirazlıköprü Dam. Primarily, data sets are prepared as input files incorporating data that represents required information for the modeling of each failure scenarios discussed in previous section. Some rules are followed to form these data sets such that *FLDWAV*

can read and run to completion. In other words, each data has to be entered in its correct location and order in the data file. Otherwise, the model will not run the input file. All of these input data files can be found in the CD-ROM supplied together with this study.

During the execution of the model, mixed flow option is used for all scenarios. This is a characteristic of the model which enables handling subcritical and supercritical flows at the same time. This means, both subcritical and supercritical flow may occur simultaneously in the routing reach. The model contains a solution method for treating the mixed flow. It consists of an algorithmic procedure which automatically subdivides the total routing reach into sub-reaches in which only subcritical or supercritical flow occurs. The transition locations where the flow changes from subcritical to supercritical or vice versa are treated as boundary conditions. This avoids the application of Saint-Venant equations to the transition flow.

The *FLDWAV* model generates very detailed output file that makes it easy to troubleshoot problems encountered during execution of the model. It also gives all hydraulic information required to evaluate flood routing results. Detailed output files belonging to each of the scenarios defined before can be accessed in the CD-ROM presented with this thesis study. The files can be easily identified by taking advantage of their file names, since they carry the label of runs defined in Tables 5.1, 5.2 and 5.3. Moreover, output summary can be found in the following tables, which summarize peak flooding conditions for each input cross section. These sections are places where flood forecasting results are sought and dam break hazard evaluations are performed. Specifically, following tables summarize peak flows, peak water surface elevations and their occurrence times for each input cross section.

Table 5.4 Summary table of peak flows and their occurrence times for Scenario 1

Run Number	Cross Section B1 0+888 Km		Cross Section B2 3+738 Km		Cross Section B3 7+988 Km		Cross Section B4 10+388 Km		Cross Section B6 18+788 Km		Cross Section B7 20+438 Km	
	Max. Flow (m ³ /s)	Occurrence Time (hr)	Max. Flow (m ³ /s)	Occurrence Time (hr)	Max. Flow (m ³ /s)	Occurrence Time (hr)	Max. Flow (m ³ /s)	Occurrence Time (hr)	Max. Flow (m ³ /s)	Occurrence Time (hr)	Max. Flow (m ³ /s)	Occurrence Time (hr)
1.1	23982	6.25	21329	6.41	18938	6.67	16105	6.94	9987	7.92	9463	8.12
1.2	41932	6.21	36420	6.34	30681	6.54	24618	6.71	12116	7.56	11285	7.77
1.3	52425	6.20	44747	6.29	35938	6.46	27444	6.62	12139	7.44	11191	7.66
1.4	21835	6.70	19784	6.85	17909	7.10	15681	7.33	10095	8.30	9614	8.48
1.5	34488	6.70	31249	6.78	27153	6.95	22922	7.10	12175	7.93	11391	8.13
1.6	37132	6.70	34475	6.73	29805	6.88	24624	7.03	12161	7.80	11290	8.00
1.7	17886	7.70	16489	7.80	15328	8.00	14111	8.20	10063	9.10	9703	9.25
1.8	21811	7.50	20923	7.60	19667	7.80	18029	7.95	11775	8.65	11225	8.85
1.9	21413	7.30	20580	7.45	19322	7.60	17764	7.80	11552	8.55	10960	8.70

Table 5.5 Summary table of peak water surface elevations and their occurrence times for Scenario 1

Run Number	Cross Section B1 0+888 Km		Cross Section B2 3+738 Km		Cross Section B3 7+988 Km		Cross Section B4 10+388 Km		Cross Section B6 18+788 Km		Cross Section B7 20+438 Km	
	Max. Stage (m)	Occurrence Time (hr)	Max. Stage (m)	Occurrence Time (hr)	Max. Stage (m)	Occurrence Time (hr)	Max. Stage (m)	Occurrence Time (hr)	Max. Stage (m)	Occurrence Time (hr)	Max. Stage (m)	Occurrence Time (hr)
1.1	64.58	6.30	51.71	6.44	35.64	6.81	32.12	7.09	22.20	8.16	20.55	8.44
1.2	68.30	6.26	54.52	6.34	37.43	6.62	33.48	6.82	22.82	7.76	20.89	7.92
1.3	69.97	6.22	55.77	6.30	38.00	6.54	33.80	6.72	22.78	7.65	20.86	7.81
1.4	64.06	6.75	51.25	6.88	35.52	7.23	32.07	7.48	22.22	8.53	20.48	8.80
1.5	67.13	6.73	53.75	6.78	37.09	7.03	33.31	7.23	22.83	8.13	20.83	8.30
1.6	67.91	6.70	54.24	6.75	37.44	6.95	33.53	7.13	22.79	8.00	20.79	8.20
1.7	63.00	7.70	50.23	7.80	35.11	8.10	31.83	8.30	22.23	9.25	20.40	9.50
1.8	64.26	7.60	51.62	7.65	36.06	7.85	32.63	8.00	22.75	8.85	20.73	9.00
1.9	64.19	7.40	51.52	7.45	35.99	7.70	32.57	7.90	22.66	8.70	20.66	8.90

Table 5.6 Summary table of peak flows and their occurrence times for Scenario 2

Run Number	Cross Section B1 0+888 Km		Cross Section B2 3+738 Km		Cross Section B3 7+988 Km		Cross Section B4 10+388 Km		Cross Section B6 18+788 Km		Cross Section B7 20+438 Km	
	Max. Flow (m ³ /s)	Occurrence Time (hr)	Max. Flow (m ³ /s)	Occurrence Time (hr)	Max. Flow (m ³ /s)	Occurrence Time (hr)	Max. Flow (m ³ /s)	Occurrence Time (hr)	Max. Flow (m ³ /s)	Occurrence Time (hr)	Max. Flow (m ³ /s)	Occurrence Time (hr)
2.1	25298	12.79	22743	12.98	20377	13.22	17763	13.47	11618	14.44	11283	14.64
2.2	43504	12.78	38094	12.90	32468	13.09	26542	13.26	14010	14.06	13449	14.24
2.3	54250	12.76	46616	12.85	37977	13.01	29644	13.17	14078	13.95	13405	14.12
2.4	23313	13.27	21365	13.40	19487	13.65	17459	13.85	11854	14.77	11549	14.97
2.5	36477	13.25	33188	13.32	29233	13.50	25042	13.65	14252	14.42	13755	14.57
2.6	39820	11.62	36899	11.67	32001	11.80	26667	11.95	13512	12.72	12723	12.90
2.7	19591	14.25	18242	14.35	17060	14.55	15837	14.70	11865	15.55	11687	15.70
2.8	23900	14.10	23021	14.20	21761	14.35	20150	14.45	13940	15.15	13673	15.30
2.9	23619	13.95	22808	14.00	21547	14.20	20037	14.35	13785	15.00	13503	15.15

Table 5.7 Summary table of peak water surface elevations and their occurrence times for Scenario 2

Run Number	Cross Section B1 0+888 Km		Cross Section B2 3+738 Km		Cross Section B3 7+988 Km		Cross Section B4 10+388 Km		Cross Section B6 18+788 Km		Cross Section B7 20+438 Km	
	Max. Stage (m)	Occurrence Time (hr)	Max. Stage (m)	Occurrence Time (hr)	Max. Stage (m)	Occurrence Time (hr)	Max. Stage (m)	Occurrence Time (hr)	Max. Stage (m)	Occurrence Time (hr)	Max. Stage (m)	Occurrence Time (hr)
2.1	64.98	12.89	52.06	12.99	36.00	13.37	32.49	13.62	22.84	14.62	20.95	14.76
2.2	68.63	12.83	54.77	12.90	37.77	13.19	33.87	13.37	23.48	14.22	21.27	14.35
2.3	70.27	12.79	56.06	12.86	38.36	13.10	34.20	13.27	23.46	14.11	21.26	14.24
2.4	64.53	13.32	51.73	13.42	35.92	13.75	32.48	14.00	22.92	14.95	20.97	15.10
2.5	67.57	13.27	54.04	13.32	37.48	13.57	33.76	13.75	23.56	14.55	21.29	14.67
2.6	68.42	11.62	54.59	11.67	37.81	11.87	33.91	12.02	23.24	12.87	21.06	13.05
2.7	63.54	14.25	50.78	14.35	35.53	14.60	32.24	14.80	22.97	15.65	21.00	15.75
2.8	64.93	14.10	52.15	14.20	36.51	14.40	33.12	14.55	23.56	15.25	21.32	15.30
2.9	64.88	13.95	52.09	14.00	36.47	14.25	33.09	14.45	23.50	15.10	21.28	15.20

Table 5.8 Summary table of peak flows and their occurrence times for Scenario 3

Run Number	Cross Section B1 0+888 Km		Cross Section B2 3+738 Km		Cross Section B3 7+988 Km		Cross Section B4 10+388 Km		Cross Section B6 18+788 Km		Cross Section B7 20+438 Km	
	Max. Flow (m ³ /s)	Occurrence Time (hr)	Max. Flow (m ³ /s)	Occurrence Time (hr)	Max. Flow (m ³ /s)	Occurrence Time (hr)	Max. Flow (m ³ /s)	Occurrence Time (hr)	Max. Flow (m ³ /s)	Occurrence Time (hr)	Max. Flow (m ³ /s)	Occurrence Time (hr)
3.1	26047	16.53	23360	16.70	20879	16.93	18352	17.16	12278	18.05	12040	18.20
3.2	43773	16.51	38261	16.63	32503	16.81	26884	16.98	15048	17.71	14629	17.86
3.3	53857	16.50	46247	16.59	37736	16.74	30094	16.90	15311	17.60	14803	17.75
3.4	23482	17.00	21423	17.15	19481	17.35	17481	17.55	12164	18.42	11956	18.55
3.5	35255	17.00	32197	17.08	28368	17.23	24518	17.38	14792	18.10	14450	18.22
3.6	37334	16.98	35159	17.03	30865	17.18	26330	17.30	14993	17.97	14589	18.10
3.7	18370	18.00	17181	18.05	16133	18.25	15029	18.40	11548	19.20	11431	19.30
3.8	21672	17.70	20906	17.80	19976	18.00	18701	18.15	13580	18.80	13415	18.90
3.9	21628	17.55	20853	17.70	19828	17.90	18575	18.05	13495	18.75	13335	18.85

Table 5.9 Summary table of peak water surface elevations and their occurrence times for Scenario 3

Run Number	Cross Section B1 0+888 Km		Cross Section B2 3+738 Km		Cross Section B3 7+988 Km		Cross Section B4 10+388 Km		Cross Section B6 18+788 Km		Cross Section B7 20+438 Km	
	Max. Stage (m)	Occurrence Time (hr)	Max. Stage (m)	Occurrence Time (hr)	Max. Stage (m)	Occurrence Time (hr)	Max. Stage (m)	Occurrence Time (hr)	Max. Stage (m)	Occurrence Time (hr)	Max. Stage (m)	Occurrence Time (hr)
3.1	65.17	16.60	52.21	16.71	36.12	17.06	32.62	17.29	23.08	18.18	21.09	18.29
3.2	68.67	16.55	54.79	16.63	37.83	16.90	33.99	17.09	23.83	17.84	21.48	17.94
3.3	70.22	16.53	56.00	16.59	38.41	16.83	34.35	16.99	23.87	17.73	21.49	17.84
3.4	64.55	17.05	51.74	17.15	35.93	17.48	32.49	17.68	23.05	18.52	21.06	18.62
3.5	67.35	17.00	53.90	17.08	37.38	17.30	33.73	17.48	23.77	18.20	21.43	18.27
3.6	67.98	17.00	54.33	17.03	37.74	17.23	33.97	17.38	23.81	18.07	21.44	18.17
3.7	63.21	18.00	50.44	18.05	35.33	18.30	32.07	18.50	22.90	19.30	21.00	19.35
3.8	64.24	17.80	51.62	17.85	36.18	18.05	32.85	18.25	23.50	18.90	21.35	18.90
3.9	64.26	17.65	51.61	17.70	36.15	18.00	32.83	18.15	23.48	18.80	21.33	18.85

Table 5.10 Summary table of peak flows and their occurrence times for Scenario 4

Run Number	Cross Section B1 0+888 Km		Cross Section B2 3+738 Km		Cross Section B3 7+988 Km		Cross Section B4 10+388 Km		Cross Section B6 18+788 Km		Cross Section B7 20+438 Km	
	Max. Flow (m ³ /s)	Occurrence Time (hr)	Max. Flow (m ³ /s)	Occurrence Time (hr)	Max. Flow (m ³ /s)	Occurrence Time (hr)	Max. Flow (m ³ /s)	Occurrence Time (hr)	Max. Flow (m ³ /s)	Occurrence Time (hr)	Max. Flow (m ³ /s)	Occurrence Time (hr)
4.1	52425	6.20	44747	6.29	35938	6.46	27444	6.62	12139	7.44	11191	7.66
4.2	54080	11.98	46414	12.05	37730	12.22	29267	12.39	13554	13.19	12786	13.36
4.3	54398	13.51	46780	13.60	38178	13.76	30002	13.93	14522	14.67	13907	14.84
4.4	54324	14.30	46709	14.39	38106	14.55	30099	14.70	14835	15.44	14277	15.60
4.5	54074	15.23	46482	15.31	37938	15.48	30135	15.63	15114	16.34	14585	16.49
4.6	3203	18.60	3196	18.80	3179	19.20	3155	19.70	3111	21.10	3113	21.20
4.7	3109	19.30	3109	19.40	3108	19.80	3107	20.30	3103	21.50	3104	21.70
4.8	3208	18.60	3208	18.70	3207	19.10	3205	19.60	3200	20.90	3201	21.00
4.9	3551	16.10	3550	16.30	3547	16.70	3540	17.20	3526	18.50	3528	18.60

Table 5.11 Summary table of peak water surface elevations and their occurrence times for Scenario 4

Run Number	Cross Section B1 0+888 Km		Cross Section B2 3+738 Km		Cross Section B3 7+988 Km		Cross Section B4 10+388 Km		Cross Section B6 18+788 Km		Cross Section B7 20+438 Km	
	Max. Stage (m)	Occurrence Time (hr)	Max. Stage (m)	Occurrence Time (hr)	Max. Stage (m)	Occurrence Time (hr)	Max. Stage (m)	Occurrence Time (hr)	Max. Stage (m)	Occurrence Time (hr)	Max. Stage (m)	Occurrence Time (hr)
4.1	69.97	6.22	55.77	6.30	38.00	6.54	33.80	6.72	22.78	7.65	20.86	7.81
4.2	70.23	11.99	56.03	12.06	38.30	12.30	34.13	12.49	23.28	13.35	21.15	13.49
4.3	70.29	13.54	56.08	13.61	38.41	13.85	34.28	14.03	23.61	14.82	21.34	14.94
4.4	70.28	14.33	56.07	14.40	38.42	14.63	34.31	14.80	23.72	15.57	21.40	15.69
4.5	70.25	15.25	56.03	15.31	38.42	15.55	34.34	15.73	23.81	16.48	21.46	16.59
4.6	55.74	18.60	43.47	18.80	31.09	19.40	28.14	19.90	18.94	21.10	18.17	21.00
4.7	55.66	19.30	43.41	19.40	31.05	20.00	28.11	20.40	18.93	21.40	18.16	21.00
4.8	55.74	18.60	43.48	18.70	31.11	19.30	28.18	19.70	18.99	20.70	18.19	20.30
4.9	56.04	16.20	43.73	16.30	31.31	16.90	28.41	17.30	19.19	18.40	18.32	18.10

Table 5.12 Summary table of peak flows and peak water surface elevations together with their occurrence times for Scenario 5

Run Number	Cross Section B1 0+888 Km		Cross Section B2 3+738 Km		Cross Section B3 7+988 Km		Cross Section B4 10+388 Km		Cross Section B6 18+788 Km		Cross Section B7 20+438 Km	
	Max. Flow (m ³ /s)	Occurrence Time (hr)	Max. Flow (m ³ /s)	Occurrence Time (hr)	Max. Flow (m ³ /s)	Occurrence Time (hr)	Max. Flow (m ³ /s)	Occurrence Time (hr)	Max. Flow (m ³ /s)	Occurrence Time (hr)	Max. Flow (m ³ /s)	Occurrence Time (hr)
5.1	52200	6.20	42079	6.31	29618	6.56	20609	6.81	8124	8.11	7562	8.42
1.3	52425	6.20	44747	6.29	35938	6.46	27444	6.62	12139	7.44	11191	7.66
5.2	53516	6.20	48173	6.26	42312	6.39	35098	6.49	17840	7.01	16672	7.11
Run Number	Cross Section B1 0+888 Km		Cross Section B2 3+738 Km		Cross Section B3 7+988 Km		Cross Section B4 10+388 Km		Cross Section B6 18+788 Km		Cross Section B7 20+438 Km	
	Max. Stage (m)	Occurrence Time (hr)	Max. Stage (m)	Occurrence Time (hr)	Max. Stage (m)	Occurrence Time (hr)	Max. Stage (m)	Occurrence Time (hr)	Max. Stage (m)	Occurrence Time (hr)	Max. Stage (m)	Occurrence Time (hr)
5.1	73.69	6.24	58.87	6.34	39.13	6.67	34.45	6.96	23.29	8.39	21.07	8.64
1.3	69.97	6.22	55.77	6.30	38.00	6.54	33.80	6.72	22.78	7.65	20.86	7.81
5.2	66.56	6.21	53.78	6.27	36.55	6.44	32.95	6.56	21.55	7.15	20.42	7.27

Table 5.13 Summary table of peak flows and their occurrence times for Scenario 6

Run Number	Cross Section B1 0+888 Km		Cross Section B2 3+738 Km		Cross Section B3 7+988 Km		Cross Section B4 10+388 Km		Cross Section B6 18+788 Km		Cross Section B7 20+438 Km	
	Max. Flow (m ³ /s)	Occurrence Time (hr)	Max. Flow (m ³ /s)	Occurrence Time (hr)	Max. Flow (m ³ /s)	Occurrence Time (hr)	Max. Flow (m ³ /s)	Occurrence Time (hr)	Max. Flow (m ³ /s)	Occurrence Time (hr)	Max. Flow (m ³ /s)	Occurrence Time (hr)
6.1	25535	1.01	21547	1.06	19351	1.23	16447	1.40	8907	2.28	8182	2.53
6.2	32854	1.03	25327	1.13	21678	1.33	17553	1.53	8985	2.43	8237	2.65
6.3	33540	1.00	26755	1.15	22498	1.36	18059	1.58	9050	2.48	8292	2.73
6.4	15207	1.46	13481	1.60	12823	1.86	11819	2.05	7941	2.90	7387	3.10
6.5	21334	1.96	18251	2.00	16453	2.20	14340	2.35	8412	3.20	7766	3.45
6.6	27567	2.01	21751	2.10	18832	2.25	15674	2.45	8579	3.35	7890	3.55
6.7	11483	1.80	10350	2.03	9946	2.26	9317	2.48	6869	3.45	6538	3.68
6.8	14624	2.63	12871	2.78	12264	3.00	11311	3.15	7643	4.05	7191	4.20
6.9	19391	2.85	16826	3.00	15099	3.16	13175	3.38	8020	4.20	7479	4.43

Table 5.14 Summary table of peak water surface elevations and their occurrence times for Scenario 6

Run Number	Cross Section B1 0+888 Km		Cross Section B2 3+738 Km		Cross Section B3 7+988 Km		Cross Section B4 10+388 Km		Cross Section B6 18+788 Km		Cross Section B7 20+438 Km	
	Max. Stage (m)	Occurrence Time (hr)	Max. Stage (m)	Occurrence Time (hr)	Max. Stage (m)	Occurrence Time (hr)	Max. Stage (m)	Occurrence Time (hr)	Max. Stage (m)	Occurrence Time (hr)	Max. Stage (m)	Occurrence Time (hr)
6.1	64.86	0.98	51.81	1.08	35.75	1.30	32.11	1.50	21.59	2.50	19.87	2.70
6.2	66.27	1.03	52.68	1.13	36.04	1.40	32.25	1.63	21.61	2.65	19.88	2.85
6.3	66.41	1.10	52.95	1.18	36.16	1.46	32.32	1.68	21.64	2.70	19.89	2.90
6.4	61.85	1.50	49.00	1.65	34.50	1.96	31.23	2.15	21.22	3.15	19.59	3.40
6.5	63.73	2.00	50.86	2.05	35.23	2.28	31.74	2.45	21.38	3.45	19.65	3.70
6.6	65.12	2.01	51.86	2.11	35.61	2.35	31.96	2.55	21.43	3.55	19.67	3.80
6.7	60.41	1.95	47.38	2.03	33.74	2.41	30.60	2.63	20.75	3.68	19.19	3.98
6.8	61.60	2.63	48.73	2.78	34.36	3.08	31.10	3.27	21.07	4.20	19.42	4.50
6.9	63.24	3.00	50.38	3.00	34.96	3.23	31.49	3.45	21.21	4.43	19.48	4.73

CHAPTER 6

EVALUATION OF THE RESULTS

Sensitivity studies of variables defined in this thesis are carried out by evaluating the output results of each scenario among itself. Comparison of the results of all scenarios also comes up with a sound understanding of effect of defined parameters on the dam break flood routing. After evaluating the importance of each parameter, dam break hazard evaluation shall be performed in order to sort out regions that are estimated to be adversely affected as a result of probable failure of Kirazlıköprü Dam.

The results of dam break analyses simulated under six different failure scenarios are tabulated in Tables 5.4 through 5.14. Output data in these tables pertain to the six input cross sections. These sections are situated in the downstream valley of the dam and each section represents a centre of population. Hazard evaluation of such settlement regions are made by making use of these output results listed in the above mentioned tables. However, the sensitivity analyses and comparison of scenarios shall be made in the continuous domain of routing reach. In other words, graphs presented in this chapter represent data which are continuously available throughout the routing reach. The frequency of available data is dependent on the dimension of computational time or distance step, since the numerical model FLDWAV gives results for each of these computation nodes.

6.1 EVALUATION OF SCENARIO 1 RESULTS

The main cause of dam break failures is reported to be inadequate spillway capacity. Most of the dam break incidents were observed to occur by the overtopping of the dam crest due to inability of spillways to convey the inflow entering into the reservoir. Since, the failure of dams happens in a short period of time and there is slight indication of possible future dam failure, most of the time spillway gates can not be opened. Thus, the dam experiences the incoming flood wave while the spillway gates are closed. Based on this realistic approach, scenario 1 is chosen to be the major failure scenario among the others. In this scenario, spillway gates are closed and maximum catastrophic inflow hydrograph is assumed to enter to the dam reservoir. In this scenario, the initial water level in the reservoir is at the maximum level.

Figure 6.1 shows the spatial variation of peak discharge for different dam breach parameters. In this scenario, the variables are failure time and size of breach opening. The characteristics of each run from 1.1 to 1.9 can be found in the breach variation matrix of Table 5.1. The uppermost curve in this graph represents the results of run 1.3. By inspecting table 5.1, one can easily notice that, this run has the shortest failure time of 0.5 hr and largest breach opening of 6881 m². On the other hand, the lowest curve gives the results of run 1.7. This sub-scenario has a 2 hr failure time and the breach forms in the shape of a triangle that corresponds to a breach opening of 2835 m². In fact, this sub-scenario possesses the longest failure time and smallest breach opening in the dam body. The next highest flow values are given by run 1.2. Because, while the failure time is the same, breach opening size is less than run 1.3 for this sub-scenario. The next highest curve is for run 1.6. Although, failure time is 1 hr for this run, it yields higher results than those of run 1.1, which has a shorter failure time. This shows that, breach opening size is more influential on the results than failure time.

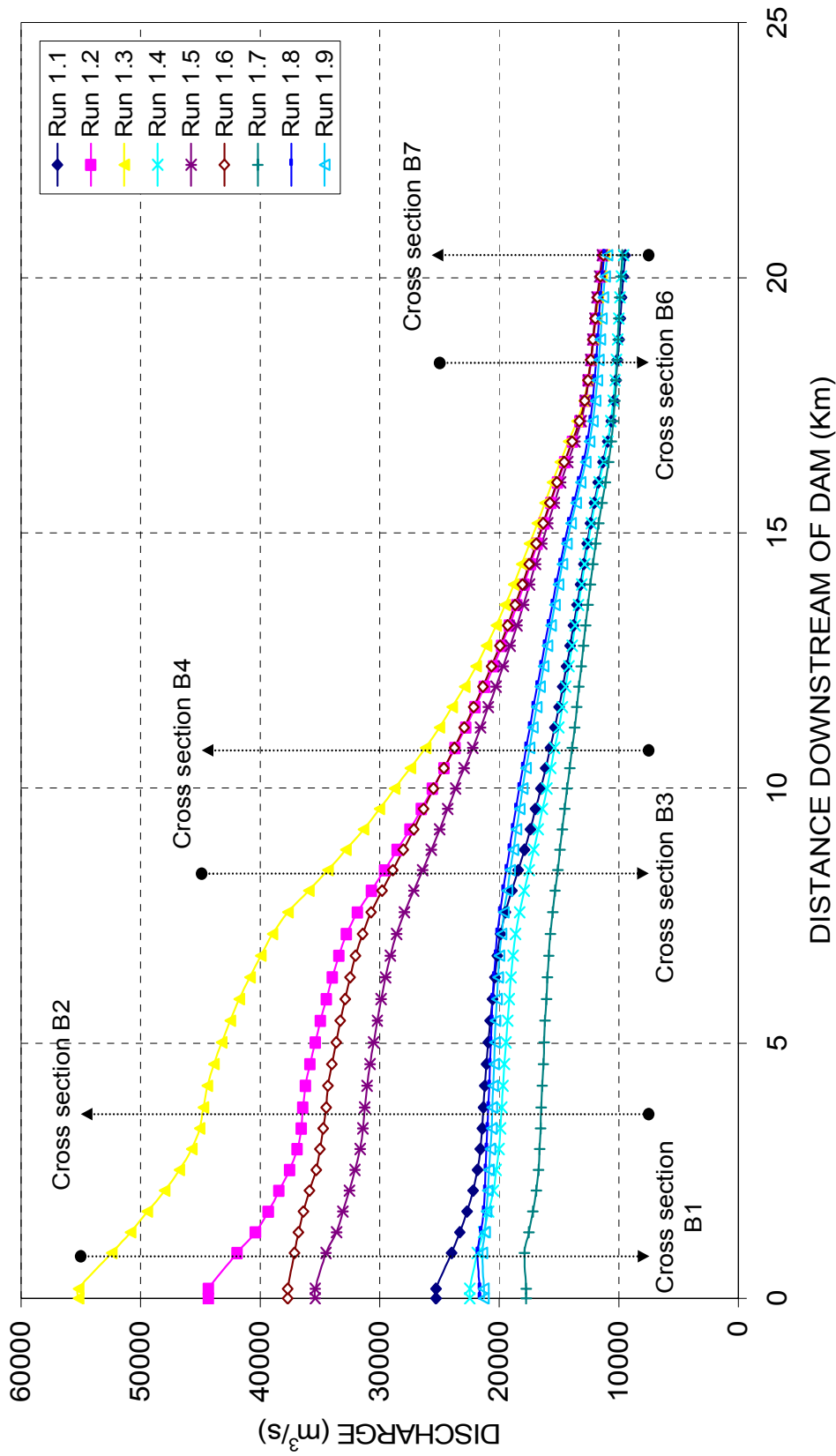


Figure 6.1 Peak discharge profiles for different breach parameters

To sum up, it can be generalized that, as the breach opening increases, peak flow increases. Additionally, as the failure time increases, the peak flow rate decreases. Therefore, it is obvious that, breach with a maximum size and minimum failure time gives the most unfavorable flooding conditions downstream. It has to be noted that, the effect of dam breach parameters damp out to the downstream of the routing reach and there is extreme peak flow attenuation for each sub-scenario. The tendency for this extreme attenuation and rapid damping of differences in the peak discharge may be devoted to the presence of very wide downstream valley.

Figure 6.2 shows the spatial variation of peak flow occurrence time along the routing reach. If the graph is examined carefully, it can be realized that, flood wave spends the shortest travel time for run 1.3; and the longest for run 1.7. This is very normal due to the fact that run 1.3 has the greatest peak flow compared to the others. Larger flows mean greater velocities, which enables the wave to travel a certain distance in a comparatively shorter period of time. For run 1.7, the breach opening is the smallest, which means relatively small peak discharges, and failure time is the longest. Therefore, it is inevitable for run 1.7 to have longest peak flow occurrence times. The peak flow occurrence time for the closest cross section to the dam is nearly the same for sub-failure groups that have the same failure time. But, as the distance from the dam axis increases, the effect of geometrical breach parameters on the peak flow occurrence time is more pronounced. It is also found out that, this time effect of failure time is more dominant on the results than breach parameters. It has to be remembered that, this is the reverse for peak flow variation. Consequently, failure time has significant impact on peak flow occurrence time. Additionally, greater breach openings result in shorter occurrence times.

Figure 6.3 displays the peak water surface profile for each sub-scenario of scenario 1. Needless to say, run 1.3 has the highest peak water surface profile, and run 1.7 has the lowest.

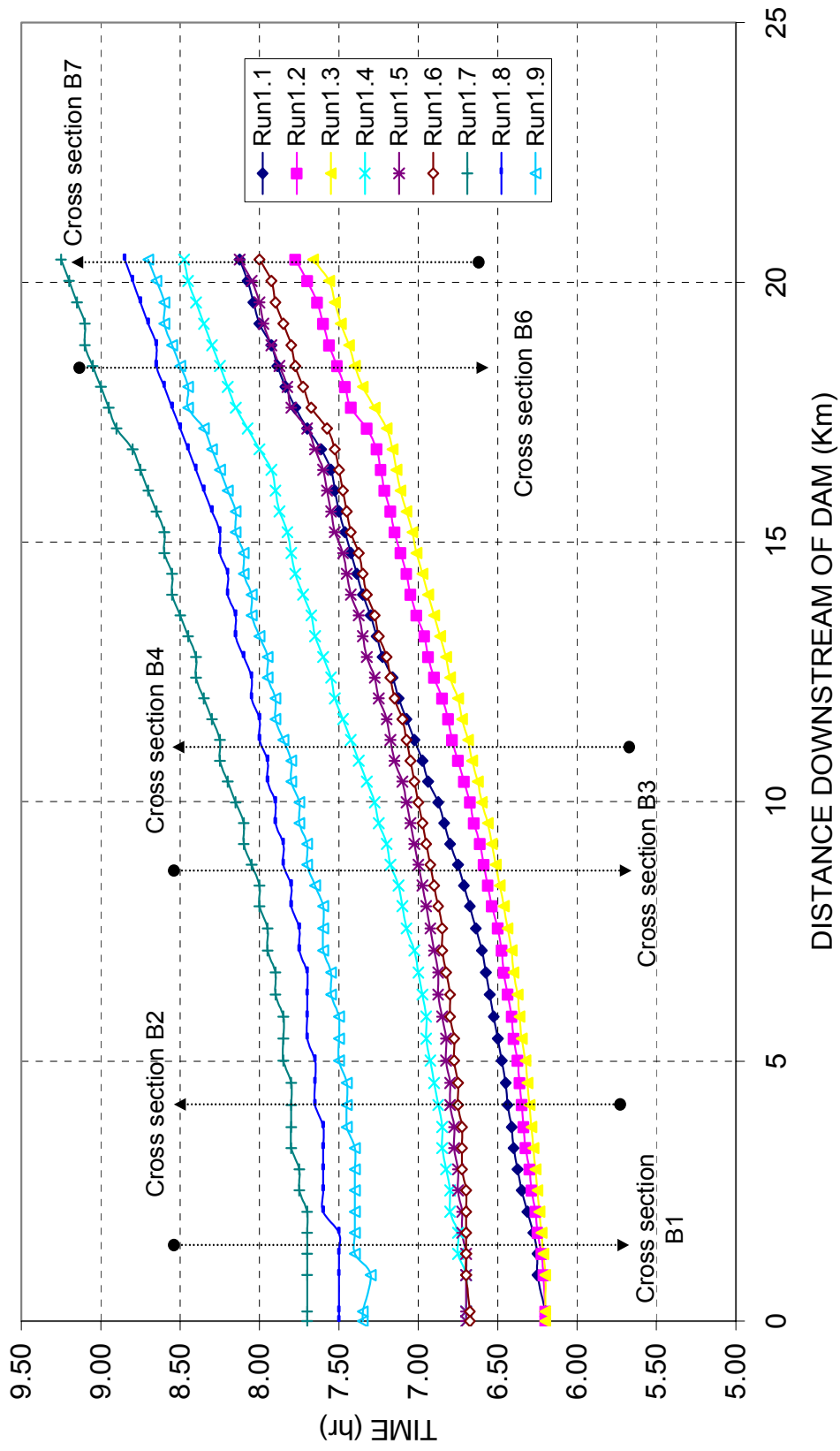


Figure 6.2 Peak flow occurrence time profiles for different breach parameters

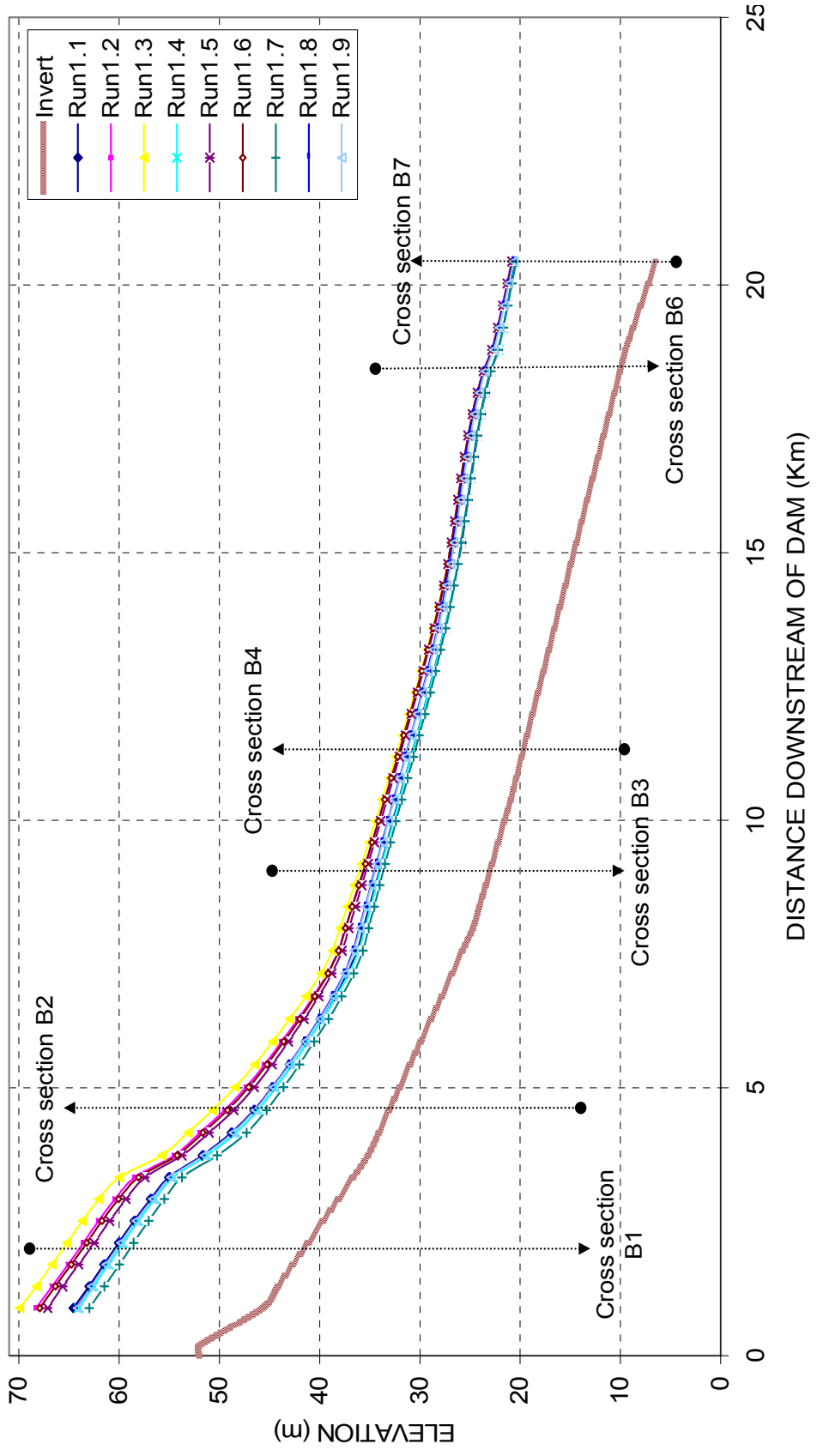


Figure 6.3 Peak water surface elevation profiles for different breach parameters

Again, the effect of breach parameters diminishes, as the flood wave progresses downstream. When compared to the peak flow variation as per different breach parameters, the peak water surface profile is slightly affected by breach parameters. In other words, the impact of breach formation is less for peak water surface elevation than for peak flow.

The final graph for scenario 1 can be seen in Figure 6.4. This figure clearly shows how a discharge hydrograph is routed along the valley. In fact, this graph can be generated for any scenario that comprises of any breach or other parameters. But, since scenario 1 is selected to be the most realistic one, it is better to generate this graph for this scenario. It is easily figured out that, the hydrograph is attenuated, lagged, and distorted as it is routed through the valley due to the effects of floodplain storage, frictional resistance to flow, flood wave acceleration components, flow losses, and downstream channel constrictions and/or flow control structures. Modifications to the flood wave are manifested as attenuation of the peak flow magnitude, spreading out or dispersion of the temporal varying flood wave volume, and changes in the celerity or travel time of the flood wave. Furthermore, since the routing reach contains wide floodplain, which acts as a significant storage volume, the flood wave is extensively attenuated as shown in Figure 6.4.

6.2 EVALUATION OF SCENARIO 2, 3 and 4 RESULTS

Scenario 1 is examined under the assumption that spillway gates can not be lifted during the entrance of catastrophic inflow hydrograph to the reservoir that resulted from heavy precipitation. However, if someone predicts in advance the possible danger of dam overtopping, the first thing that comes to his mind may be opening the radial gates of the dam, so that flood wave can pass through the gate opening. Due to an operational problem, he may not be able to raise the gates properly at all, or he may succeed to open the

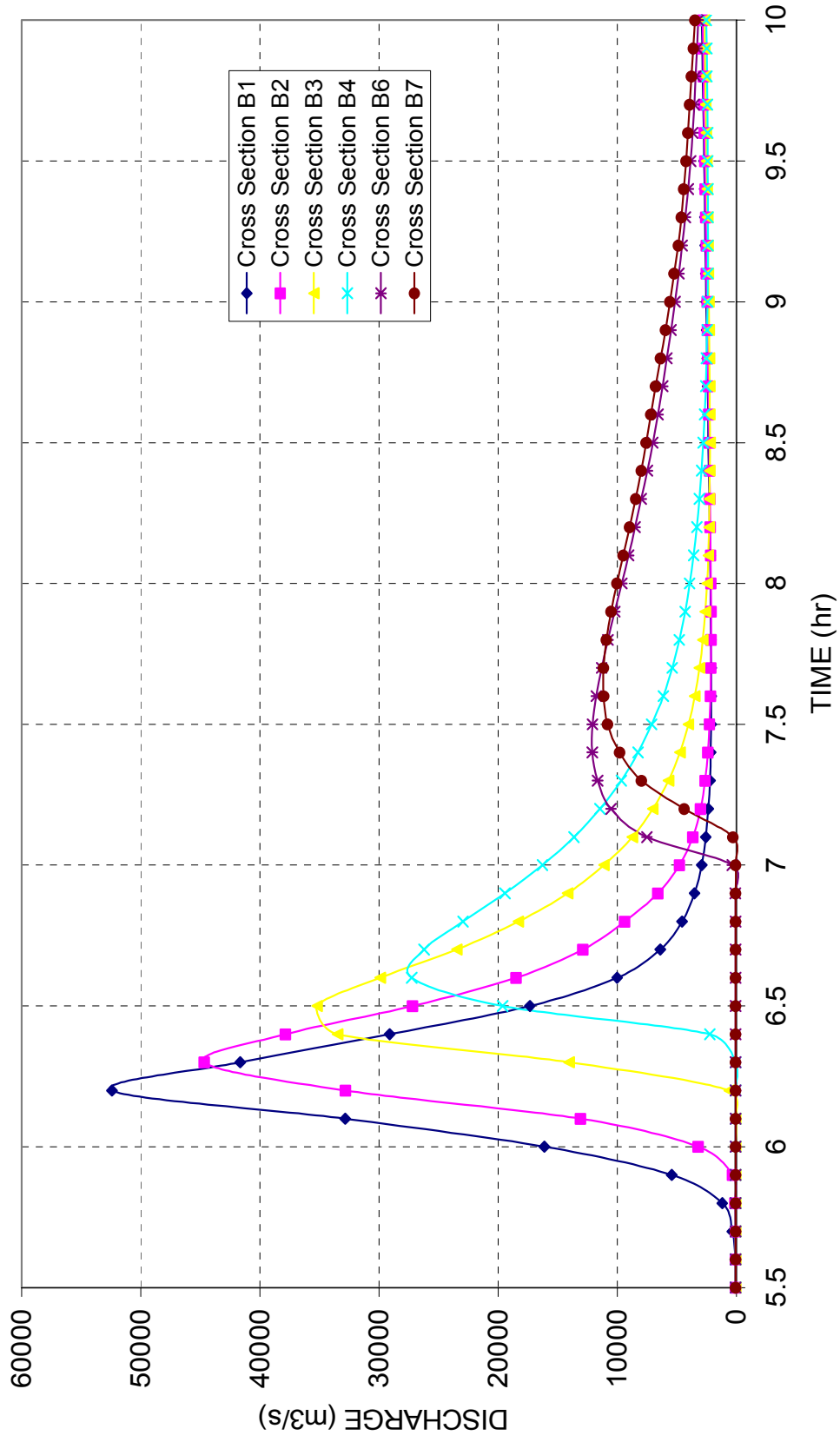


Figure 6.4 Dam break flood wave attenuation along the routing reach for scenario 1

gates partially. Since, the former is examined in scenario 1, it is considered to explore the effect of spillway gate opening in scenarios 2 and 3. Spillway rating curve is available for each gate opening in the increments of one meter. In order to see if gate opening affects routing results significantly, it is decided to test all sub-scenarios of scenario 1 under gate opening of 2 m and 6 m for scenario 2, and 3, respectively. Gate opening of 2 m represents smaller gate openings, while a gate opening of 6 m represents relatively larger gate openings. Comparing results of scenarios 1, 2, and 3, it is found out that gate opening has slight influence on peak flow and peak water surface elevation. Scenarios 2 and 3 came up with greater peak flows and peak water surface elevations as compared to scenario 1. This may be due to the larger total amount of water that is conveyed through the spillway opening. Since, the spillway continuously discharges water; the inflow hydrograph continually releases water to the spillway. But, when the spillway gates are closed, the water shall accumulate behind the dam up to a maximum level until breaching of the dam body occurs. Therefore, the amount of accumulated water that is released through the breach opening is less than the amount of water that is continually released through the spillway opening when the gates are open. Essentially, the impact of spillway gate opening can be observed in occurrence time of peak flow. It is worth to notice that, scenarios 2 and 3 lead to significantly longer occurrence times of peak flow. While the peak occurrence times are around 6-7 hours for scenario 1, these values are 13-14, and 17-18 hours for scenarios 2 and 3, respectively. A gate opening of 2 m, which is a small opening indeed, may increase the occurrence time twice as the value when the gates are closed. This means, the spillway gate opening is very important in determining the warning and evacuation time. So, it is vital to have spillway gates open as wide as possible, to increase the warning time required to evacuate populations living downstream. In order to have a better idea on the effect of spillway gate opening amount on the downstream flooding conditions, graphs shown in Figures 6.5 through 6.7 are created.

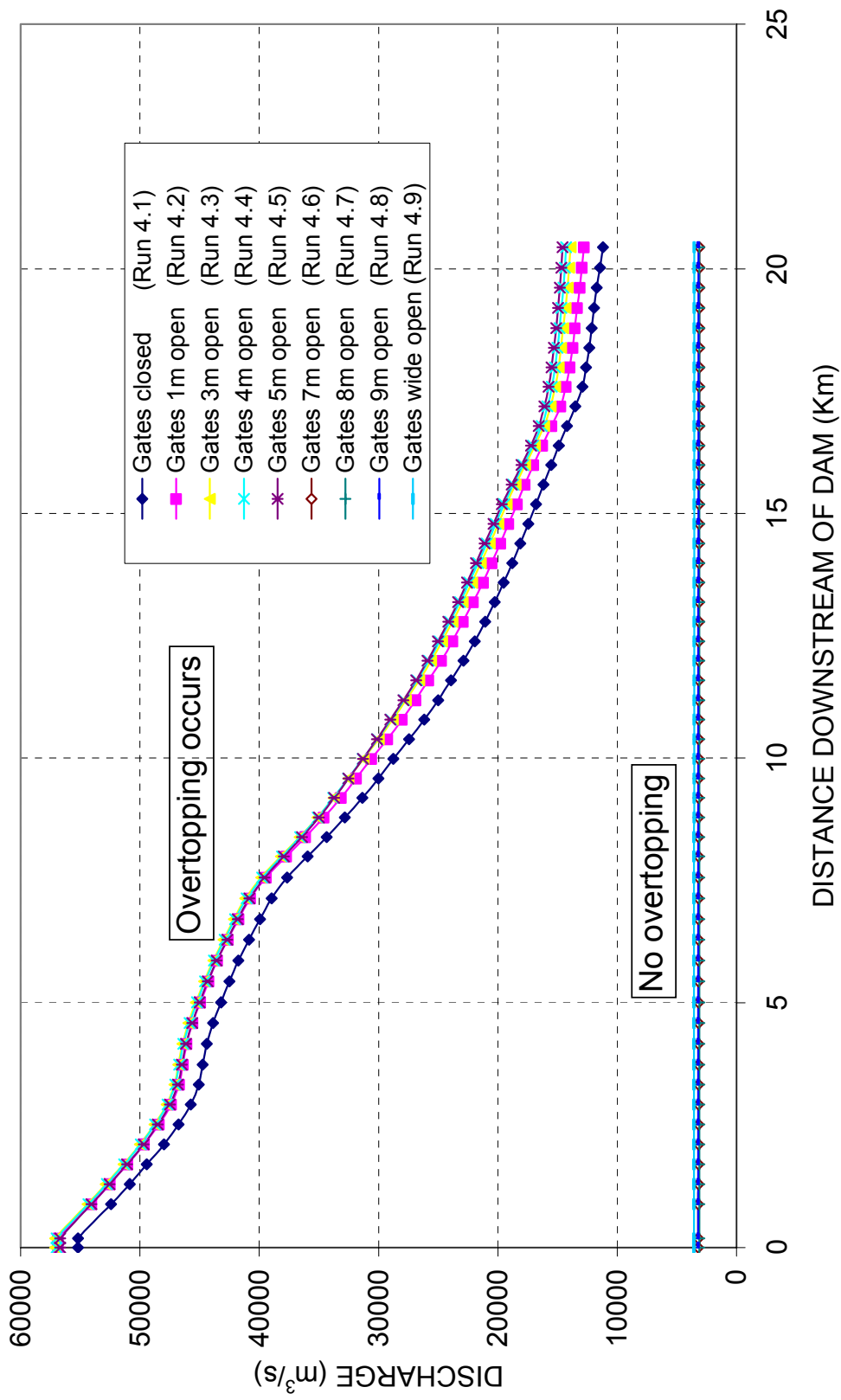


Figure 6.5 Peak discharge profiles for different spillway gate openings

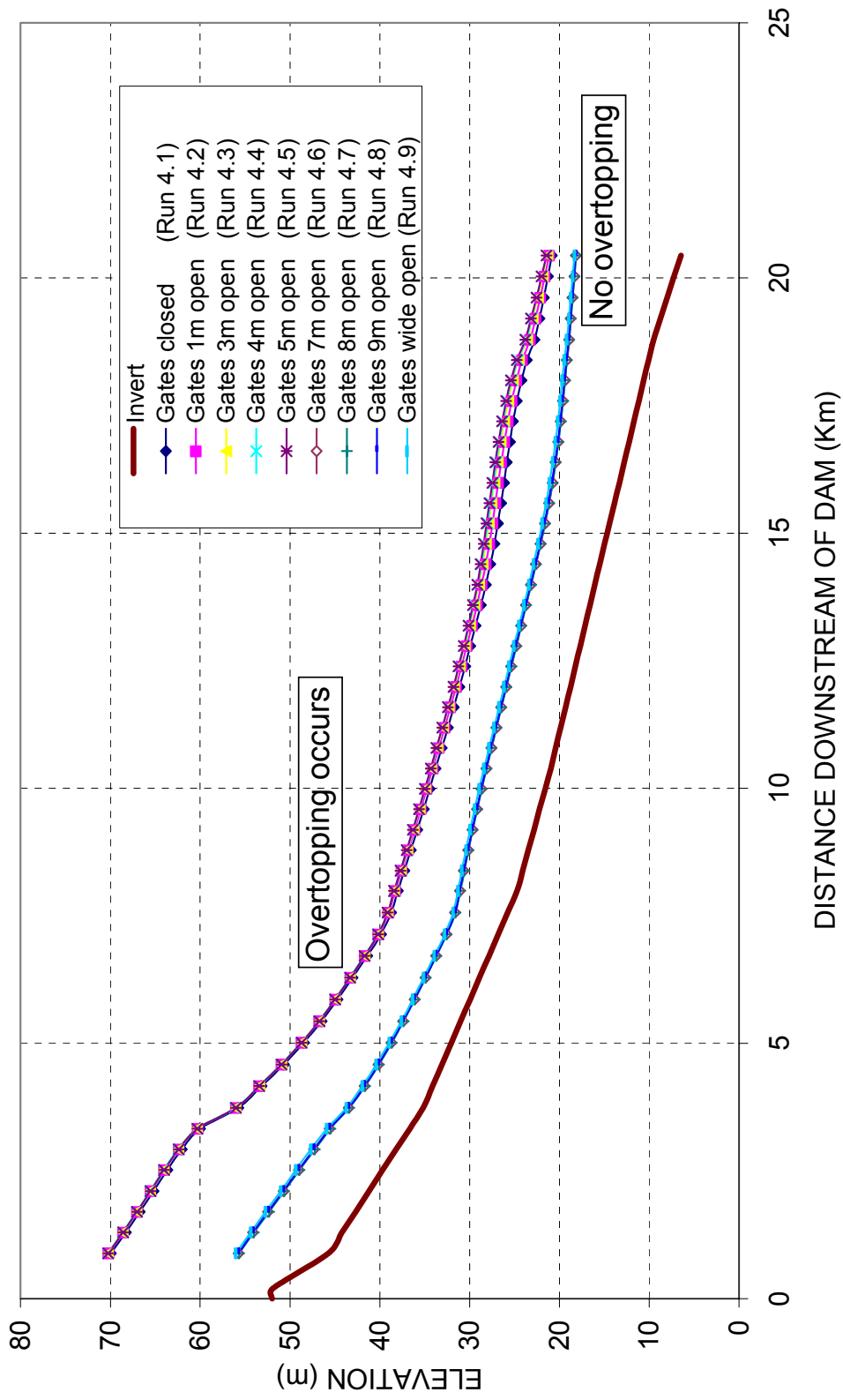


Figure 6.6 Peak water surface elevation profiles for various spillway gate openings

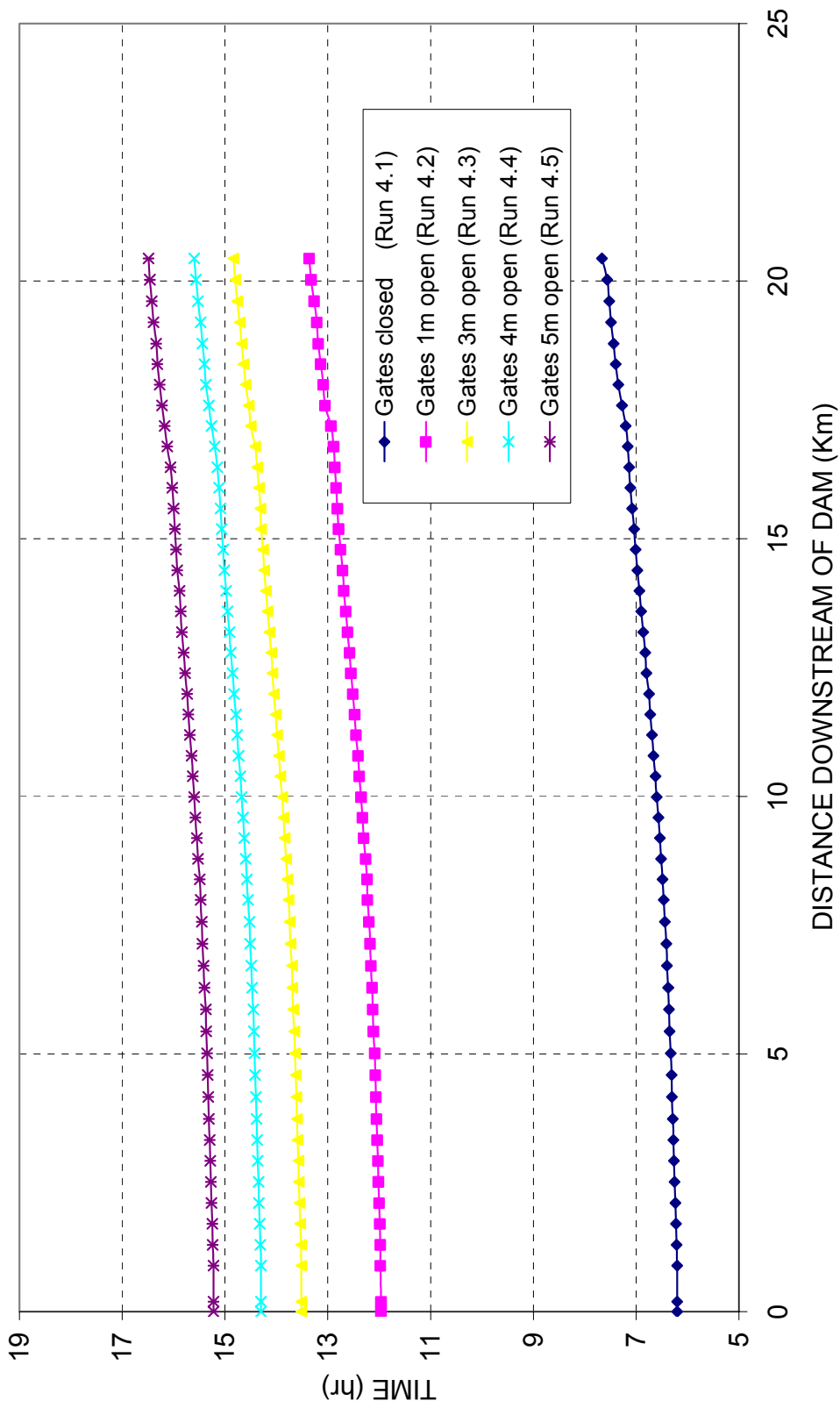


Figure 6.7 Peak flow occurrence time profiles for spillway gate openings that lead to dam failure

Preceding graphs are generated from the output data of scenario 4. This scenario is individually intended to expose the impact of spillway gate opening on the results. Since 2 m and 6 m gate openings are examined in scenarios 2 and 3, this scenario searches for results of remaining available gate openings. Figure 6.5 shows the variation of peak flow along the routing reach under different spillway gate openings. Peak flows are extremely large and there is a great attenuation of discharges for sub-scenarios starting from run 4.1 to run 4.5. Afterwards, peak flows are considerably small and almost constant. This is a nice indication of critical gate opening that will prevent overtopping failure of the dam. The abrupt change in the values of peak flow is due to the occurrence of dam failure. The dam fails in runs 4.1 to 4.5 and does not fail for runs 4.6 to 4.9. This can also be sorted out by looking at the discharge values in Table 5.10. The peak discharge at cross section B1 is 54074 m³/s in run 4.5, and it is 3203 m³/s in run 4.6. This is the limit where dam failure occurs. The spillway gate opening in run 4.5 is 5 m as per table 5.2, and the gate opening is 7 m in run 4.6. Additionally, gate opening of 6 m leads to a peak discharge of 53857 m³/s for cross section B1 in run 3.3. This means, if the spillway gate opening is 6 m, the dam fails and results in a huge peak discharge. But, if the spillway gate opening is 7 m, as in the case of run 4.6, the dam does not fail and the spillway achieves to release the flood water to the downstream valley before the overtopping of the dam occurs. Consequently, spillway gates have to be opened at least 7 m from the gate sill to prevent dam failure of Kirazlıkopru Dam if catastrophic inflow hydrograph enters to the reservoir.

In Figure 6.5, the peak discharge is almost constant for spillway gate openings of 7 m, 8 m, 9 m, and for wide open case. The dam does not fail in these runs, and the flow is almost supercritical along the routing reach. The flow conveyed in these runs is not dam break originated; hence, great attenuation of hydrographs is not encountered.

Figure 6.6 displays the profile of peak water surface elevation under several spillway gate openings. As in the case of previous scenarios, the peak water surface elevations are slightly affected. But, it has to be noted that, when the dam does not fail since spillway gates are opened more than 7 m, the water surface elevations are very low. On the other hand, when the spillway gates are opened less than 7 m, the dam fails and peak water surface elevations increase considerably.

Final comments on scenario 4 can be made on occurrence time of peak flow. Figure 6.7 is generated for this purpose. It is obvious that, as the gate opening increases, peak flow occurrence time also increases. This fact is very important for the determination of warning times. The presence of gate opening retards the occurrence time of peak flow, since it prevents accumulation of great amounts of water behind the dam, which in turn reduces the velocity of the dam break flood wave. The flood may travel in great amounts due to continuous discharge through the gate opening. But, the arrival time of flood wave is lagged due to reduced velocity. As seen in Figure 6.7, the shortest occurrence time is given by the run in which spillway gates are closed. If the gates can be opened as large as possible, warning and evacuation time of people living downstream shall be longer which will impede great amount of lives being lost. It has to be noted that the results of scenario 4 are obtained for the largest breach opening, which is shown in Figure 5.3, and for the shortest failure time, which is 0.5 hour.

6.3 EVALUATION OF SCENARIO 5 RESULTS

Manning n is one of the parameters that contain high level of uncertainty. In order to see if the selection of Manning n can be quite significant for dam break flooding, scenario 5 is examined. For the previous scenarios, Manning n value of 0.04 is used for the channel and 0.06 for the floodplain. These values are taken from the study of Bozkuş (1992) about water surface

profiles along the Bartın River. In this scenario, two other sets of Manning n are used for the sensitivity analyses of Manning n values. The details of sub-scenarios 5.1 and 5.2 can be found in Table 5.2.

The spatial variation of peak flow with respect to three different Manning n value sets can be seen in Figure 6.8. This figure reveals that, as the Manning n values increase, peak flow values decrease. This outcome is reasonable, since discharge is inversely proportional to Manning n. The role of Manning n on the peak flow values gets more significant as the distance from the dam axis increases. This complies with the fact that, the dissipated energy increases as the distance along which frictional resistance is applied increases. Manning n values of 0.02 and 0.04 give the highest peak flows, since the resistance to flow is very low in this run.

Figure 6.9 stresses on the spatial variation of peak water surface elevation along the routing reach. Water surface elevations are higher when Manning n values are greater. It is well known that, discharge is directly proportional to flow depth, while it is inversely proportional to Manning n. Therefore, in order to maintain the same discharge, water depth has to be high when the Manning roughness coefficient is also high. It is also noted from Figure 6.9 that, the effect of Manning n is considerably damped or reduced along the downstream valley during the computation of the water surface elevations.

The effect of Manning on the peak occurrence time can be followed from Figure 6.10. This figure puts forward that, an increase in the Manning n value significantly increases the peak flow occurrence time especially for the downstream locations. For the regions that are very close to the dam are slightly affected. The flood wave encounters more resistance in case of larger Manning n values; thus, it arrives to downstream locations late. The existence of obstructions, heavy vegetation, trees, logs, and shrubs all decrease the adverse effects of dam break flooding.

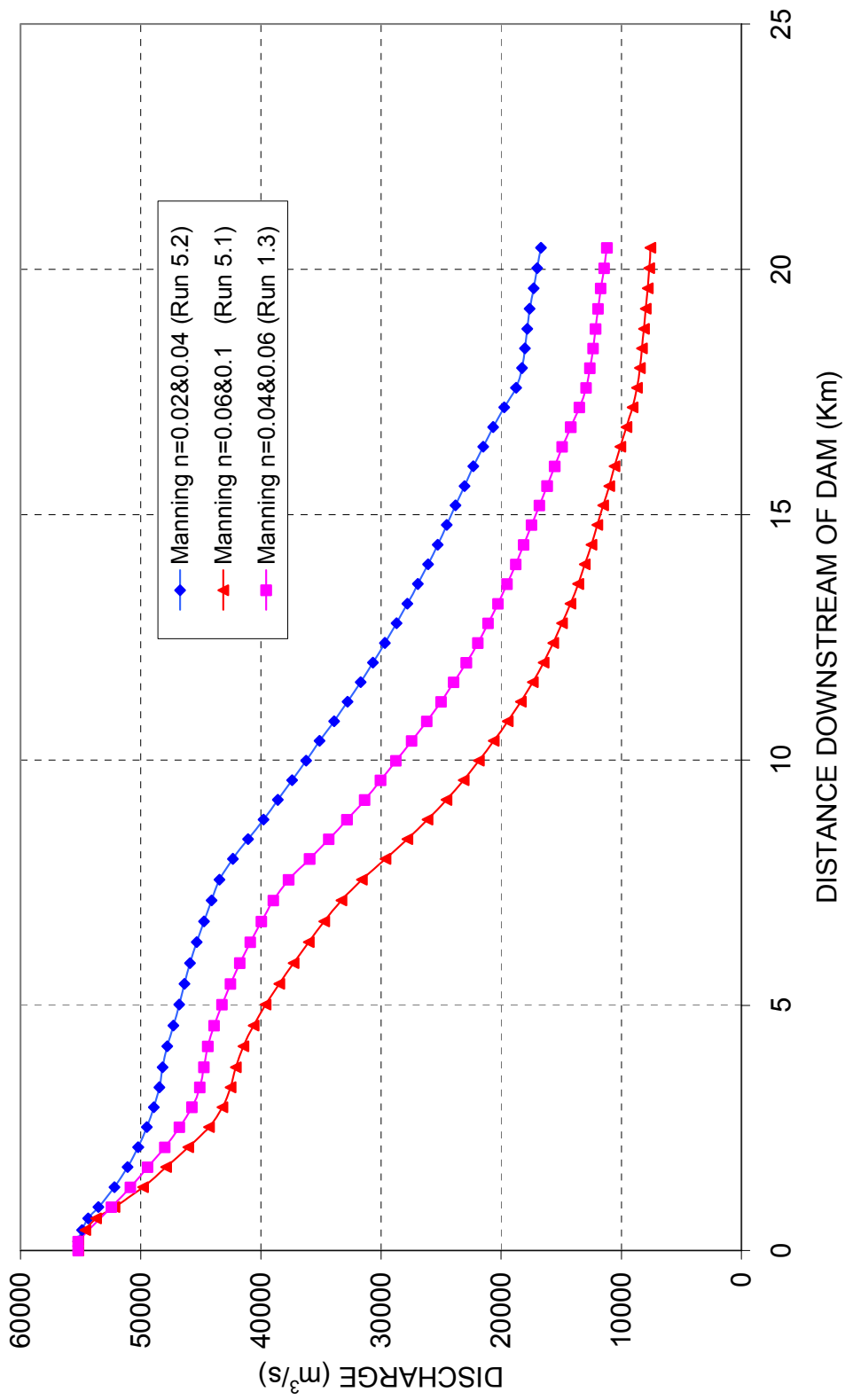


Figure 6.8 Peak discharge profiles for different Manning n values

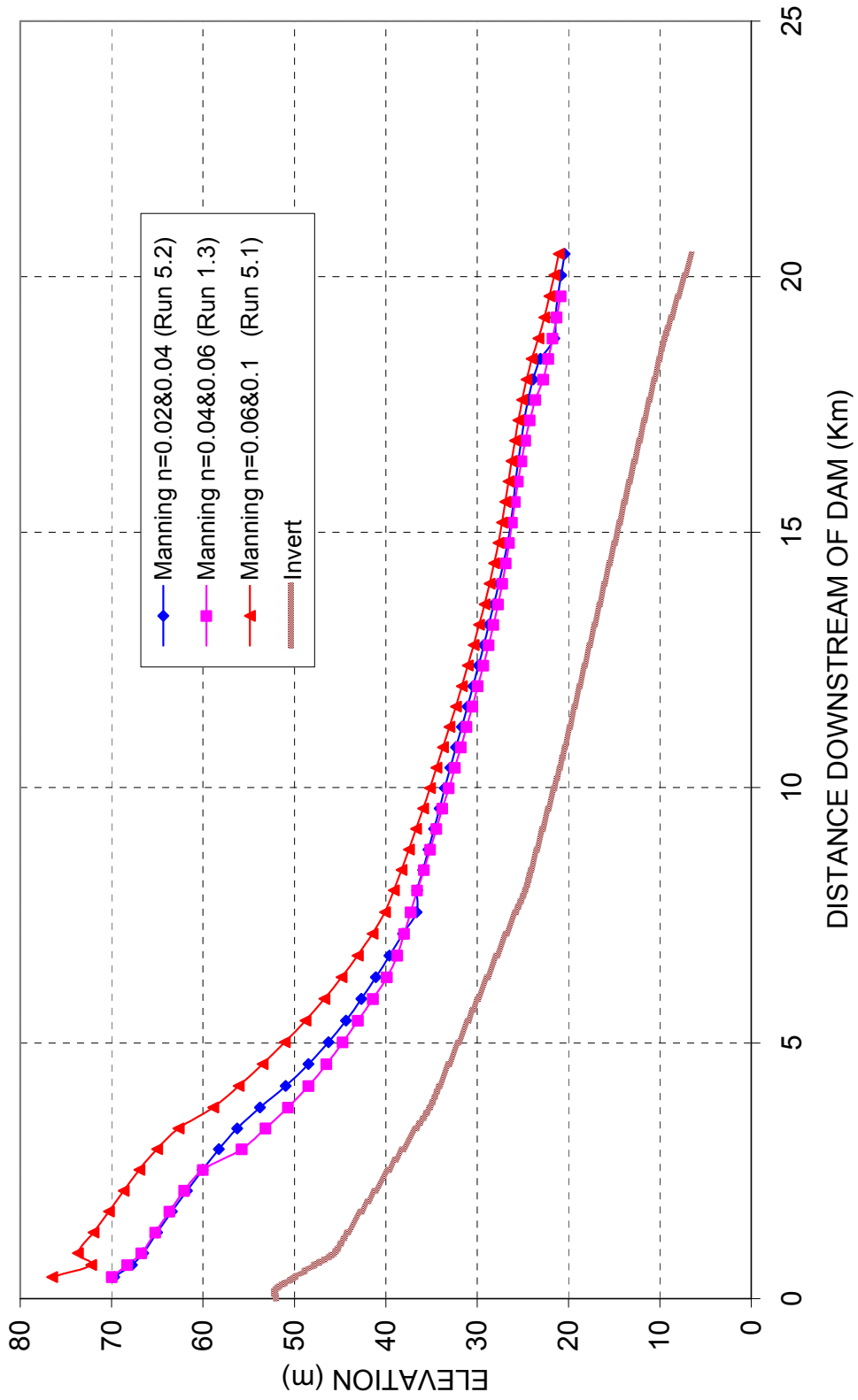


Figure 6.9 Peak water surface elevation profiles for different Manning n values

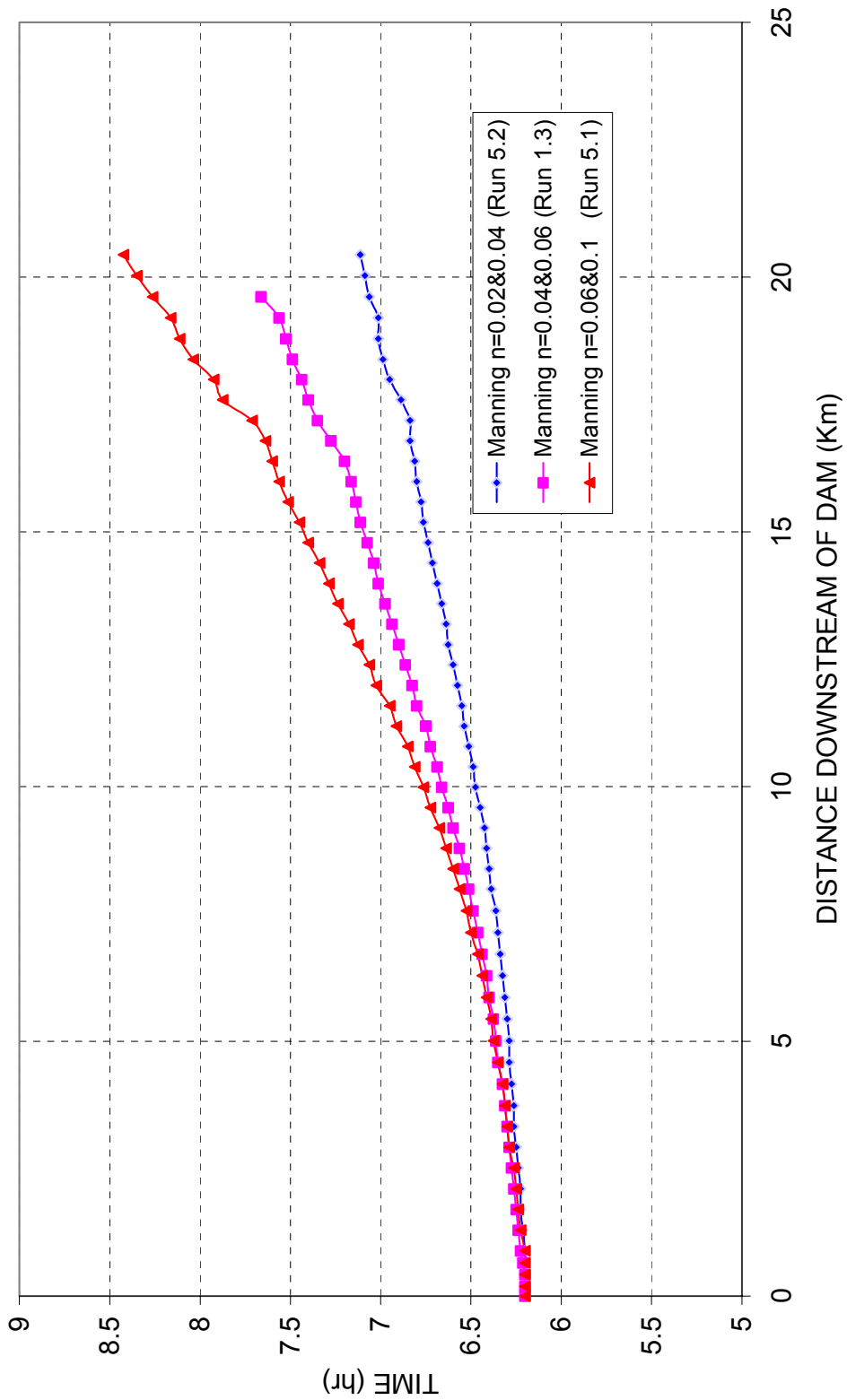


Figure 6.10 Peak flow occurrence time profiles for different Manning n values

6.4 EVALUATION OF SCENARIO 6 RESULTS

Piping failure of Kirazlıköprü Dam is simulated in this scenario. Although overtopping failures generally lead to trapezoidal breach shape, piping breach usually forms in rectangular shape. In this scenario, a certain rectangular breach is modeled with variable breach formation rates and failure times. If scenario 6 results in Tables 5.13 and 5.14 are studied, it can be noticed that peak flow and peak water surface elevations are less than the values of any overtopping failure scenario. That means piping failure leads to less critical results. This makes sense, because the breach opening formed during piping failure is considerably small when compared to size of overtopping breaches. As it is pointed out in section 6.3, as the breach opening size increases, peak flood conditions also increase. Moreover, the time of failure is usually longer for piping than overtopping failure. It is very important to note that occurrence times of piping failure scenarios in Tables 5.13 and 5.14 with those of overtopping failure can not be compared. Because, piping failure is modeled to start immediately at $t=0$, while overtopping failure starts when a certain water surface elevation is reached behind the dam. It has to be appreciated that, during overtopping failure, the reservoir elevations needs some time to fill up to the desired elevation.

Assuring that piping failures cause less critical results than overtopping failures, the main objective of this scenario is set to be investigation of breach formation rate and failure time effects on the reservoir outflow hydrograph. For this purpose, Figures 6.11 through 6.14 are generated in order to have a better visual understanding of the phenomenon.

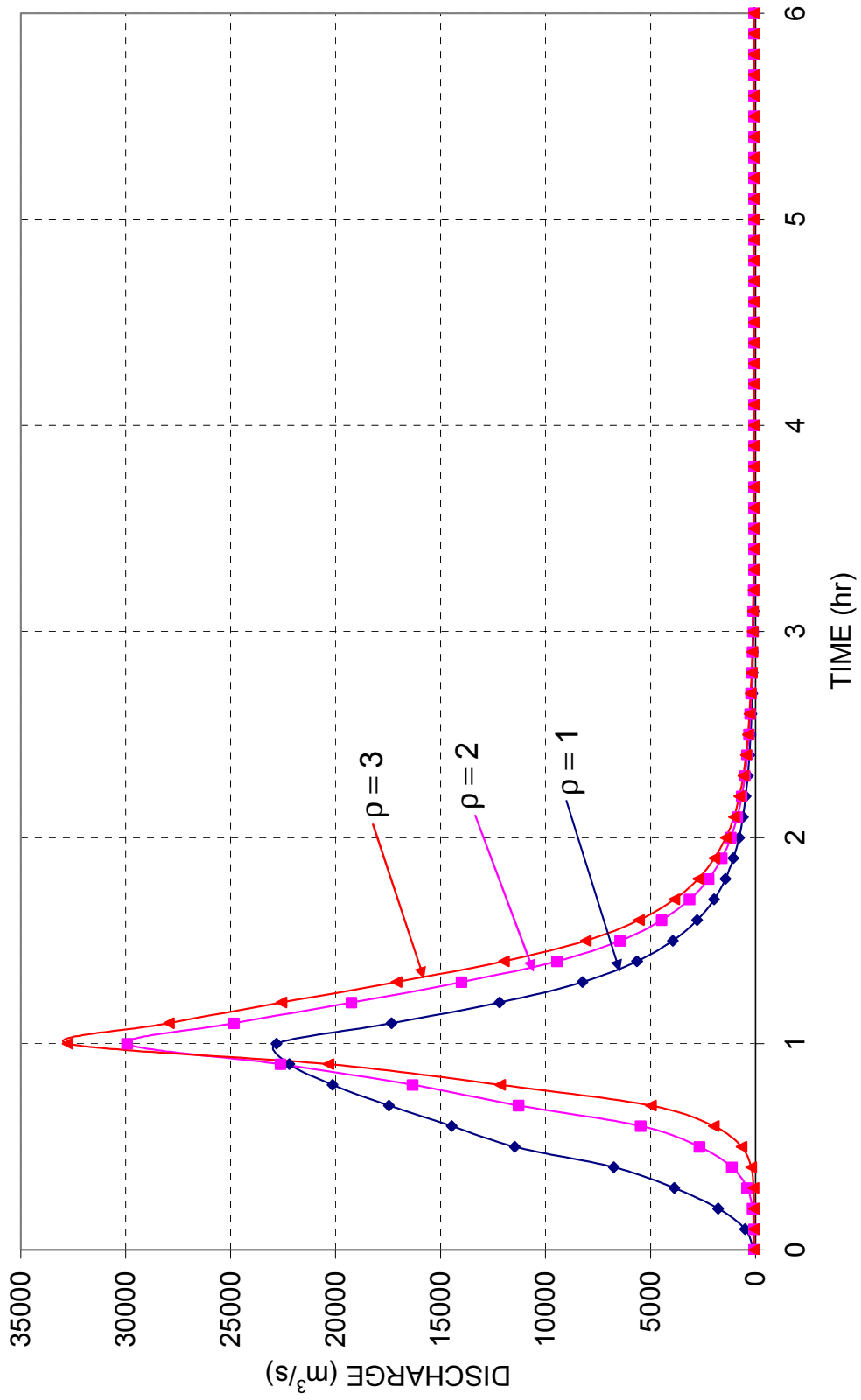


Figure 6.11 Reservoir outflow hydrograph for piping failure ($T_f = 1$ hr)

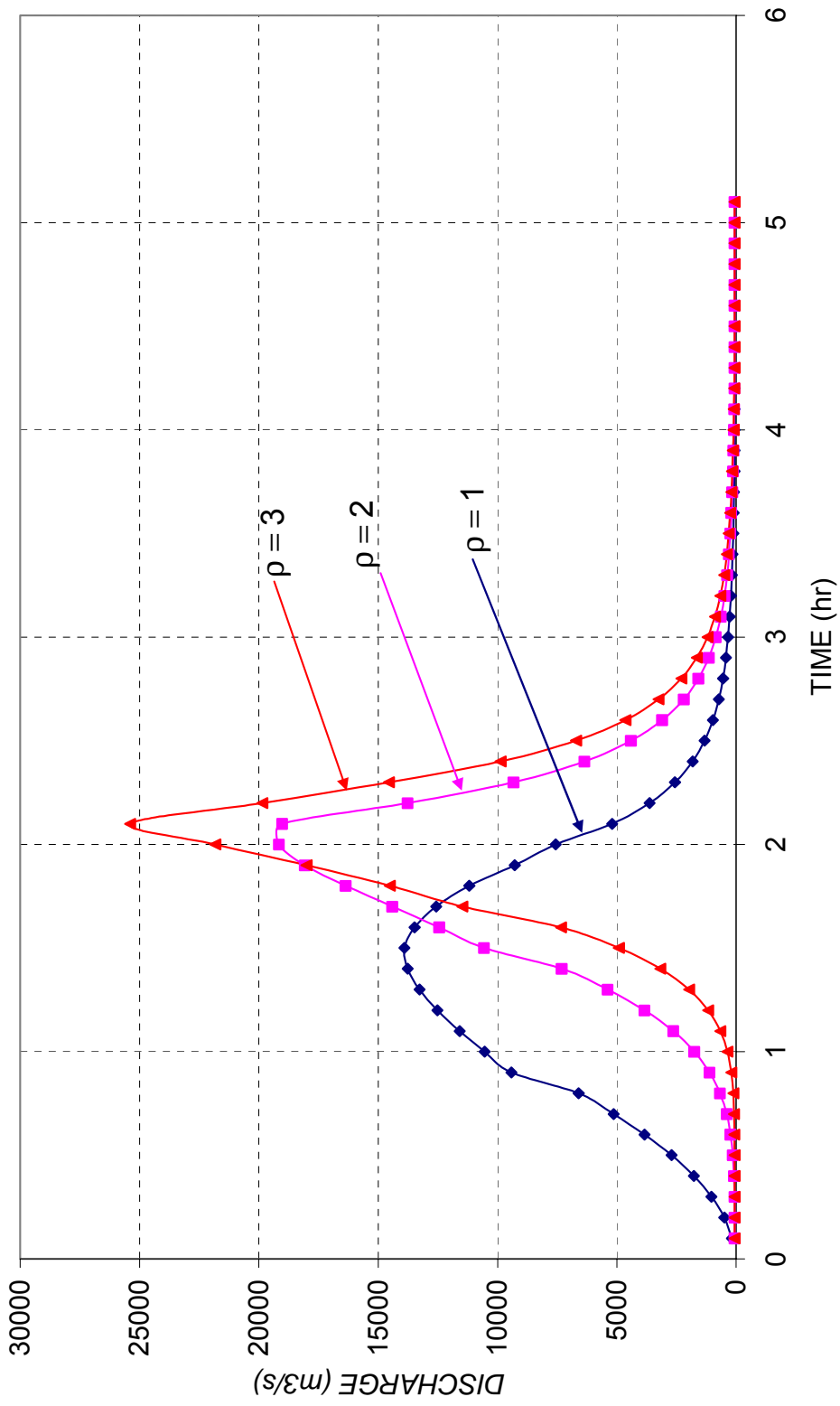


Figure 6.12 Reservoir outflow hydrograph for piping failure ($T_f = 2$ hr)

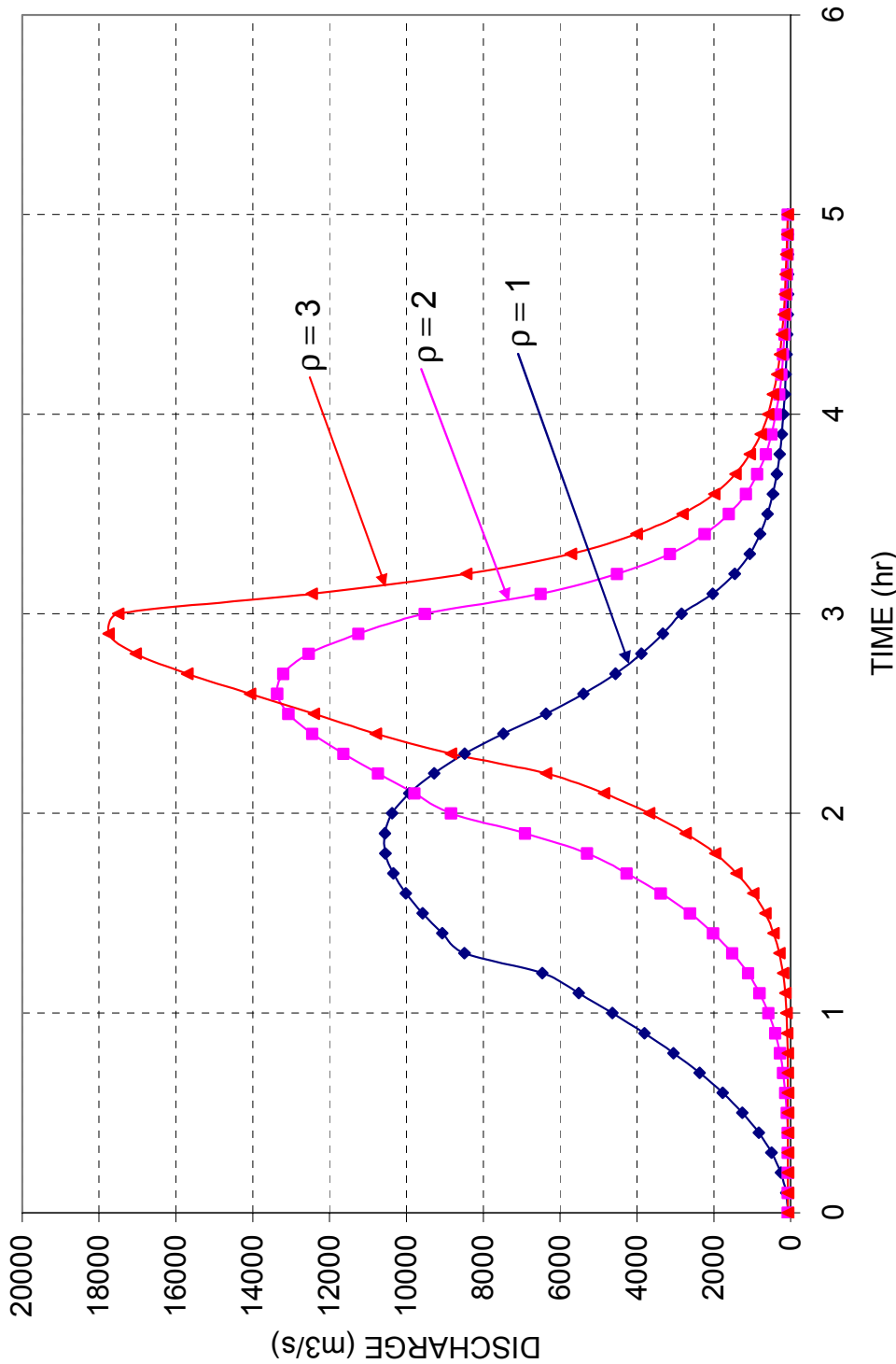


Figure 6.13 Reservoir outflow hydrograph for piping failure ($T_f = 3$ hr)

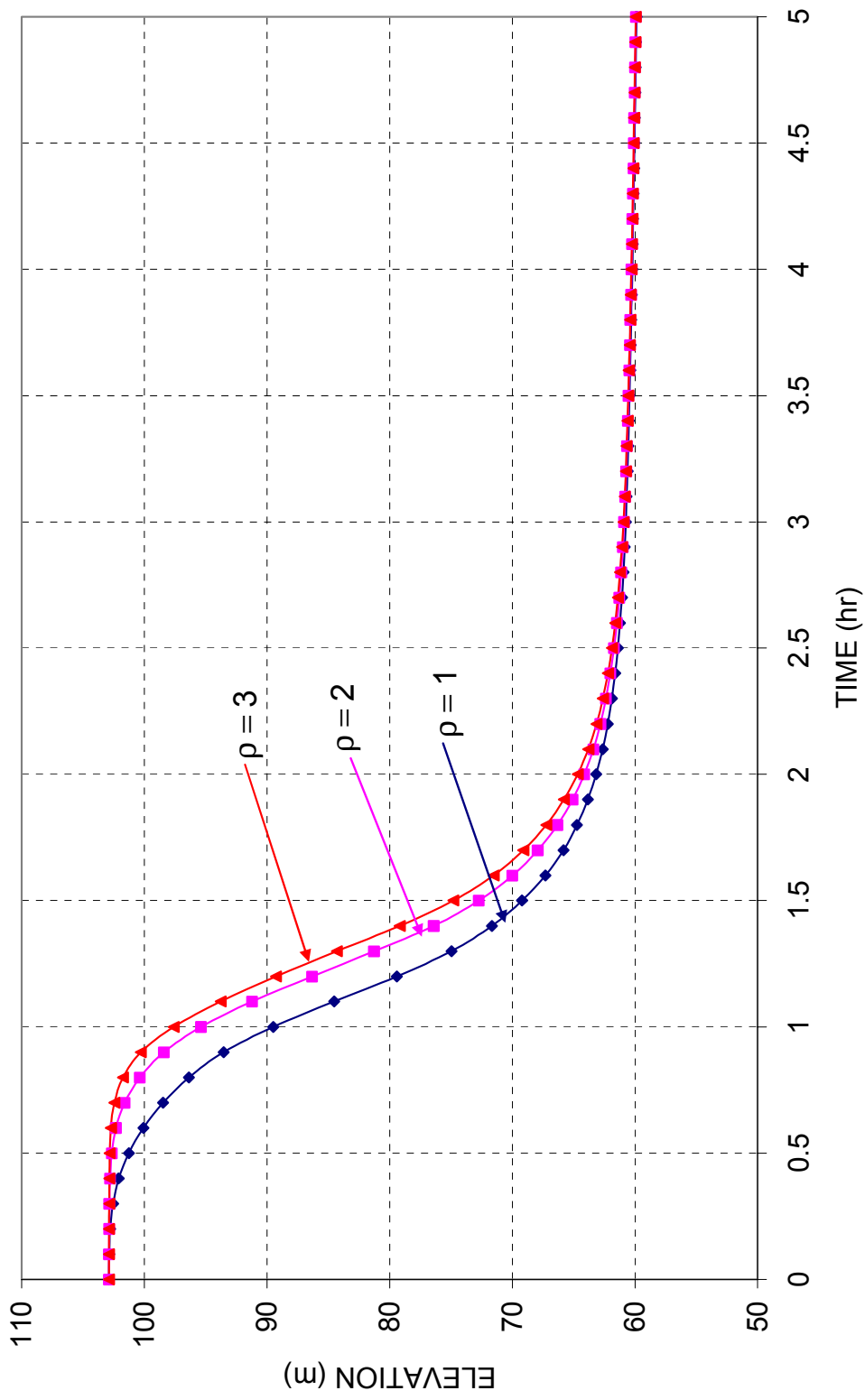


Figure 6.14 Temporal variation of water surface elevation in the reservoir for 1 hr failure time

In the literature, it is advised to use breach formation rate parameter values greater than unity for piping failure simulations. Overtopping breaches develop in a linear rate, but piping breaches form in a quadratic rate; i.e, ρ values are greater than unity. In order to see the effect of breach formation rate on the breach outflow, ρ values of 1, 2 and 3 are utilized in this scenario under different failure times.

Figures 6.11-6.14 show that as the breach formation rate increases, peak flows also increase for any failure time. In Figure 6.11, it has to be noted that, time to peak of outflow hydrographs almost coincides with the failure time. In runs 6.1 to 6.3, the failure time is 1 hr and peak flows for different ρ values occur also at 1 hr. In Figure 6.12, time to peak of outflow hydrograph corresponding to $\rho=1$ occurs before the failure time. Time of failure is 2 hr for this scenario, but peak flow occurs before 2 hr in run 6.4, which has the value of $\rho=1$. And finally, in Figure 6.13, both runs 6.7 and 6.8 have time to peaks that occur earlier than failure time. For any failure time, if the breach formation rate is 3, time to peak occurs almost at the same time as the breach completely forms. On the other hand, as the failure time increases, peak flow occurs earlier than failure time for $\rho=1$ and $\rho=2$ values. It can be concluded that, as the breach formation rate increases, time to peak of outflow hydrographs also increase up to the failure time.

If the hydrographs representative of three failure times are observed, it can be seen that the slope of rising limbs decrease as the failure time increases. The greatest rising limb slope is encountered when $\tau=1$ hr and $\rho=3$. As ρ increases, slope of the rising limb also increases. The falling limbs of the hydrographs are more or less parallel to each other. This may be due to the fact that, even the breach formation rates are different, the terminal breach shape and size is the same for all.

The slope of the rising limb is the mildest for linear breach formation. Furthermore, the limb starts rising immediately after $t=0$. However, the early stage of piping failures are said to occur very slowly; therefore, utilization of a linear breach formation is not realistic and values greater than unity has to be used when simulating piping failures.

Finally, Figure 6.14 shows the temporal variation of water surface elevation in the reservoir for different ρ values. In this figure, the failure time is kept constant and the effect of breach formation rate on the peak water surface elevation is sought. It is easily noted that, peak water surface elevation is effected by the breach formation rate. Greater breach formation rates result in higher water surface elevations. Time of failure is 1 hr in this graph, but the variation in water surface elevations for each ρ value starts before peak flows occur at 1 hr.

6.5 HAZARD EVALUATION OF DOWNSTREAM REGIONS

The analyses results presented in previous sections are needed to perform hazard evaluation of the populations settled downstream of the dam. With the availability of these forecasting results, the regions which are under danger of flooding due to Kirazlıköprü Dam failure can be determined. In order to achieve this, first of all, the regions that are very close to the location of input cross sections have to be designated. This can be done by the aid of 1/25000 or 1/100000 topographic maps. This work is done in this study and the settlements nearby each input cross section can be found in Table 6.1 together with their populations for the year 2000. The approximate elevation of these regions from the mean sea level is also included in this table.

Knowing the elevation of each settlement, the most critical flooding conditions due to dam break has to be sorted out from the analyses results.

In fact, the most unfavorable conditions are resulted from run number 5.1. This scenario is examined under very low Manning roughness coefficients. However, based on the previous study on the region, and the experience of operational staff in that region, Manning n values are considerably higher than those. Therefore, the results of this sub-scenario are not used for the sake of more realistic hazard evaluation of Kirazlıköprü Dam failure. Besides, since the occurrence times are greatly increased when the spillway gates can be raised, scenarios that examine this matter are also excluded in the hazard evaluation. The peak flow and water surface elevation conditions may be slightly more critical, but occurrence time is more critical in determining warning and evacuation times. Therefore, it is vital to perform hazard evaluation under scenario 1, which assumes that spillway gates can not be opened during the flood.

The downstream valley mainly consists of wide floodplains which are used for agricultural purposes. There are many agricultural areas located along both sides of Gökırmak Creek as well as tile factories, motor pumps, bridges, schools, mosques, government buildings, housings and highways. To evaluate the flooding risk of any region, maximum water surface elevation at that region and the elevation of the region itself have to be compared. This comparison can be made by making use of Table 6.1. Derbent district is located nearby cross section B1. The center of this region is at an elevation of around 90 m from the mean sea level. But, there are some small villages such as Çimce which are at an elevation of less than 70 m. Since the maximum water surface elevation in this region is about 70 m, all the agricultural areas, houses, schools and highways of this village may be flooded. Since, this region is very close to dam site, flood wave is expected to arrive in a small period of time. The warning time to evacuate people in this region is only 6 hours. On the other hand, for the Keller village, which is situated at elevations higher than 70m, there is no flooding problem.

Similarly, the center of Çamlık district is not expected to encounter any

flooding; because, it is located at an elevation that is higher than the maximum expected water surface elevation. Unfortunately, Kayaaltı village is not as lucky as Çamlık district. Since, it is located 50m from the mean sea level it is flooded when the flood wave arrives to this region at 6.3 hr. The roadway and the bridge may face severe flooding.

Kurtköy and Nefsigeriş are situated in a wide valley, and the floodplains of the Gökırmak are extensively used for agricultural purposes. These locations are also under great danger. The mean elevation of this region is around 30 m, and around 1600 people live here. Kirazlıköprü dam break forecasting results endangers the lives of these people, since the flood wave is expected to rise to a maximum elevation of 38 m. Only, 6.5 hr is available to alert these people and to evacuate them to safe places. This time starts when the first drop of catastrophic inflow enters to the reservoir. Fortunately, the school at elevation 40 m may be able to survive.

Yanaz and Terkihaliller are located 10 km away from the dam axis, and their elevation is approximately 30 m from the sea level. Since the inundation level for this region is 33.8 m, all the housings, agricultural areas, tile factory and concrete plant have high risk to get flooded. Same observations can be made for Tabanözü and Muratbey districts which are 19 km far from the dam axis. Since these regions are considerably far from the dam site, required time for the evacuation and warning of the people is longer as compared to regions that are closer to dam axis. About 8 hour warning time is available for these regions.

Situated very close to the input cross section B7, Ağıdacı district is located 10 m from the mean sea level. It is foreseen that, peak water surface elevation rises to 20 m elevation, and severe flooding of this region is likely to occur. The peak flow is expected to arrive to this region at about 8 hr. More details of above discussion on hazard evaluation can be found in Table 6.1 below.

Table 6.1 Hazard evaluation of downstream regions

Cross Section	St.Km	Nearby Region	Elevation (m)(MSL)	Population (2000)	Max WSEL (m)(MSL)	Occurrence Time (hr)	Run Number	Max Flow (m ³ /s)	Occurrence Time (hr)	Run Number
B1	0.888	Çimce District	60-70		69.97	6.22	1.3	52425	6.2	1.3
		Keller District	70-90							
		DERBENT	90	411						
		Roadway	60							
B2	3.738	Kayaaltı District	50		55.77	6.3	1.3	44747	6.29	1.3
		ÇAMLIK	60	169						
		Roadway	≈ 50							
		Bridge	≈ 50							
B3	7.988	Nazikoğlu District	30		38	6.54	1.3	35938	6.46	1.3
		KURTKÖY	30	670						
		NEFSİGERİŞ	30	958						
		Roadway	≈ 30							
		Bridge	≈ 30							
		School	40							
B4	10.388	Mutaf District	30		33.8	6.72	1.3	27444	6.62	1.3
		YANAZ	30	690						
		TERKİHALİLLER	30	1009						
		Tile factory	< 30							
		Concrete plant	< 31							
		Roadway	< 32							
B6	18.788	Değirmenalçağı District	10		22.78	7.65	1.3	12139	7.44	1.3
		TABANÖZÜ	10	683						
		MURATBEY	10	484						
		Roadway	10							
B7	20.438	Türbealtı District	10		20.89	7.92	1.2	11191	7.66	1.3
		AĞDACI	10	1125						
		Roadway	10							

CHAPTER 7

CONCLUSION

The dam break analysis of Kirazlıköprü Dam is conducted in this study under several failure scenarios. It is intended to investigate the adverse effects of dam break event on the downstream settlements. For this purpose, a numerical model developed by the National Weather Service in the United States is used. This model is an enhanced one dimensional unsteady flow routing tool used widely in the world. The dam under discussion is situated within the borders of Bartın Province of Turkey. This city is notorious for frequent devastating floods that have occurred in the past years. Due to the climatic characteristics of this region, it is not surprising to expect new flood incidents. This means, Kirazlıköprü Dam is one of the dams that bear the greatest probability of dam break event.

The output results of dam break simulation are quite sensitive to input data. Dam break phenomenon contains many parameters that constitute considerable uncertainty. In order to overcome this disadvantage of uncertainty, a sensitivity study is desired. In other words, instead of using certain parameters that depend on historical dam break incidents, sets of variable parameters are utilized in the analyses. Nothing is definite in dam break simulation, and the results may change significantly even for a small alteration in the input parameters. Based on this decision, several scenarios are established to cover all possible failure and flooding conditions.

The principal parameters that vary among the scenarios are, breach formation time, breach formation rate, terminal breach size and shape,

spillway gate openings and Manning n values. The effect of each of these parameters is explored and their significance on the output results is interpreted in this study. It is found out that, terminal breach opening size and failure time incredibly affects downstream flooding conditions such as peak flow rate and peak water surface elevations. Therefore, it is crucial to select sensible breach parameters for dam break flood forecasting. Additionally, selection of Manning n is quite important in simulating dam break failures. Fortunately, Manning n data for the routing reach is available from the previous studies that were conducted in the same region. Nevertheless, it is worth to perform simulations under different sets of Manning n values, as done in Scenario 5 of this study.

There is limited number of cross sections whose data is available. For high elevations, cross section data can be deduced from topographic maps, but this is not possible for generating the channel data of the river. In this study, cross sections are located where physical data is available. There are only eight cross sections with available data and two of them are deleted since they create numerical difficulties during the solution of Saint-Venant equations. Due to lack of data such as, presence and properties of levees, bridge constrictions across the river and off-channel storage areas, the effect of these can not be studied herein. Moreover, existence of more cross sectional data might yield to more accurate modeling of the routing reach and more precise output results afterwards.

Apart from overtopping failure, piping failure of Kirazlıköprü Dam is also investigated in this study. It is found out that, overtopping failure leads to more devastative results than piping failure. Moreover, the available time for warning and evacuation of people is much less for overtopping failure than piping failure. But, potential of piping failure always exist due to the fact that it can happen in any time, even in a sunny day with no precipitation at all. When there is water in the reservoir, there is always risk of piping failure. Therefore, it has to be treated with great care.

Analyses results indicate that, most of the regions downstream of the dam are facing danger of flooding if the dam failure of Kirazlıköprü Dam occurs. Hazard evaluation study is performed for Scenario 1, because this is the major scenario which reflects the physical properties of the modeling domain the best. Manning n values, spillway gate condition and breach parameters are very realistic for this scenario. The output results support the idea that this scenario gives the most critical flooding conditions in the downstream valley. As per the results, many agricultural areas, houses, roads, and residential areas may be flooded. A certain district nearby each cross section is under danger and the people living there have to be alerted before the flood wave arrives. Almost in all cross sections, highway gets flooded. This highway connects the province of Karabük to Bartın. A touristic place, Safranbolu is located in Karabük, and most of the tourists travel from Safranbolu to another touristic place Amasra of Bartın province. Therefore, this state highway is frequently used and it is usually crowded. Needless to say, it is vital to warn these traveling people on time if any undesired incident of dam failure is about to occur.

It appears that it is a must to prepare emergency action plans based on the results presented in this study. This is needed for the use of public officials for their use in a real-time emergency management. Early warning systems to alert people on time have to be established. This will also aid proper evacuation of people living downstream and save lives being lost.

Finally, the author would like to recommend another flow routing model for future studies. *BOSS DAMBRK* serves the same functions as *NWS FLDWAV*, but *BOSS DAMBRK* has a more user friendly interface, and it is easier to learn and use. *BOSS DAMBRK* displays over 30 different presentation-quality graphs, including an initial conditions plot, flood inundation map, hydrograph plots, summary hydrograph plots, time history plots, and 3D river valley plots, allowing the user to quickly evaluate his work.

REFERENCES

2000 Genel Nüfus Sayımı, *Nüfusun Sosyal ve Ekonomik nitelikleri, il 74 Bartın*, T.C. Başbakanlık Devlet İstatistik Enstitüsü, Necatibey Cad. No:114, 06100 Ankara/TÜRKİYE, 2002.

Amein, M., and Fang, C.S., *Implicit Flood Routing in Natural Channels*, Journal of Hydraulics Division, ASCE, Vol.96, No.HY12, pp.2481-2500, 1970.

Baltzer, R.A., and Lai, C., *Computer Simulation of Unsteady Flow in Waterways*, Journal of Hydraulics Division, ASCE, Vol.94, No.HY4, pp.1083-1117, 1968.

Bozkuş, Z., *Bartın İl Merkezinin Bartın Irmağı Taşkınlarından Korunması ile ilgili Matematiksel Model Çalışmaları Ara Raporu*, Model No.277, DSİ Hidrolik Laboratuvarı, 1992.

Bozkuş, Z., *Baraj Yıkılması Analizleri için Geliştirilmiş Bir Model*, DSİ Teknik Araştırma ve Kalite Kontrol Dairesi Başkanlığı Yayını, YN:Hİ-879, 1994.

Bozkuş, Z., *Baraj Yıkılma Analizlerinde Kullanılan Matematiksel Modellerin Kıyaslanması ve Uygulamalı Örnekler*, DSİ Su ve Toprak Kaynaklarının Geliştirilmesi Konferansı Bildirileri, Ankara, 2, 731-747, 1994.

Bozkuş, Z., Kasap, A., *Comparison of Physical and Numerical Dam-Break Simulations*, Tr. J. of Engineering and Environmental Science, Vol.22, pp.429-443, 1998.

Bozkuş, Z., Güner, A.İ., *Pre-Event Dam Failure Analyses for Emergency Management*, Tr. J. of Engineering and Environmental Science, Vol.25, pp.627-641, 2001.

Brater, E., *Hydraulics, Civil Engineering Handbook*, edited by L.C. Urquhart, Sect. 4, McGraw-Hill Book Co., New York, pp.4.44-4.60, 1959.

Chow, V.T., *Open Channel Hydraulics*, McGraw-Hill Book Co., New York, 1959.

Costa, J.E., *Floods from Dam Failures*, U.S. Geological Survey Open-File Report 85-560, Denver, Colorado, p.54, 1985.

DeLong, L.L., *Extension of the Unsteady One-Dimensional Open Channel Flow Equations for Flow Simulation in Meandering Channels with Floodplains*, Selected papers in Hydrologic Science, U.S. Geological Survey Water Supply Paper 2220, pp.101-105, 1986.

DeLong, L.L., *Mass Conversation: 1-D Open Channel Flow Equations*, Journal of Hydraulics Division, Vol.115, No.2, pp.263-268, 1989.

Ellingwood, B. et al., *Assessing Cost of Dam Failure*, Journal of Water Resources Planning and Management, ASCE, Vol.119, No.1, January/February, pp. 64-82, 1993.

Fread, D.L., and Harbaugh, T.E., *Open Channel Profiles by Newton's Iteration Technique*, Journal of Hydrology, Vol.13, pp.70-80, 1971.

Fread, D.L., *Technique for Implicit Dynamic Routing in Rivers with Tributaries*, Water Resources Research, Vol.9, No.4, pp.918-926, 1973.

Fread, D.L., *Implicit Dynamic Routing of Floods and Surges in the Lower Mississippi*, Presented at American Geophysical Union Spring Meeting in Washington D.C., April, pp.26, 1974.

Fread, D.L., *Numerical Properties of Implicit Four-Point Finite Difference Equations of Unsteady Flow*, HRL-45, NOAA Tech. Memo NWS HYDRO-18, Hydrologic Research Laboratory, National Weather Service, Silver Spring, Maryland, 1974.

Fread, D.L., *The Development and Testing of a Dam-Break Flood Forecasting Model*, Proc. of Dam-Break Flood Modeling Workshop, U.S. Water Resources Council, Washington D.C., pp.164-197, 1977.

Fread, D.L., *Theoretical Development of Implicit Dynamic Routing Model*, HRL-113, Hydrologic Research Laboratory, National Weather Service, Silver Spring, Maryland, 1978.

Fread, D.L., *Channel Routing, Chapter 14, Hydrologic Forecasting*, (Eds: Anderson, M.G., and Burt, T.P.), John Wiley Sons, New York, Chapter 14, pp.437-503, 1985.

Fread, D.L., *Flood Routing and the Manning n*, Proc. Of the International Conference for Centennial of Manning's formula and Kuichling's Rational Formula, ed. B.C.Yen, Charlottesville, Va., pp.699-708, 1989.

Fread, D.L., *The NWS Dambreak Model: Theoretical Background/User Documentation*, Hydrologic Research Laboratory, Office of Hydrology, National Weather Service (NWS), Silver Spring, Maryland, June 1988 (Revision 4, August 1991).

Fread, D.L., *Flow Routing, Chapter 10, Handbook of Hydrology*, ed. E.R. Maidment, McGraw-Hill Book Co., New York, pp.10.1-10.36, 1992.

Fread, D.L., *Dam-Breach Floods*, NOAA, National Weather Service, Office of hydrology, Silver Spring, Maryland, 1997.

Fread, D.L., *Dam-Break Modeling and Flood Routing: A Perspective on Present Capability and Future Directions*, Presented at International Workshop on Dam Break Processes, Stillwater, OK, March 10-11, 1998.

Fread, D.L., *The NWS FLDWAV Model: Theoretical Description/User Documentation*, Hydrologic Research Laboratory, Office of Hydrology, National Weather Service (NWS), NOAA, Silver Spring, Maryland, 1998.

Graham, W., *Human and Economic Consequences of Dam Failure*, Proceedings Fema Workshop, Oklahoma City, OK, June 26-28, 2001.

Hagen, V.K., *Re-Evaluation of Design Floods and Dam Safety*, Presented at Fourteenth ICOLD Congress, Rio de Janeiro, 1982.

Paquier, A., Nogues, P., and Herledan, R., *Model of Piping in order to Compute Dam Break Wave*, CADAM Proceedings, Munich meeting, 1998.

Preissmann, A., *Propagation of Translatory Waves in Channels and Rivers*, First Congress of French Assoc. for Computation, Grenoble, France, pp.433-442, 1981.

Serafim, L., *Safety of Dams Judged from Failures*, Water Power and Dam Constructions, December, pp.32-35, 1981.

U.S. Army Corps of Engineers, *National Program of Inspection of Dams*, Bul. I-4, Dept. of the Army, Office of Chief of Engineers, Washington D.C., 1975.

Wahl, T.L., *Predicting Embankment Dam Breach Parameters-A needs Assessment*, 27th IAHR Congress, San Francisco, California, August 10-15, 1997.

Wahl, T.L., *Prediction of Embankment Dam Breach Parameters-A Literature Review and Needs Assessment*, U.S. Dept. of the Interior, Bureau of Reclamation, Dam Safety Report DSO-98-004, Denver C.O., 1998.

Weatmore, J.N., and Fread, D.L., *The NWS Simplified Dam Break Flood Forecasting Model*, Printed and Distributed by the Federal Emergency Management Agency (FEMA), pp.122, 1984.

Wurbs, R.A., *Dam-Breach Flood Wave Models*, Journal of Hydraulic Engineering, Vol.113, No.1, pp.29-46, 1987.

Yazıcılar, F., *Water Surface Profile Computations in Floodplain Channels*, MSc. Thesis in Civil Engineering at Middle East Technical University, Ankara-Turkey, Dec., 1997.

APPENDIX A



Layout of modeling reach